

Diss. ETH No. 25697

# Time-optimal Control of the Formula 1 Hybrid Electric Power Unit

A thesis submitted to attain the degree of  
DOCTOR OF SCIENCES of ETH Zürich

(Dr. Sc. ETH Zürich)

presented by

MAURO RUBÉN ULISSE SALAZAR VILLALON

M. Sc. ETH in Mechanical Engineering

born on 23 March 1990  
citizen of Switzerland and Spain

accepted on the recommendation of

Prof. Dr. Christopher H. Onder, examiner

Dr. Carlo Bussi, co-examiner

Prof. Dr. Lino Guzzella, co-examiner

Prof. Dr. Theo Hofman, co-examiner

Prof. Dr. Marco Mazzotti, co-examiner

2018



# Time-optimal Control of the Formula 1 Hybrid Electric Power Unit

Mauro Rubén Ulisse Salazar Villalon

Institute for Dynamic Systems and Control  
ETH Zürich  
2018

Institute for Dynamic Systems and Control  
ETH Zürich  
Switzerland

© 2018 Mauro Rubén Ulisse Salazar Villalon. All rights reserved.

*A Loria*

*"Non si può descrivere la passione,  
la si può solo vivere."  
Enzo Ferrari*



# Abstract

Since 2014, Formula 1 racing cars have been equipped with a hybrid electric power unit composed of an electrically turbocharged internal combustion engine and an electric motor used for boosting and regenerative braking. The energy management system that controls this hybrid electric powertrain strongly influences the achievable lap time, as well as the consumption of fuel and battery energy.

In this thesis we study models and control strategies to achieve the best possible lap time. First, we identify a convex model of the power unit and use it to numerically assess the time-optimal control strategies. Second, we leverage the convex model to analytically derive a time-optimal control policy that can be implemented on the ECU in a feedforward fashion and in compliance with the sporting regulations. Third, we develop two feedback control algorithms to counteract disturbances and track the optimal strategies in a lap-time-optimal way: the first one in the form of a two-level optimality tracking MPC scheme, and the second one inspired by ECMS and consisting of PID controllers continuously adjusting the optimal control policy in real-time. We perform numerical tests using convex and high-fidelity simulation environments to validate the optimality and the robustness of the proposed control approaches under realistic disturbances.

# Riassunto

Dal 2014 le vetture da corsa di Formula 1 sono equipaggiate con un gruppo motopropulsore ibrido elettrico composto da un motore a combustione interna a turbocompressione elettrica e da un motore elettrico utilizzato per l'accelerazione e la frenata rigenerativa. Il sistema di gestione dell'energia che controlla questo gruppo motopropulsore influenza fortemente il tempo sul giro raggiungibile, nonché il consumo di carburante e batteria.

In questa tesi studiamo modelli e strategie di controllo per raggiungere il miglior tempo sul giro possibile. In primo luogo, identifichiamo un modello convesso del motopropulsore e lo utilizziamo per calcolare numericamente le traiettorie di controllo ottimali in termini di tempo sul giro. In secondo luogo, sfruttiamo il modello convesso per ricavare analiticamente una strategia di controllo in anello aperto che può essere implementata nella centralina in conformità al regolamento sportivo. In terzo luogo, sviluppiamo due algoritmi di controllo in retroazione per contrastare disturbi esterni ed inseguire le traiettorie ottimali: il primo sotto forma di uno schema di controllo a modello predittivo a due livelli per inseguimento ottimale ed il secondo ispirato a ECMS e costituito da controllori PID che regolano continuamente ed in tempo reale la strategia di controllo ottimale. Per validare l'ottimalità e la robustezza degli approcci di controllo proposti, svolgiamo investigazioni numeriche utilizzando ambienti di simulazione convessi e ad alta fedeltà in presenza di disturbi realistici.







# Acknowledgement

First, I would like to thank my supervisor, Chris Onder, for proposing this most fascinating research project to me and welcoming me to his lab. He has been a real *Doktorvater* to me. Under his guidance I could not only extend and deepen my scientific and academic background, but also understand the importance of human values such as ethic responsibility and integrity. His tireless patience and deep-rooted human qualities were of paramount importance to me. Sometimes I see him as a Zen master.

Second, I express my utmost gratitude to Lino Guzzella, not only for being my co-examiner, but for supporting and advising me throughout my studies at ETH Zürich. He was a real mentor to me. The true passion and energy he put into all his lecture courses are the reason why I decided to delve into this scientific career. I still remember him calling me *ungeduldig* in one of the classes of Control Systems I, eight years ago, and afterwards recognizing the importance of restless curiosity in research and education.

Third, I am very grateful to Marco Mazzotti for accepting to be my co-examiner. He has been a mentor and a point of reference throughout my studies at ETH, and I am really glad that he will be there at the end of the first part of my career at ETH.

Fourth, I would like to thank Theo Hofman for being my co-examiner and for warmly welcoming me at TU Eindhoven. I appreciated the possibility of discussing my PhD thesis with him and meeting with the Control Systems Technology group.

Fifth, my gratitude goes to Ferrari S.p.A. Gestione Sportiva for supporting and believing in this project, and to Carlo Bussi, for the invaluable and fruitful discussions, his challenges and his patience, also when he was *murato con trombette*, and for agreeing to be a co-examiner of this thesis. Moreover, thank you to Fernando Grando, for his support, his kindness and cheerful optimism, and to Alberto Cerofolini and Luca Arzilli, for the great work together in the last phase of my PhD.

Sixth, I would really like to thank all the students I had the honour and pleasure to supervise. Special thanks go to Pol Duhr for following part of my project with passion and dedication while I was at Stanford, and for joining our lab as an invaluable and very supportive team member. Moreover, I would like to thank Nicolas Lanzetti for being an amazing Bachelor, Master and ping pong student. Finally, I thank both of them for carefully revising this thesis.

A paragraph full of thanks goes to Camillo Balerna, my first Master student and now awesome colleague. From him I have learned a lot. First, how to – and how not to – supervise students. He made me realize how important it is to change perspective and accept people as they are. Second, his full commitment and tireless patience are qualities I personally find of utmost importance for the great results he could achieve during his

PhD studies. He is a brilliant and solar human being, whose behaviour sets an example for everyone. Third, he was a great companion on the working trips to Maranello and able to transform the burden of long driving hours and staying away from home to a real treat. Last, but not least, he has become a very dear friend to me and I wish him all the best for his PhD thesis, which I am sure will turn out great, also thanks to the inspiration gathered at Ristorante Montana. *Se lo puoi sognare, lo puoi fare.*

A big thank you goes to my great post-docs and co-authors Søren Ebbesen, for introducing me to the project, and to *Superflip* Elbert, for teaching me how to write scientific publications and for the amazing concerts together. I also thank Brigitte Rohrbach for carefully revising most of my publications, including this thesis. Special thanks to our administrative assistants Kerstin Fischer and Helen Hanimann, to Katharina Munz for the amazing Yoga lessons, and Annina Fattor for her warmth and for persuading me to join a meditation class: It has changed my life. I also thank my meditation teacher Sabina Ritzmann for letting me sit with her for so many hours. Finally, I would like to thank all my IDSC friends and colleagues, in particular Raffi Hedinger, Richi Hutter, Hansi Ritzmann, Stijn Van Dooren, Sevi Hänggi, Giordano Moretto, Thiva Albin, Tammo Zobel, Andi Ritter, Andrea Carron, Nico Robuschi, Ale Zanardi and Elena Arcari, for the great times together.

My warm thanks also go to Raffaello D'Andrea, Florian Dörfler and Melanie Zeilinger for their advice, and to Emilio Frazzoli for encouraging me to opt for an exchange semester at Stanford. I am very grateful to David Norris, Manfred Morari and Colin Jones for mentoring me and generously sharing with me their expert advice and their guidance during my ETH studies and PhD.

*Gratias ago Marco Pavoni* and to the Autonomous Systems Lab for welcoming me at Stanford University and allowing me to work on fascinating research topics in a very stimulating environment. I have learned a lot and I am looking forward to learning more! In particular, I would also like to thank Max Schiffer, Federico Rossi, Matt Tsao and Izzy Aguiar for the fruitful cooperation on the AMoD projects. Many thanks also to Chris Gerdes for welcoming me to his stimulating class on vehicle dynamics and sharing his expertise with me, and thanks to Tushar Goel for teaching me how to drive fast. I thank Denise Gigante for admitting me to her very challenging and inspirational seminar on the Illuminated Works of William Blake. I deeply enjoyed the possibility of being part of such high-level literary discussions. I would like to thank the Stanford Zen Society for welcoming me in their Sangha and sharing their practice with me, and my Zen teachers for their wisdom and guidance. Moreover, a big thank-you to Robert Cusick for shining his compassionate light on me and for allowing me to join his Compassion Cultivation Training. It has been an unforgettable experience. *Grazie* to Chrissie Dinca, Simone Fasciati, Ale Breschi, Silvia Mostoni, Andrea Stifani, Giuseppe Trainiti and Raffaele Manna for making me feel at home when I was homesick on the other side of the planet.

I wish to thank the ETH Foundation for supporting me throughout my Master studies and connecting me with very interesting people, in particular mí hermana Eva Avilla.

I am grateful to the Swiss Study Foundation for allowing me to participate in extremely fascinating seminars and for introducing me to a network of amazing people. Thanks a lot to my NMUN friends for their friendship and the fantastic reunions.

My gratitude extends to my Middleschool Maths teacher Margherita Tavarini: Thanks to her I fell in love with the fabulous world of Maths and Science at an early stage in my life! Many thanks also to my Highschool Maths teacher Gianandrea Bernasconi for imparting to me the importance of notation and precision in Science, and to my chemistry teacher Carlo Devittori for supervising with passion and dedication my first research project.

I owe my deepest gratitude to my dear friend Ilse New for guiding me through the amazing world of English literature and teaching me that *signs are small measurable things, but interpretations are illimitable*. I am very thankful to her for proofreading all of my publications, including this thesis, and for reviewing all of my poems and lyrics.

I am very thankful to the Topsy Road family for our musical journey together. Together we have crossed Bridges of Fire, sailed Another Sea and soared Beyond the Veil. In particular, I would like to thank Christian Zatta for his friendship. Writing and playing music with him has always been a great source of joy and inspiration. In the past years, as his talent was growing, driven by an inextinguishable passion, I have learned a lot from him. I hope he knows I consider him the younger brother I never had. I would like to thank my brother Jacopo Schürch for being such a great friend for the past two decades. He is one of the most caring persons I know and I am grateful that I could always count on his help and advice. Many special thanks go to Andrea Agazzi for being always there for me, wherever he happened to be, all around the world. I am deeply grateful for his relentless and unconditional support throughout these years and I hope he knows that I have always admired him for his academic curiosity and his deep humanity. I am happy and honoured to be a brother to him, as he is one to me.

I owe so much to my family, a safe haven where I have always felt welcome and loved. I am happy I could always count on so many caring persons with whom I share such a strong bond. Words cannot express how grateful I am to my parents for their love and support: to my father Antonio for his warm loving kindness and his deeply human advice, and to my mother Yvonne for being the most compassionate, caring and intelligent mentor one could ever dream of. It is thanks to them that I have come this far.

Last, I would like to thank Ursina, from the bottom of my heart. She is one of the strongest and most marvellous persons I have ever met in my entire life, and I feel extremely grateful to have her walking beside me, wherever I am, whatever it takes, no matter how far.

*Grazie.*



# Contents

<b>1. Introduction</b>	1
<b>2. Model Identification</b>	5
2.1 Longitudinal Dynamics and Powertrain Model	7
2.2 Energy Management Problem for One Race Lap	14
2.3 Simulation Environments	16
<b>3. Time-optimal Control Strategies: The Numerical Solution</b>	19
3.1 Optimal Control Problem in the Space Domain	20
3.2 Nonlinear Optimization Problem in the Space Domain	30
3.3 Numerical Results	31
<b>4. Time-optimal Control Policy: The Analytical Solution</b>	41
4.1 Optimal Control Problem in Time Domain	42
4.2 Optimal Control Policy	47
4.3 Numerical Results	51
<b>5. A Two-level MPC Scheme</b>	57
5.1 High-level MPC Optimization Problem	59
5.2 High-level MPC Implementation	62
5.3 Low-level Optimality Tracking Zone MPC	64
5.4 Numerical Results	66
<b>6. Equivalent Lap Time Minimization Strategies</b>	73
6.1 Controller Structure	74
6.2 Controller Design	75
6.3 Numerical Results	77
<b>7. Conclusion and Future Directions</b>	81
<b>A. Appendix</b>	83
A.1 Second-order Conic Constraints	83
A.2 Non-smooth Pontryagin's Minimum Principle	84
A.3 Derivation of the Optimal Control Policy	88
A.4 Linearized System	92
<b>References</b>	93

*Contents*

<b>Curriculum Vitae</b> . . . . .	101
-----------------------------------	-----



# Foreword

This thesis documents part of the research carried out by the author during his doctoral studies under the supervision of Professor Christopher H. Onder at the Institute for Dynamic Systems and Control at ETH Zürich between March 2015 and September 2018.

The research was conducted in cooperation with Ferrari S.p.A. For reasons of confidentiality, only the contents of the journal articles and conference proceedings that have been published during the doctoral studies will be presented.

The original publications can be found in [1]–[4]. For the sake of consistency, the publications [5]–[11] are not included, neither are the projects [12]–[14], carried out from January to July 2018 in the Autonomous Systems Lab at Stanford University.

This thesis consists of seven chapters: Chapter 1 provides an introduction to the work, the motivation, and a literature review on related work. Chapter 2 presents the problem tackled, namely the time-optimal energy management of the Formula 1 power unit and the identification of a continuous-time model of the system. Chapters 3 and 4 provide offline approaches to solve the optimal control problem and compute an implementable optimal control policy. Chapters 5 and 6 present two feedback control algorithms, whilst Chapter 7 discusses possible future work directions.

## *Contents*

# Introduction

Lap time is of crucial importance in Formula 1 (F1) racing. It is defined as the amount of time it takes a race car to finish one lap and it is strongly influenced not only by the driver, but also by the performance of the propulsion system of the race car. Since 2014, F1 racing cars have been equipped with a hybrid electric powertrain, as shown in the upper part of Fig. 1.1. The control and coordination of such an inherently complex system is of paramount importance to achieve the best possible lap time and maximize the chances to win a race.

Herein, a 1.6l turbocharged internal combustion engine (ICE) is combined with an electric energy recovery system consisting of a battery and two electric motor/generator units (MGU). The first one is labeled kinetic, with the technical acronym MGU-K. It is connected to the traction system, to be used for electric boosting and regenerative braking. The heat unit (MGU-H) acts on the turbocharger shaft, improving the engine operation during transients and recovering waste heat from the exhaust gas. As shown in the lower part of Fig. 1.1, the power unit control system of the F1 car depends on the

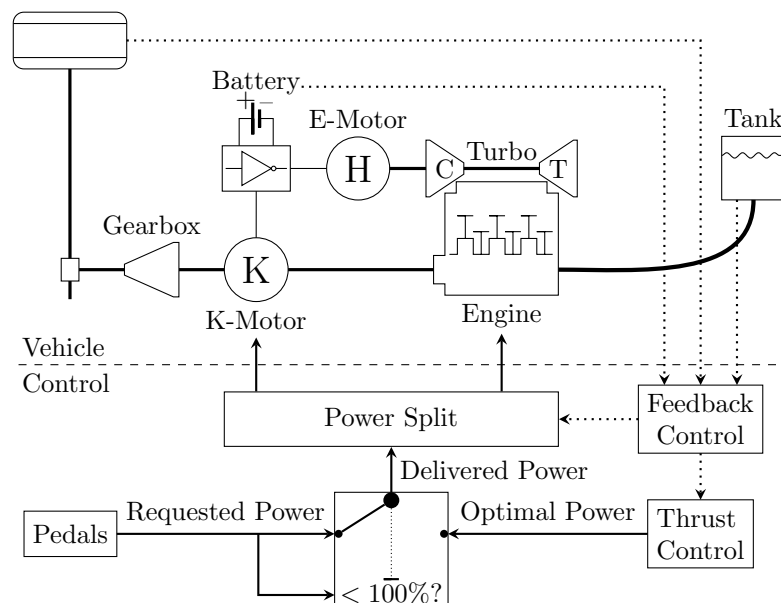


Figure 1.1: The F1 power unit with the energy management feedback control system.

pedal operation. If the driver is not requesting full power, the control system must deliver the amount of power requested by the driver, and the energy management system can only decide how to split it between the ICE and the MGU-K. Conversely, if the driver is requesting maximum power, the regulations allow the energy management system to decide the amount of propulsive power to provide and the split between the actuators. The degree of freedom offered by the thrust controller allows to trade off lap time against energy consumption and cope with the finite size of the battery and the fuel consumption limit of 105 kg per race [15]–[18].

We identify three main areas of research related to the minimum lap time energy management for hybrid electric race cars: First, the minimum fuel power split for hybrid electric vehicles; second, eco-driving strategies for hybrid electric vehicles; third, the minimum time vehicle maneuvering problem. The first two areas of research have emerged with the recent push to improve the fuel economy and reduce the carbon footprint of a wide range of vehicles by downsizing, turbocharging and electrifying their combustion engines. The complexity of these hybrid electric powertrains entails the need for elaborate high-level control algorithms coordinating the energy flows among the various components. Since these high-level control algorithms are crucial to achieve a good overall fuel efficiency, they need to be carefully designed and implemented. Researchers have used model-based techniques [19] as well as the theory of optimal control [20], [21] to derive fuel-optimal energy management strategies [22], to optimize the powertrain design in extensive parameter studies [23]–[25], to trade off drivability against fuel economy [26], [27], as well as to evaluate the potential efficiency improvement of compound turbocharging [28]–[33].

Specifically, the first area of research comprehends the minimum fuel control problem for hybrid electric passenger vehicles or heavy-duty trucks, whereby the propulsive power is decided by the driver and the vehicle speed is treated as an exogenous signal. Researchers have studied the optimal power split problem using non-causal approaches based on dynamic programming [34], [35], convex optimization [36]–[38] and Pontryagin’s minimum principle (PMP) [19], [22], [39], [40]. The implementation of real-time control algorithms relied on adapting the optimal solution obtained with PMP using equivalent consumption minimization strategies (ECMS) [41]–[45], model predictive control (MPC) algorithms [46], [47], or heuristic rule-based strategies [19], [48].

The second area of research has emerged more recently, with the introduction of adaptive cruise control systems and autonomous driving. Under the assumption that the power unit torque, and therefore the speed of the vehicle, can be controlled, eco-driving strategies were assessed for longitudinal dynamic models offline using dynamic programming [49], [50], nonlinear optimization [51], [52] and PMP [53], [54], whereby the implementation in real-time was mostly based on MPC [55], [56]. Nevertheless, such approaches aim at minimizing the fuel consumption and sometimes also pollutant emissions as well as battery wearing, but never solve minimum time control problems.

A third area of research optimizes the velocity profile simultaneously with the driving path of race cars and motorbikes in a two- or even three-dimensional framework [57]–[66],

occasionally including the energy recovery system [67]–[69], using nonlinear optimization techniques which result in long computational times and lack global optimality guarantees. Minimum time path following receding horizon controllers for autonomous vehicles are presented in [70]–[78].

The contribution of this thesis is fourfold. First, we assume that the driving path cannot be influenced by the energy management, but is rather determined by the driver’s steering input and is therefore fixed. By carefully introducing convex approximations and relaxations in the vehicle model, we formulate the time-optimal energy management problem as a convex optimal control problem that can be solved efficiently using dedicated numerical solvers. Of course, the approximations will introduce modeling errors to some extent. However, our validation against a detailed nonlinear third-party simulator demonstrates that the modeling errors introduced are acceptable. Therefore, the use of convex optimization enables the rapid evaluation of the optimal solution, while accuracy is maintained at a satisfactory level and, more importantly, the relative influence of changes in the control strategy is reproduced with precision. Furthermore, the global optimality of the solution found is guaranteed, which leads to a high level of robustness [1].

Second, we solve the optimal energy management problem analytically and propose a feedforward controller that is implementable in real-time. Using PMP, we derive the optimal control policy analytically [2], where the integral constraints are handled via non-smooth convex analysis. The control policy expresses the optimal power split and the optimal thrust as functions of the costate variable associated with the kinetic energy of the vehicle. The optimal value of the costate variable at each position along the racetrack can be evaluated using an offline optimization algorithm prior to a race, if necessary for a number of scenarios. Doing so, we provide an effective way to implement the globally optimal control strategies on the car in a feedforward fashion that can be easily tuned [5].

Third, to introduce feedback, we design a two-level MPC scheme which was shown to react in a lap-time-optimal way to realistic disturbances while delivering satisfying results over multiple laps [3]. However, such an approach holds the drawback that optimization algorithms must run on-board, which is not always possible for an ECU.

Fourth, as an alternative, we present a feedback control approach which achieves a performance that is equivalent to, if not better than the MPC algorithms presented, while requiring a negligible computational effort. Leveraging techniques inspired by ECMS, we propose equivalent lap time minimization strategies to adapt the optimal power split and thrust control strategies using PID controllers in order to react to disturbances and respect the consumption limits in a lap-time-optimal way [4].

The remainder of this thesis is structured as follows: We identify a longitudinal dynamic model of the F1 car in Chapter 2, where we also present the time-optimal energy management problem for one race lap and introduce the simulation environments used throughout the thesis to test the control approaches proposed. In Chapter 3, using convex optimization, we compute the optimal control strategies numerically, while we derive the optimal control policy analytically, leveraging a non-smooth version of PMP in Chapter 4. Thereafter, we present feedback control algorithms for the real-time energy management

of the F1 powertrain. Specifically, we introduce a two-level MPC scheme in Chapter 5 and equivalent lap time minimization strategies in Chapter 6. Chapter 7 concludes the thesis, summarizing the results and discussing possible future research directions.

# 2

## Model Identification

This section describes the F1 power unit in detail, presents the formulation of the time-optimal energy management problem for one race lap, and introduces the simulation environments used throughout the thesis. The model identification was presented in [1], whilst the problem formulation in the time domain and the simulation environments were introduced in [2].

Fig. 2.1 depicts a schematic representation of the F1 power unit. In addition to the turbocharged ICE, which converts the chemical energy stored in the fuel into mechanical propulsion energy, the power unit is equipped with two MGUs. The first one, labeled K, can either be used to recover kinetic energy during braking phases and recharge the battery in the energy storage (ES) system, or to supply additional boosting power to the wheels during acceleration phases. The second MGU, labeled H, is used both to recover excess heat from the ICE exhaust gas via the turbine of the turbocharger and to improve the engine's torque response during transients. The input variables are the fuel power  $P_f$ , i.e., the amount of fuel energy entering the ICE, the MGU-K mechanical power  $P_k$ , and the power extracted with the hydraulic brakes  $P_{brk}$ . The state variables are the kinetic energy of the vehicle  $E_{kin}$ , the fuel energy consumed  $E_f$ , and  $E_b$ , the battery state of energy. The racing regulations of the Fédération Internationale de l'Automobile (FIA) limit the amount of fuel to be used over the whole race and the battery size, as well as the amount of boosting and regenerative braking per lap [15]–[17]. To account for the latter

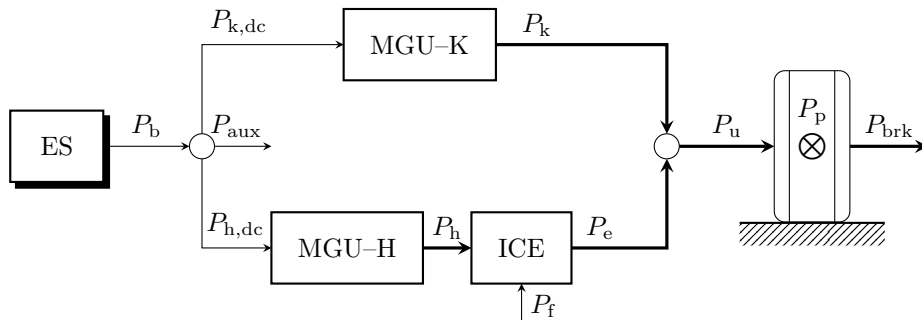


Figure 2.1: Schematic representation of the F1 power unit. Bold lines indicate mechanical connections; arrows denote positive energy flow directions. The blocks represent the ES, the MGU-K, the MGU-H and the ICE.

two energy budgets, two additional state variables must be introduced: the amount of electric energy transferred from the Energy Storage (ES) to the MGU-K, termed  $E_{\text{ES2K}}$ , and the amount of electric energy transferred in the opposite direction, i.e., from the MGU-K to the ES, termed  $E_{\text{K2ES}}$ . The remaining energy flows are the auxiliary power  $P_{\text{aux}}$ , the battery terminal power  $P_{\text{b}}$ , the MGU-K and H electrical power flows  $P_{\text{k,dc}}$  and  $P_{\text{h,dc}}$ , respectively, the MGU-H and the ICE mechanical power flows  $P_{\text{h}}$  and  $P_{\text{e}}$ , the powertrain power  $P_{\text{u}}$ , and the propulsive power  $P_{\text{p}}$ .

We condense the vehicle dynamics and the three-dimensional fixed driving path on the racetrack in the following track-dependent parameters: the maximum speed profile  $v_{\text{max}}(s)$ , the track curvature  $\gamma(s)$ , and the track inclination  $\theta(s)$ , where  $s$  is the longitudinal position of the car on the race track. The maximum speed profile combines the grip-limitations during cornering with the longitudinal acceleration constraints and can be computed using a higher-order non-convex tire model or be directly inferred from telemetry data.



## 2.1 Longitudinal Dynamics and Powertrain Model

The model of the F1 car presented in this subsection and shown in Fig. 2.1 is derived using [19] as the main reference. The car is represented as a point with mass  $m$  at the longitudinal position  $s$  moving with speed  $v$  and kinetic energy  $E_{\text{kin}} = \frac{1}{2} \cdot m \cdot v^2$ , and subject to the propulsive power  $P_p$  and the drag power  $P_d$  as

$$\frac{d}{dt}E_{\text{kin}}(t) = P_p(t) - P_d(t) . \quad (2.1)$$

The propulsive power  $P_p$  can be related to the power unit power  $P_u$  at the rear wheels by

$$P_p = C_s(P_u, v, \gamma, \dots) \cdot P_u - P_{\text{brk}} , \quad (2.2)$$

where  $C_s(P_u, v, \gamma, \dots)$  is a function describing the instantaneous percentage of wheel slip and  $P_{\text{brk}} \geq 0$  represents the power of the hydraulic brakes. The slip depends on a large number of variables, but it can be estimated by comparing measurements of the front and rear axle rotational speeds. Fig. 2.2 shows recorded measurement data of  $P_u$  and  $P_p$  during time intervals with  $P_{\text{brk}} = 0$  in an actual race. For reasons of confidentiality, we normalized the data whenever deemed necessary. To quantify the modeling error, we use the normalized mean error

$$\bar{e} = \frac{1}{y_0 \cdot N} \cdot \sum_{i=1}^N |y_{\text{model},i} - y_{\text{meas},i}| , \quad (2.3)$$

where  $y_{\text{model}}$  is the predicted value of the variable  $y$ ,  $y_{\text{meas}}$  the measured one and  $y_0$  a normalizing term. We use two datasets: the first one to identify the model parameters and the second one for validation purposes. The solid line shows a second-order polynomial fit of the form

$$C_s(P_u, v, \gamma, \dots) \cdot P_u \cong c_{s,1} \cdot P_u^2 + c_{s,2} \cdot P_u , \quad (2.4)$$

where the constant coefficients  $c_{s,1} \leq 0$  and  $c_{s,2}$  are subject to identification.

The drag power  $P_d$  is a sum of the aerodynamic drag  $P_a = (c_{d,0} + c_{d,1} \cdot \gamma) \cdot v^3$ , the rolling friction  $P_r = c_r \cdot m \cdot g \cdot \cos(\theta) \cdot v$  and the gravitational power  $P_g = m \cdot g \cdot \sin(\theta) \cdot v$ , where  $\gamma$  and  $\theta$  are the position-dependent path curvature and track inclination,  $g$  is the gravity, and  $c_{d,i}$  and  $c_r$  are the aerodynamic drag and rolling friction coefficients, respectively. The aerodynamic drag differs from the general formulation [19] by an additional term describing the effect of the path curvature  $\gamma$  and the open-wheel design of the F1 car on the air flow. The drag coefficients  $c_{d,0}$ ,  $c_{d,1}$  and  $c_r$  are identified by fitting the longitudinal vehicle dynamics to recorded measurement data of the velocity. The input to the model in this case is the corresponding propulsive power  $P_p$ . Fig. 2.3 shows the validation of the fit, indicating a good agreement between the vehicle and the model.

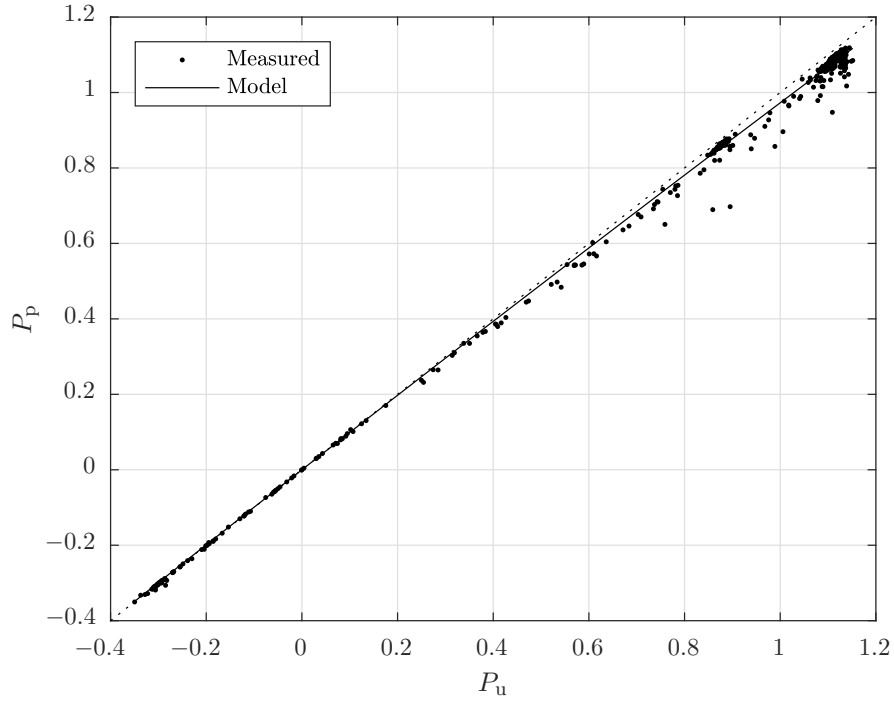


Figure 2.2: Quadratic wheel-slip model. The normalized mean error is 1.0%. The outliers are related to the neglected velocity-dependent slip and measurement noise.

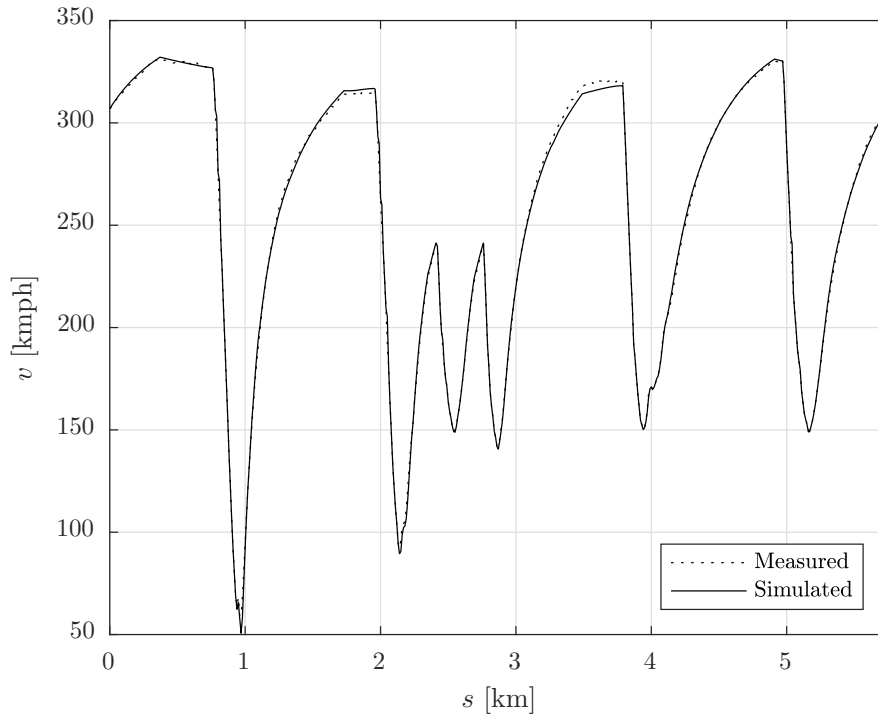


Figure 2.3: Measured and simulated vehicle speed profiles on the Monza circuit with a normalized mean error of 0.4%.

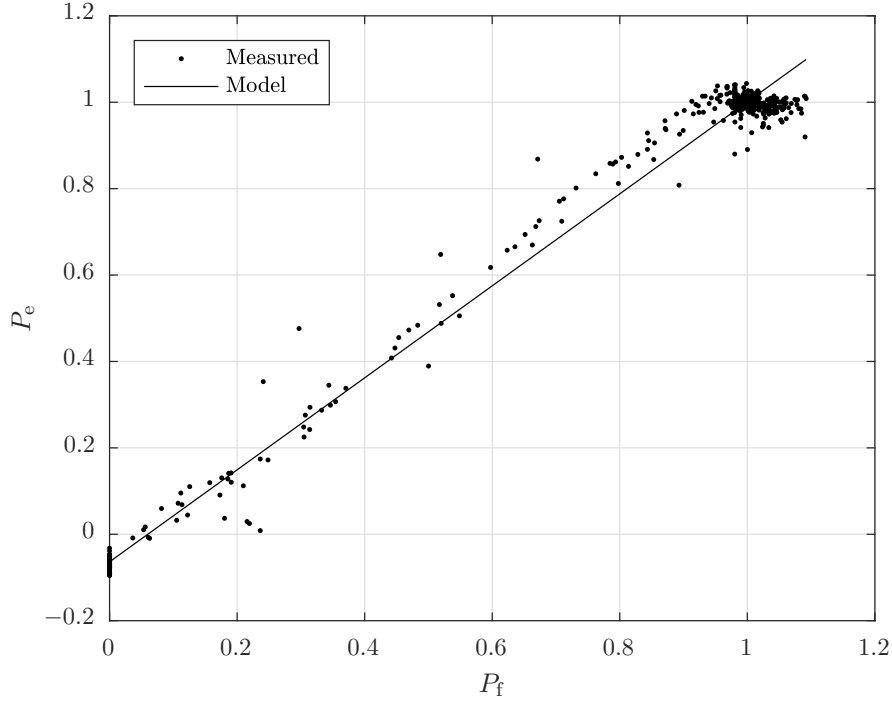


Figure 2.4: The indicated engine efficiency  $\eta_e$  (slope) and drag power  $P_{e,0}$  (offset) are identified by a linear regression. The normalized mean error is 2.7%, whereas the outliers reflect the neglected speed dependence of the parameters, the short transients, and the measurement noise.

The vehicle dynamics, the shape of the path on the track, and the acceleration constraints are condensed into a position-dependent maximum speed constraint, which can be expressed as a maximum kinetic energy constraint as

$$E_{\text{kin}}(t) \leq E_{\text{kin,max}}(s(t)) = \frac{m}{2} \cdot v_{\text{max}}(s(t))^2 . \quad (2.5)$$

The powertrain power  $P_u$  is the sum of the ICE power  $P_e$  and the mechanical power delivered by the MGU-K  $P_k$ . The engine is modeled using a *Willans* approximation where the mechanical power output  $P_e$  is approximated by an affine function of the fuel power as

$$P_e = \eta_e(\omega_e) \cdot P_f - P_{e,0}(\omega_e) , \quad (2.6)$$

given that  $\omega_e$  is the engine speed,  $\eta_e$  is the indicated efficiency and  $P_{e,0}$  is the engine drag power [79]. Fig. 2.4 shows recorded measurement data of mechanical engine power plotted over the fuel power. The data suggests that the engine operates primarily at maximum or minimum (motoring) power. A fit of (2.6) to the data indicates that the speed dependency of the indicated efficiency and the drag power may be neglected without significant loss of accuracy. Thus, removing the dependency on  $\omega_e$  from (2.6) we obtain

$$P_e = \eta_e \cdot P_f - P_{e,0} \quad . \quad (2.7)$$

The FIA regulations limit the maximum fuel flow to 100 kg/h [16]. This constraint, combined with the fact that the fuel flow cannot be negative, can be converted to power, using the lower heating value of gasoline  $H_{\text{lhv}}$  as

$$0 \leq P_f \leq P_{f,\text{max}} := \frac{100 \text{ kg/h}}{3600 \text{ s/h}} \cdot H_{\text{lhv}} \quad . \quad (2.8)$$

The MGU-K electrical power  $P_{k,\text{dc}}$  is limited to 120 kW for both motor and generator operating modes. This constraint can be expressed for the mechanical power as

$$P_{k,\text{min}} \leq P_k \leq P_{k,\text{max}} \quad . \quad (2.9)$$

The turbocharger is a fundamental part of the ICE: It consists of a radial compressor mechanically connected to a radial turbine via a shaft. The role of the first component is to force fresh air into the cylinders of the ICE by using the mechanical energy extracted from the exhaust gases by the turbine. The F1 ICEs are equipped with turbochargers, whereby the turbine retracts more energy from the exhaust gas flow than the amount necessary to operate the compressor in steady-state conditions. Therefore, it is possible to collect the remaining amount of energy by converting it into electrical energy with the MGU-H. Here we assume that the control strategy of the MGU-H is determined by the engine low-level controls and cannot be influenced by the energy management strategy. Assuming steady-state conditions, we can establish a relation between the MGU-H power and the fuel power as shown in Fig. 2.5. Our linear approximation

$$P_h = -\eta_h \cdot P_f \quad , \quad (2.10)$$

where  $\eta_h$  represents the thermal-to-mechanical conversion efficiency of the turbocharger, neglects all transient phenomena. Nevertheless, it still reaches an acceptable overall accuracy, since the drivers are usually switching between zero and full load, as shown in Fig. 2.5. Considering that the MGU-H power magnitude amounts to less than 10% of the total powertrain power, the effective error would be one magnitude lower than the indicated 22.7%, hence it would have a minor effect.

The electrical power of the MGUs  $P_{x,\text{dc}}$ , with  $x = k, h$ , is modeled as

$$P_{x,\text{dc}} = \alpha_x \cdot P_x^2 + P_x \quad , \quad (2.11)$$

where the coefficients  $\alpha_x$  describe the power losses and are subject to identification. Fig. 2.6 and 2.7 show the quadratic regression of the measurement data in which  $\alpha_k$  and  $\alpha_h$  of (2.11) were identified.

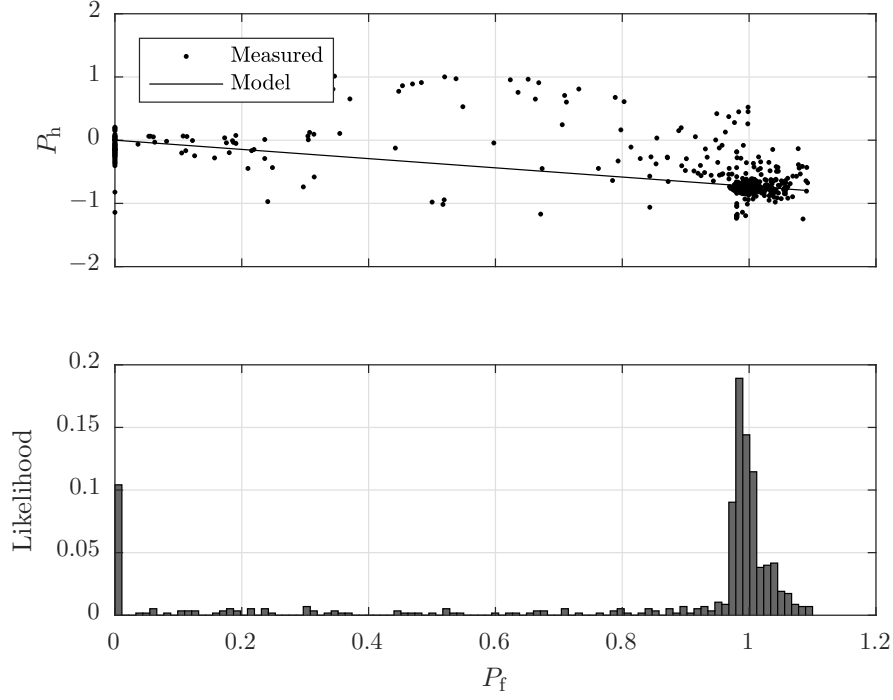


Figure 2.5: The mechanical MGU-H power is assumed to be linearly dependent on fuel power due to the likelihood of the operating points. The normalized mean error is 22.7%, whereas the outliers reflect the neglected short transients and measurement noise.

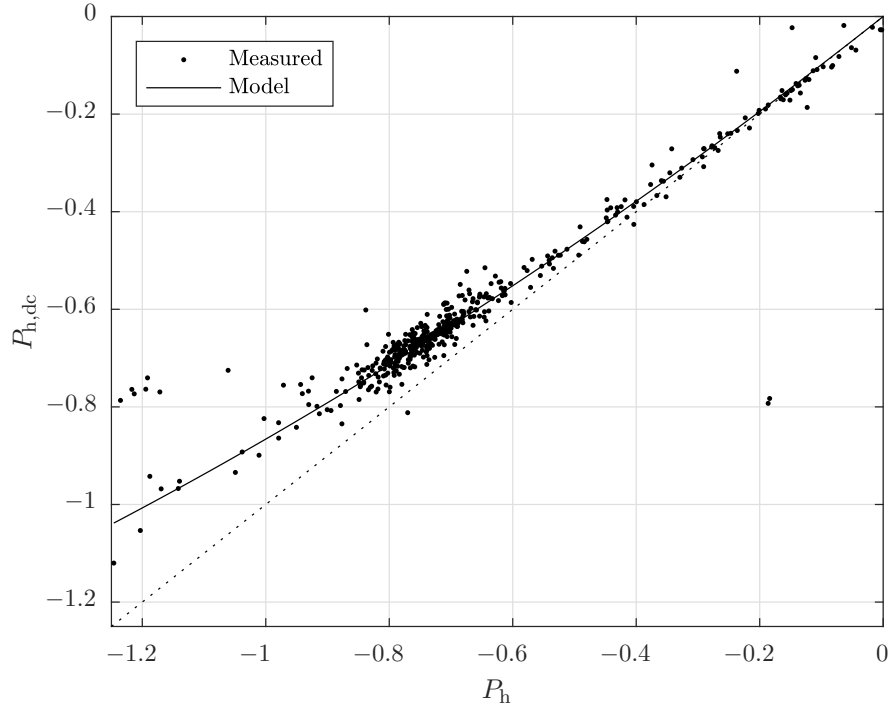


Figure 2.6: Quadratic MGU-H model. The normalized mean error is 2.3%, whereas the outliers reflect the neglected inertial effects and measurement noise.

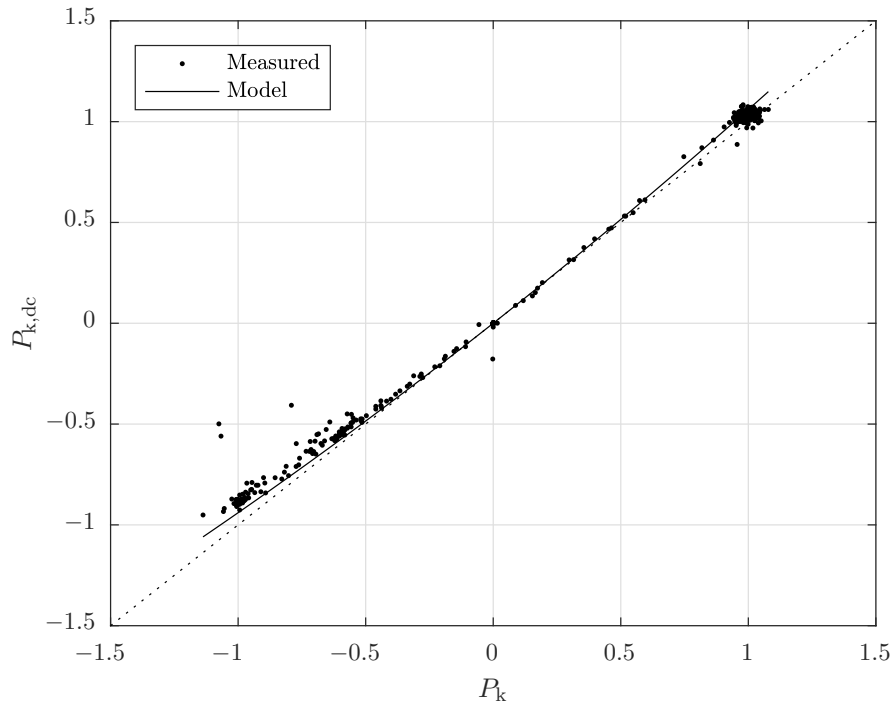


Figure 2.7: Quadratic MGU-K model. The normalized mean error is 2.4%, whereas the outliers reflect the neglected inertial effects and measurement noise.

The power extracted at the battery terminal  $P_b$  is a combination of the MGU-K and MGU-H electrical power and of a constant auxiliary power  $P_{aux} = 2 \text{ kW}$ :

$$P_b = P_{aux} + P_{k,dc} + P_{h,dc} . \quad (2.12)$$

The internal battery power  $P_i$ , which is responsible for the actual change in the state of energy of the battery  $E_b$ , is approximated by

$$P_i = \alpha_b \cdot P_b^2 + P_b . \quad (2.13)$$

Fig. 2.8 shows the quadratic fit to measured data. Most of the outliers stem from the dynamics of the battery that are not accounted for by the model.

The state variables of the powertrain are the fuel energy consumption  $E_f$  and the battery state of energy  $E_b$ , which are modeled as open integrators as

$$\begin{aligned} \frac{d}{dt} E_f(t) &= P_f(t) \\ \frac{d}{dt} E_b(t) &= -P_i(t) , \end{aligned} \quad (2.14)$$

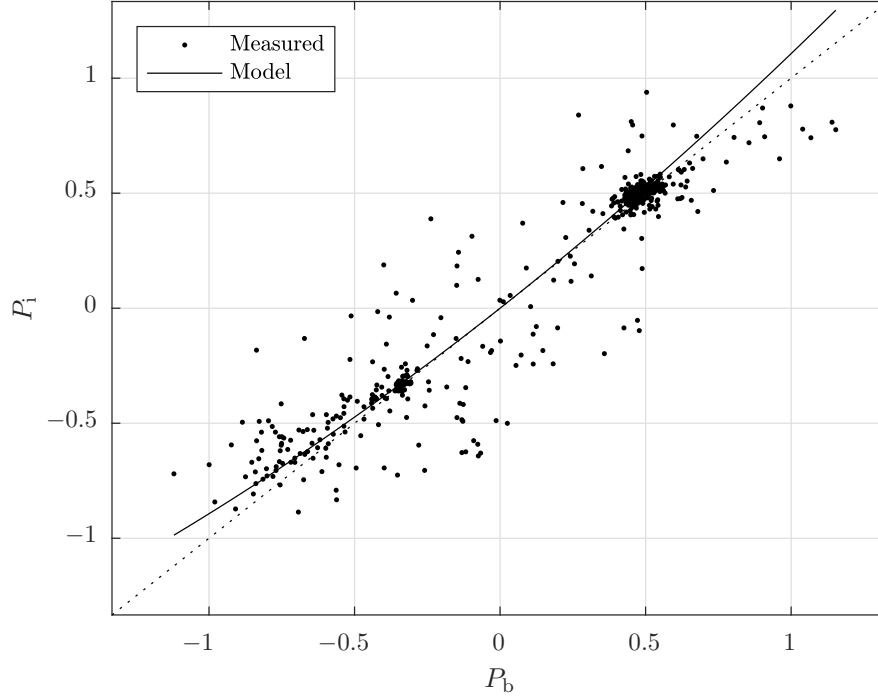


Figure 2.8: Quadratic battery model. The normalized mean error is 7.4%, whereas the outliers reflect the neglected open circuit voltage and measurement noise.

whereby the negative sign in the battery dynamics occurs because a positive battery internal power  $P_i$  would discharge the battery.

The FIA regulations state that over one lap the boosting energy directly transferred from the battery to the electric MGU-K may not exceed 4 MJ [16]. This boosting energy is labeled  $E_{\text{ES2K}}$  and its non-smooth dynamics are

$$\frac{d}{dt}E_{\text{ES2K}}(t) = \max \left\{ 0, P_{k,\text{dc}}(t) + \min \left\{ 0, P_{h,\text{dc}}(t) \right\} \right\} = \max \left\{ 0, P_{k,\text{dc}}(t) + P_{h,\text{dc}}(t) \right\}, \quad (2.15)$$

where the second equality is due to the fact that the MGU-H is considered a pure generator and, therefore,  $\min \{0, P_{h,\text{dc}}(t)\} = P_{h,\text{dc}}(t)$ . Moreover, the amount of regenerative braking energy directly transferred from the MGU-K to the battery is limited to  $-2$  MJ per lap [16]. This regenerative braking energy is labeled  $E_{\text{K2ES}}$  and its non-smooth dynamics are given by

$$\frac{d}{dt}E_{\text{K2ES}}(t) = \min \left\{ 0, P_{k,\text{dc}}(t) + \max \left\{ 0, P_{h,\text{dc}}(t) \right\} \right\} = \min \left\{ 0, P_{k,\text{dc}}(t) \right\}, \quad (2.16)$$

whereby, again, the negativity of  $P_{h,\text{dc}}(t)$  was used to simplify the equation.

## 2.2 Energy Management Problem for One Race Lap

In this section, the minimum lap time control problem is formulated for one race lap. The energy management problem for the F1 car consists of finding the optimal strategies that minimize the lap time  $T$ , i.e.,

$$\min \int_0^T dt \ , \quad (2.17)$$

subject to the dynamics presented in Section 2.1 above and the following constraints. The constraints on boosting and regenerative braking energy are given as

$$\begin{aligned} E_{\text{ES2K}}(T) &\leq 4 \text{ MJ} \\ E_{\text{K2ES}}(T) &\geq -2 \text{ MJ} \ . \end{aligned} \quad (2.18)$$

Over a whole race, the fuel consumption is limited to  $100 \text{ kg}^1$ . Depending on the number of laps  $N_{\text{tot}}$  a nominal fuel energy consumption for one lap  $\Delta E_{\text{f},0}$  can be computed as

$$\Delta E_{\text{f},0} = \frac{100 \text{ kg}}{N_{\text{tot}}} \cdot H_{\text{lhv}} \ , \quad (2.19)$$

such that on a nominal race lap we have

$$E_{\text{f}}(T) - E_{\text{f}}(0) = \Delta E_{\text{f},0} \ . \quad (2.20)$$

However, this variable is a strategy parameter and may be changed depending on the scenario, since there is no hard limitation on the fuel consumption per lap.

The battery state of energy must be contained in a window of 4 MJ throughout the race, i.e.,

$$E_{\text{b}}(t) \in [0, 4 \text{ MJ}] \quad \forall t \in [0, T] \ . \quad (2.21)$$

Under nominal conditions, we aim at keeping the battery balanced throughout a lap, i.e.,

$$E_{\text{b}}(T) - E_{\text{b}}(0) = \Delta E_{\text{b},0} = 0 \text{ MJ} \ . \quad (2.22)$$

Nevertheless, the change in the battery state of energy  $\Delta E_{\text{b},0}$  is a strategic parameter as well which can be changed depending on the stage of the race.

---

<sup>1</sup>In the 2017 and 2018 seasons such a limit was increased to 105 kg, due to the increase in drag arising from the introduction of wider tires and larger wings. However, without loss of generality, in this thesis we will always consider the vehicle specifications of the 2014-2016 seasons and, therefore, consider a maximum fuel consumption of 100 kg [16], [17].



## 2.2 Energy Management Problem for One Race Lap

Finally, for the time-domain formulation, we add the position on the racetrack  $s$  as an additional state variable, the dynamics of which are given by

$$\frac{d}{dt}s(t) = \sqrt{\frac{2 \cdot E_{\text{kin}}(t)}{m}} \quad (2.23)$$

and are subject to the initial and terminal conditions

$$\begin{aligned} s(0) &= 0 \\ s(T) &= S \quad , \end{aligned} \quad (2.24)$$

whereby  $S$  is the length of the circuit.

## 2.3 Simulation Environments

This section briefly discusses the simulation environments used in this thesis for testing and validation purposes. The first environment is based on the model derived in Section 2.1. As we will show in Chapter 3 below, for such a model we can compute the globally optimal solution and use it to benchmark the optimality of the controllers tested in this environment. The second environment is a third-party high-fidelity simulator for the F1 powertrain used to validate the performance of the controllers. Given the limited access to a F1 car, this environment will serve as a test-bench.

Without loss of generality, throughout this thesis we will consider the circuit of Barcelona, Spain, which is typically used for pre-season testing due to its challenging layout comprising a variety of low-, medium-, and high-speed corners. Fig. 2.9 depicts the track layout. Nevertheless, the results presented can be readily extended to all race-tracks without any additional burden.

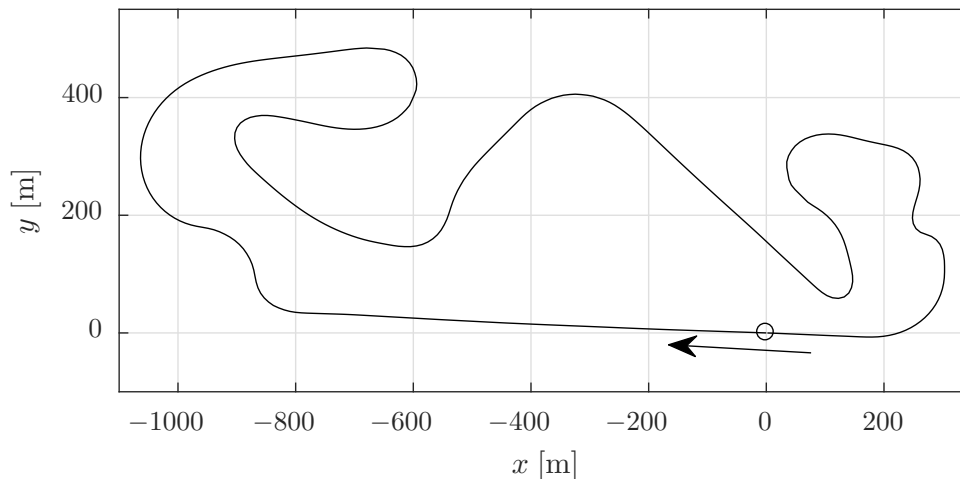


Figure 2.9: The Circuit of Barcelona. The circle and arrow indicate the start/finish line and the racing direction, respectively.

### Benchmark Simulator

In order to validate the control algorithms presented in this thesis, a benchmark simulator representing the simplified model derived in the subsections above is used as a virtual test-bench. The differential equations presented in Sections 2.1 are integrated in space domain using the Euler forward method. The advantage of such a model is that it can be used to compute the globally optimal minimum lap time strategies. Therefore, we can use it to compare the performance of causal controllers with the non-causal globally optimal solution and infer their degree of sub-optimality. The pedal operation is simulated assuming an optimal driver who would always request the thrust power  $P_{\text{req}}$  to maximize the vehicle speed, while not violating the maximum speed constraint. The FIA regulations allow the power delivered by the power unit  $P_u$  to be decided by the ECU only in a

```

 $\Delta s = \frac{S}{N}$ 
 $E_{\text{kin}}(0) = E_{\text{kin}}^{\text{start}}$ 
 $E_{\text{f}}(0) = \Delta E_{\text{b}}(0) = E_{\text{ES2K}}(0) = E_{\text{K2ES}}(0) = b_{\text{GL}}(0) = s(0) = 0$ 
for  $k=0:N$  do
     $v(k) = \sqrt{\frac{2 \cdot E_{\text{kin}}(k)}{m}}$ 
     $\Delta t(k) = \frac{\Delta s}{v(k)}$ 
    if  $b_{\text{GL}}(k) = 0$  then
         $P_{\text{u}}(k) = P_{\text{u}}^{\text{ECU}}(s(k), x(k))$ 
    else
         $P_{\text{u}}(k) = P_{\text{u,max}} = P_{\text{e,max}} + P_{\text{k,max}}$ 
    end
     $E_{\text{kin}}(k+1) = E_{\text{kin}}(k) + \left( P_{\text{p}}(P_{\text{u}}(k)) - P_{\text{d}}(E_{\text{kin}}(k), s(k)) \right) \cdot \Delta t(k)$ 
    if  $E_{\text{kin}}(k+1) > E_{\text{kin,max}}(k+1)$  then
         $E_{\text{kin}}(k+1) = E_{\text{kin,max}}(k+1)$ 
         $P_{\text{u}}(k) = \max \left\{ P_{\text{u,min}}, P_{\text{p}}^{-1} \left( \frac{E_{\text{kin}}(k+1) - E_{\text{kin}}(k)}{\Delta t(k)} + P_{\text{d}}(E_{\text{kin}}(k), s(k)) \right) \right\}$ 
         $b_{\text{GL}}(k+1) = 1$ 
    else
         $P_{\text{u}}(k) = P_{\text{u}}^{\text{ECU}}(s(k), x(k))$ 
         $b_{\text{GL}}(k+1) = 0$ 
    end
     $[P_{\text{e}}(k), P_{\text{k}}(k)] = \text{PS}^{\text{ECU}}(s(k), x(k), P_{\text{u}}(k))$ 
     $P_{\text{f}}(k) = (P_{\text{e}}(k) + P_{\text{e},0}) / \eta_{\text{e}}$ 
     $E_{\text{f}}(k+1) = E_{\text{f}}(k) + P_{\text{f}}(k) \cdot \Delta t(k)$ 
     $\Delta E_{\text{b}}(k+1) = \Delta E_{\text{b}}(k) - P_{\text{i}}(P_{\text{k}}(k), -\eta_{\text{h}} \cdot P_{\text{f}}(k)) \cdot \Delta t(k)$ 
     $E_{\text{ES2K}}(k+1) = E_{\text{ES2K}}(k) + \max \left\{ 0, P_{\text{k,dc}}(P_{\text{k}}(k)) + P_{\text{h,dc}}(-\eta_{\text{h}} \cdot P_{\text{f}}(k)) \right\} \cdot \Delta t(k)$ 
     $E_{\text{K2ES}}(k+1) = E_{\text{K2ES}}(k) + \min \left\{ 0, P_{\text{k,dc}}(P_{\text{k}}(k)) \right\} \cdot \Delta t(k)$ 
     $s(k+1) = s(k) + \Delta s$ 
end
 $T = \sum_{k=0}^N \Delta t(k)$ 

```

**Algorithm 1:** Benchmark simulator.

power-limited region, i.e., only when the driver is demanding maximum acceleration, using the thrust controller  $P_{\text{u}}^{\text{ECU}}(\cdot)$ . Otherwise, the car is in a grip-limited region in which the amount of thrust requested by the driver must be provided and thus the ECU can only decide on how to split the request between the thermal and the electrical power unit components with the power split controller  $\text{PS}^{\text{ECU}}(\cdot)$  [16], [17]. The binary variable  $b_{\text{GL}}$  is used to distinguish whether the car is in a grip- or power-limited region. Since the start/finish line is located in a straight, we initialize the car in a power-limited region, i.e.,  $b_{\text{GL}} = 0$ . Algorithm 1 describes the benchmark simulator environment, where  $x = (E_{\text{kin}}, E_{\text{f}}, \Delta E_{\text{b}}, E_{\text{ES2K}}, E_{\text{K2ES}})^{\top}$ .

### **High-fidelity Nonlinear Simulator**

We use a third-party nonlinear simulator as a high-fidelity test-bench to assess the performance of the controllers proposed in this thesis. This simulator was developed in Simulink, based on the results of [57].

# 3

## Time-optimal Control Strategies: The Numerical Solution

This chapter presents the numerical computation of the optimal control strategies for one race lap. First, we formulate the lap-time-optimal control problem in the space domain. This way, we derive a finite-horizon control problem where the position-dependent parameters introduced in Chapter 2 can be implemented in a linear fashion. Moreover, we relax the problem to a convex form, namely, a second-order conic program whose solution can be computed efficiently, using dedicated numerical solvers and is guaranteed to be globally optimal. A similar methodology was presented in [80], where the time-optimal actuation strategy for a six-degree-of-freedom industrial robot following a predefined path was evaluated, using convex optimization. Later, the idea was extended to vehicles in [81], [82] without, however, considering the optimization of the energy management strategy, as is necessary in the case of a hybrid electric race car. Second, we verify the global optimality of the solution numerically by solving a simplified version of the control problem, using dynamic programming (DP), whereby we assume an unbounded consumption of fuel and battery energy. Finally, we perform a parametric study on the impact of the fuel and battery allowances on the lap time achievable.

### 3.1 Optimal Control Problem in the Space Domain

This section presents the formulation of the time-optimal energy management problem as a second-order conic program. The simplifications and relaxations that are required to make the model convex will be described during the derivation, and their impact on the overall model quality will be discussed.

Since the track-dependent parameters are given as a function of the distance driven, we formulate the optimal control problem in the spatial domain. The equivalent time-domain formulation would result in a non-convex program due to the non-convex transformation from the spatial to the time domain via the velocity. Furthermore, the formulation in the space domain results in a fixed-horizon optimization problem. The independent variable is no longer the time  $t$ , but the position on track  $s$ .

The objective (2.17) of the time-optimal control problem is to minimize the lap time  $T$  as

$$\min \int_0^S \frac{dt}{ds}(s) ds , \quad (3.1)$$

where  $S$  is the length of the track and  $\frac{dt}{ds}(s)$  denotes the spatial derivative of time, which is often referred to as lethargy. It describes the *time-consumption* per unit distance driven and is defined as

$$\frac{dt}{ds}(s) = \frac{1}{v(s)} . \quad (3.2)$$

Note that  $\frac{dt}{ds}(s)$  itself is an optimization variable within the problem. While the objective (3.1) is linear, the constraint (3.2) is nonlinear. However, by rearranging and relaxing the equation we obtain

$$v(s) \cdot \frac{dt}{ds}(s) \geq 1 , \quad (3.3)$$

which is a geometric mean expression and can thus be formulated as a second-order conic constraint (see Appendix A.1), that is

$$\frac{dt}{ds}(s) \cdot v_0 + v(s) \cdot \frac{1}{v_0} \geq \left\| \begin{matrix} 2 \\ \frac{dt}{ds}(s) \cdot v_0 - v(s) \cdot \frac{1}{v_0} \end{matrix} \right\|_2 , \quad (3.4)$$

where  $v_0 = 1 \text{ m/s}$  is a normalization constant. Since on the basis of (3.1) it is optimal to minimize the lethargy  $\frac{dt}{ds}(s)$  when solving the convex problem, the solver will always converge to the optimal solution where (3.4) holds with equality. Furthermore, this condition may be verified a posteriori, as will be shown in the Section 3.3 Numerical Results. A more detailed analysis of this relaxation technique can be found in [83]. When the velocity is equal to zero, the lethargy is not defined and numerical issues may arise. Nevertheless,

such a scenario only occurs at the beginning of a race, in the pit lanes, or in the case of an accident. These special cases are not considered in the present work.

In the following subsections we convert the longitudinal and the powertrain dynamics from a time domain to a space domain formulation and relax them such that they can be expressed as convex constraints in the lap-time-optimization problem. The time-derivative of energy is power, while its spatial derivative is force. Therefore, we will transform the input and algebraic power variables  $P$  to their equivalent force variables  $F$  using the relation

$$F = \frac{P}{v} = P \cdot \frac{dt}{ds} . \quad (3.5)$$

The optimal power  $P^*$  can then be inferred in post-processing from the optimal force  $F^*$  as  $P^*(s) = F^*(s) \cdot v^*(s)$ .

### Longitudinal Vehicle Dynamics

In this subsection, we formulate the longitudinal vehicle dynamics presented in Section 2.1 in the space domain and express them in a convex way. First, we consider the vehicle as a point mass and apply Newton's second law

$$m \cdot v(s) \cdot \frac{d}{ds}v(s) = F_p(s) - F_d(s) , \quad (3.6)$$

where  $m$  is the mass of the vehicle, and  $F_p$  and  $F_d$  the propulsive and drag forces, respectively. The propulsive force and power are connected by the relation

$$F_p(s) = \frac{P_p(s)}{v(s)} . \quad (3.7)$$

The drag force  $F_d$  is the sum of the aerodynamic drag  $F_a$ , the gravitational force  $F_g$ , and the rolling resistance force  $F_r$ :

$$F_d(s) = F_a(s) + F_g(s) + F_r(s) . \quad (3.8)$$

In summary, the aerodynamic drag is approximated by

$$F_a(s) = (c_{d,0} + c_{d,1} \cdot \gamma(s)) \cdot v(s)^2 . \quad (3.9)$$

The gravitational force component is approximated by

$$F_g(s) = m \cdot g \cdot \sin(\theta(s)) , \quad (3.10)$$

and, finally, the rolling resistance force is approximated by

$$F_r(s) = c_r \cdot m \cdot g \cdot \cos(\theta(s)) \quad . \quad (3.11)$$

The longitudinal vehicle model presented thus far is not convex. First of all, the left-hand side of (3.6) is non-convex. However, by applying the chain rule to the left-hand side we show that it represents the change in kinetic energy, i.e.,

$$m \cdot v(s) \cdot \frac{d}{ds} v(s) = \frac{1}{2} \cdot m \cdot \frac{d}{ds} (v(s))^2 \quad . \quad (3.12)$$

Thus we reformulate the left-hand side by substituting the velocity for kinetic energy, that is

$$\frac{d}{ds} E_{\text{kin}}(s) = F_p(s) - F_d(s) \quad . \quad (3.13)$$

Similarly, the aerodynamic drag (3.9) which is contained in the right-hand side of (3.13) is quadratic in  $v$  and thus linear in the kinetic energy, that is

$$F_a(s) = (c_{d,0} + c_{d,1} \cdot \gamma(s)) \cdot \frac{2}{m} \cdot E_{\text{kin}}(s) \quad . \quad (3.14)$$

In order to establish a connection between the objective and the vehicle dynamics, we include the convex quadratic constraint

$$E_{\text{kin}}(s) \geq \frac{1}{2} \cdot m \cdot v(s)^2 \quad . \quad (3.15)$$

The relaxation of (3.15) does not change the optimal solution, which can be explained as follows: The left-hand side of equation (3.15) is fixed via the equality constraint (3.13) and therefore represents an upper bound for the velocity. Since the goal is to minimize lap time, any solver aiming to find the optimal solution converges to a solution that fulfills (3.15) with equality [83]. This condition will be verified in the Section 3.3 Numerical Results.

The final two issues to be resolved are (3.7), which is bilinear, and (2.2), which is quadratic. As we are not interested in the braking power, we use the knowledge that  $P_{\text{brk}}(s) \geq 0$  and combine (2.2) with (2.4) to obtain

$$P_p(s) \leq c_{s,1} \cdot P_u(s)^2 + c_{s,2} \cdot P_u(s), \quad c_{s,1} \leq 0 \quad . \quad (3.16)$$

Next, we express (3.16) in terms of forces

$$\frac{F_p(s)}{v(s)} \leq c_{s,1} \cdot F_u(s)^2 + c_{s,2} \cdot \frac{F_u(s)}{v(s)} \quad , \quad (3.17)$$



which we rearrange to

$$\frac{dt}{ds}(s) \cdot (c_{s,2} \cdot F_u(s) - F_p(s)) \geq -c_{s,1} \cdot F_u(s)^2 . \quad (3.18)$$

This constraint is a geometric mean expression and as such can be expressed as a second-order conic constraint

$$\frac{dt}{ds}(s) \cdot v_0 + (c_{s,2} \cdot F_u(s) - F_p(s)) \cdot \frac{1}{F_0} \geq \left\| \begin{array}{c} 2 \cdot \sqrt{-c_{s,1}} \cdot F_u(s) \cdot \sqrt{\frac{v_0}{F_0}} \\ \frac{dt}{ds}(s) \cdot v_0 - (c_{s,2} \cdot F_u(s) - F_p(s)) \cdot \frac{1}{F_0} \end{array} \right\|_2 , \quad (3.19)$$

where  $F_0 = 1 \text{ N}$  is a normalization constant. This conic constraint establishes a convex connection between the propulsive force  $F_p(s)$  and the power unit force  $F_u(s)$ , thereby bypassing (3.7). The case where (3.19) holds with inequality corresponds to the case where the hydraulic brakes are applied. In the energy-constrained case, i.e., if all the fuel available is required to minimize the lap time, the optimization criterion will make the solver converge to a solution where braking is minimized. In the energy-unconstrained case, i.e., if the minimum lap time is constrained by operational limits of the powertrain rather than by the availability of energy, the solver is allowed to waste some of the excess energy in the hydraulic brakes by choosing a solution where (3.19) holds with inequality. With respect to the optimization criterion chosen (3.1) accounting for lap time only, the solution found this way is optimal, despite the fact that another solution with the same lap time but with a reduced fuel consumption may exist. To handle this case, a small regularization term may be added in the optimization criterion, but it is omitted here since the focus of our contribution is not on the braking strategy.

Finally, the power of the power unit is split into the engine power  $P_e$  and the MGU-K power  $P_k$ , that is

$$P_u(s) = P_e(s) + P_k(s) , \quad (3.20)$$

which can be expressed in terms of the mechanical ICE and MGU-K forces  $F_e$  and  $F_k$  as

$$F_u(s) = F_e(s) + F_k(s) . \quad (3.21)$$

To account for grip limitations during cornering and longitudinal acceleration constraints, the upper bound on the kinetic energy (2.5) is imposed:

$$E_{\text{kin}}(s) \leq E_{\text{kin,max}}(s) . \quad (3.22)$$

Furthermore, for a standard race lap we assume the initial and final velocities to be equal, i.e.,

$$E_{\text{kin}}(S) = E_{\text{kin}}(0) . \quad (3.23)$$

### Internal Combustion Engine

Formulating the *Willans* approximation (2.7) in terms of forces, we obtain the ICE force  $F_e$  as

$$F_e(s) = \eta_e \cdot F_f(s) - P_{e,0} \cdot \frac{dt}{ds}(s) , \quad (3.24)$$

which is linear in the fuel force  $F_f(s)$  and  $\frac{dt}{ds}(s)$ . The notion of fuel *force* is, of course, a purely mathematical abstraction: It relates to the fuel energy consumption by

$$\frac{d}{ds} E_f(s) = F_f(s) . \quad (3.25)$$

The maximum fuel flow rate is enforced together with its positiveness by the linear inequality constraints

$$0 \leq F_f(s) \leq P_{f,\max} \cdot \frac{dt}{ds}(s) . \quad (3.26)$$

Setting  $E_f(0) = 0$ , the maximum fuel consumption allowance per lap is enforced in terms of fuel energy by

$$E_f(S) \leq E_{f,\max} , \quad (3.27)$$

where the maximum fuel energy consumption at the end of the lap is defined as  $E_{f,\max} = r_f \cdot \Delta E_{f,0}$ . The relative fuel load  $r_f$  is a strategy-dependent parameter which usually ranges between 95% and 105%.

### Turbocharger

The linear relation (2.10) can also be expressed in forces as

$$F_h(s) = -\eta_h \cdot F_f(s) . \quad (3.28)$$

### Electric Motors Generator Units (MGUs)

The quadratic losses in the electric motors MGU-K and MGU-H (2.11) are both expressed in terms of forces as

$$F_{x,dc}(s)/v(s) \geq \alpha_x \cdot F_x(s)^2 + F_x(s)/v(s), \quad \text{for } x = k, h . \quad (3.29)$$

We rewrite (3.29) as a geometric mean expression

$$\frac{dt}{ds}(s) \cdot (F_{x,dc}(s) - F_x(s)) \geq \alpha_x \cdot F_x(s)^2 \quad (3.30)$$

and then as a second-order conic constraint

$$\frac{dt}{ds}(s) \cdot v_0 + (F_{x,dc}(s) - F_x(s)) \cdot \frac{1}{F_0} \geq \left\| \begin{array}{c} 2 \cdot \sqrt{\alpha_x} \cdot F_x(s) \cdot \sqrt{\frac{v_0}{F_0}} \\ \frac{dt}{ds}(s) \cdot v_0 - (F_{x,dc}(s) - F_x(s)) \cdot \frac{1}{F_0} \end{array} \right\|_2 . \quad (3.31)$$

The case where (3.31) holds with inequality corresponds to the non-physical case where part of the electric energy disappears and vanishes. Similar as for (3.19), if all energy available is required to minimize lap time, the optimization criterion will make the solver converge to a solution where (3.31) holds with equality. The upper and lower bounds on the MGU-K power are taken into account by

$$P_{k,min} \cdot \frac{dt}{ds}(s) \leq F_k(s) \leq P_{k,max} \cdot \frac{dt}{ds}(s) . \quad (3.32)$$

### Energy Storage System

The DC power at the battery terminals (2.12) is expressed in terms of forces as

$$F_b(s) = F_{k,dc}(s) + F_{h,dc}(s) + P_{aux} \cdot \frac{dt}{ds}(s) . \quad (3.33)$$

Equation (2.13) can be expressed in terms of forces and in turn by means of a second-order conic constraint as follows:

$$\frac{dt}{ds}(s) \cdot v_0 + (F_i(s) - F_b(s)) \cdot \frac{1}{F_0} \geq \left\| \begin{array}{c} 2 \cdot \sqrt{\alpha_b} \cdot F_b(s) \cdot \sqrt{\frac{v_0}{F_0}} \\ \frac{dt}{ds}(s) \cdot v_0 - (F_i(s) - F_b(s)) \cdot \frac{1}{F_0} \end{array} \right\|_2 . \quad (3.34)$$

As for (3.19) and (3.31), the equality in (2.13) was relaxed to an inequality, which will hold with equality if all energy available is required to minimize the lap time. The dynamics of the battery state of energy  $E_b(s)$  are modeled through the change in the energy level  $\Delta E_b(s) = E_b(s) - E_b(0)$  as

$$\frac{d}{ds} \Delta E_b(s) = -F_i(s) . \quad (3.35)$$

We set a lower bound on the difference between the final and the initial state of charge as

$$\Delta E_b(S) \geq \Delta E_{b,min} , \quad (3.36)$$

where  $\Delta E_{b,min}$  can be chosen on a window of at the most  $\pm 4$  MJ around  $\Delta E_{b,0} = 0$  MJ, due to the finite size of the battery. Generally, an upper bound does not have to be defined since lap time is minimized by using as much energy per lap as possible.

### ES2K and K2ES Constraints

In this subsection, the dynamics of the limited energy budgets for the boosting and the regenerative braking energy  $E_{\text{ES2K}}$  and  $E_{\text{K2ES}}$ , respectively, are presented and expressed in a convex way. The regulations limit the boosting to a maximum value of 4 MJ per lap, and the regenerative braking energy to a minimum value of  $-2$  MJ per lap. The corresponding energy flows can be expressed as follows:

$$P_{\text{ES2K}}(s) = \max\{0, P_{\text{k,dc}}(s) + \min\{0, P_{\text{h,dc}}(s)\}\} \quad (3.37)$$

$$P_{\text{K2ES}}(s) = \min\{0, P_{\text{k,dc}}(s) + \max\{0, P_{\text{h,dc}}(s)\}\} . \quad (3.38)$$

Due to the assumption that the MGU-H is operated in generator mode only, the power  $P_{\text{h,dc}}(s)$  is always non-positive and therefore (3.37)–(3.38) can be reformulated as

$$P_{\text{ES2K}}(s) = \max\{0, P_{\text{k,dc}}(s) + P_{\text{h,dc}}(s)\} \quad (3.39)$$

$$P_{\text{K2ES}}(s) = \min\{0, P_{\text{k,dc}}(s)\} . \quad (3.40)$$

The constraint (3.39) can be relaxed to convex terms by

$$\begin{aligned} P_{\text{ES2K}}(s) &\geq P_{\text{k,dc}}(s) + P_{\text{h,dc}}(s) \\ P_{\text{ES2K}}(s) &\geq 0 , \end{aligned} \quad (3.41)$$

while the constraint (3.40) can be relaxed to

$$\begin{aligned} P_{\text{K2ES}}(s) &\leq P_{\text{k,dc}}(s) \\ P_{\text{K2ES}}(s) &\leq 0 . \end{aligned} \quad (3.42)$$

Once these power flows are transformed to forces, the changes in the corresponding cumulative values are

$$\frac{d}{ds} E_{\text{ES2K}}(s) \geq F_{\text{k,dc}}(s) + F_{\text{h,dc}}(s) \quad (3.43)$$

$$\begin{aligned} \frac{d}{ds} E_{\text{ES2K}}(s) &\geq 0 \\ \frac{d}{ds} E_{\text{K2ES}}(s) &\leq F_{\text{k,dc}}(s) \\ \frac{d}{ds} E_{\text{K2ES}}(s) &\leq 0 , \end{aligned} \quad (3.44)$$

with the upper and lower bounds

$$0 \leq E_{\text{ES2K}}(s) \leq 4 \text{ MJ} \quad (3.45)$$

$$0 \geq E_{\text{K2ES}}(s) \geq -2 \text{ MJ} , \quad (3.46)$$

and the initial conditions  $E_{\text{ES2K}}(0) = E_{\text{K2ES}}(0) = 0$ . The constraints (3.41)–(3.42) are relaxations of the original constraints (3.39)–(3.40). Nevertheless, due to their monotonicity and due to the bounds (3.45)–(3.46), the physical values of ES2K and K2ES, which can be obtained integrating (3.39) and (3.40), respectively, are bounded above and below by their relaxed versions defined in Equations (3.41)–(3.42). This way we can ensure that the terminal constraints (2.18) are respected.

### Convex Optimization Problem in the Space Domain

To summarize, the state variables of our problem are  $x = (E_{\text{kin}}, E_{\text{f}}, \Delta E_{\text{b}}, E_{\text{ES2K}}, E_{\text{K2ES}})^\top$ , whereas the input variables are  $u = (F_{\text{f}}, F_{\text{k}})^\top$ , which are the equivalent of power in the space domain. The time-optimal energy management problem is then

$$\min \int_0^S \frac{dt}{ds}(s) ds \quad (3.47)$$

subject to the dynamics

$$\begin{aligned} \frac{d}{ds} E_{\text{kin}}(s) &= F_{\text{p}}(s) - F_{\text{d}}(s) \\ \frac{d}{ds} E_{\text{f}}(s) &= F_{\text{f}}(s) \\ \frac{d}{ds} \Delta E_{\text{b}}(s) &= -F_{\text{i}}(s) \\ \frac{d}{ds} E_{\text{ES2K}}(s) &\geq 0 \\ \frac{d}{ds} E_{\text{ES2K}}(s) &\geq F_{\text{k,dc}}(s) + F_{\text{h,dc}}(s) \\ \frac{d}{ds} E_{\text{K2ES}}(s) &\leq 0 \\ \frac{d}{ds} E_{\text{K2ES}}(s) &\leq F_{\text{k,dc}}(s) , \end{aligned} \quad (3.48)$$

the state and input constraints

$$\begin{aligned}
 F_f(s) &\in [0, P_{f,\max}] \cdot \frac{dt}{ds}(s) \\
 F_k(s) &\in [P_{k,\min}, P_{k,\max}] \cdot \frac{dt}{ds}(s) \\
 E_{\text{kin}}(s) &\leq E_{\text{kin},\max}(s) \\
 E_{\text{kin}}(S) &= E_{\text{kin}}(0) \\
 E_f(0) = \Delta E_b(0) &= E_{\text{ES2K}}(0) = E_{\text{K2ES}}(0) = 0 \\
 E_f(S) &\leq E_{f,\max} \\
 \Delta E_b(S) &\geq \Delta E_{b,\min} \\
 E_{\text{ES2K}}(S) &\leq 4 \text{ MJ} \\
 E_{\text{K2ES}}(S) &\geq -2 \text{ MJ} ,
 \end{aligned} \tag{3.49}$$

and the physical constraints

$$\begin{aligned}
 \frac{dt}{ds}(s) \cdot v_0 + v(s) \cdot \frac{1}{v_0} &\geq \left\| \frac{2}{\frac{dt}{ds}(s) \cdot v_0 - v(s) \cdot \frac{1}{v_0}} \right\|_2 \\
 E_{\text{kin}}(s) &\geq \frac{1}{2} \cdot m \cdot v(s)^2 \\
 F_d(s) &= F_a(s) + F_g(s) + F_r(s) \\
 F_a(s) &= (c_{d,0} + c_{d,1} \cdot \gamma(s)) \cdot \frac{2}{m} \cdot E_{\text{kin}}(s) \\
 F_g(s) &= m \cdot g \cdot \sin(\theta(s)) \\
 F_r(s) &= c_r \cdot m \cdot g \cdot \cos(\theta(s)) \\
 \frac{dt}{ds}(s) \cdot v_0 + (c_{s,2} \cdot F_u(s) - F_p(s)) \cdot \frac{1}{F_0} &\geq \left\| \frac{2 \cdot \sqrt{-c_{s,1}} \cdot F_u(s) \cdot \sqrt{\frac{v_0}{F_0}}}{\frac{dt}{ds}(s) \cdot v_0 - (c_{s,2} \cdot F_u(s) - F_p(s)) \cdot \frac{1}{F_0}} \right\|_2 \\
 F_u(s) &= F_e(s) + F_k(s) \\
 F_e(s) &= \eta_e \cdot F_f(s) - P_{e,0} \cdot \frac{dt}{ds}(s) \\
 F_h(s) &= -\eta_h \cdot F_f(s) \\
 \frac{dt}{ds}(s) \cdot v_0 + (F_{k,dc}(s) - F_k(s)) \cdot \frac{1}{F_0} &\geq \left\| \frac{2 \cdot \sqrt{\alpha_k} \cdot F_k(s) \cdot \sqrt{\frac{v_0}{F_0}}}{\frac{dt}{ds}(s) \cdot v_0 - (F_{k,dc}(s) - F_k(s)) \cdot \frac{1}{F_0}} \right\|_2 \\
 \frac{dt}{ds}(s) \cdot v_0 + (F_{h,dc}(s) - F_h(s)) \cdot \frac{1}{F_0} &\geq \left\| \frac{2 \cdot \sqrt{\alpha_h} \cdot F_h(s) \cdot \sqrt{\frac{v_0}{F_0}}}{\frac{dt}{ds}(s) \cdot v_0 - (F_{h,dc}(s) - F_h(s)) \cdot \frac{1}{F_0}} \right\|_2 \\
 F_b(s) &= F_{k,dc}(s) + F_{h,dc}(s) + P_{\text{aux}} \cdot \frac{dt}{ds}(s) \\
 \frac{dt}{ds}(s) \cdot v_0 + (F_i(s) - F_b(s)) \cdot \frac{1}{F_0} &\geq \left\| \frac{2 \cdot \sqrt{\alpha_b} \cdot F_b(s) \cdot \sqrt{\frac{v_0}{F_0}}}{\frac{dt}{ds}(s) \cdot v_0 - (F_i(s) - F_b(s)) \cdot \frac{1}{F_0}} \right\|_2.
 \end{aligned} \tag{3.50}$$

### 3.2 Nonlinear Optimization Problem in the Space Domain

In order to verify the optimality of the solutions found, a comparable benchmark solution must be computed. The full problem has too many state and input variables to be solved with conventional DP techniques, while any solution found with a nonlinear programming algorithm is not guaranteed to be globally optimal. To circumvent this problem, a simplified version of the control problem is set up in order to evaluate an ideal lower bound for the lap time. The idealized version of the control problem corresponds to the case where unlimited battery and fuel energy is available, and both engine and motor are able to deliver full power anytime. This problem does not require any relaxation and can be solved by a nonlinear optimization algorithm, such as DP. The problem is to minimize (3.47) subject to the dynamics

$$\frac{d}{ds}E_{\text{kin}}(s) = F_p(s) - (F_a(s) + F_g(s) + F_r(s)) , \quad (3.51)$$

the state and input constraints

$$\begin{aligned} F_u(s) &\leq (\eta_e \cdot P_{f,\max} - P_{e,0} + P_{k,\max}) \cdot \sqrt{\frac{m}{2 \cdot E_{\text{kin}}(s)}} \\ E_{\text{kin}}(s) &\leq E_{\text{kin},\max}(s) \\ E_{\text{kin}}(S) &= E_{\text{kin}}(0) , \end{aligned} \quad (3.52)$$

and the physical constraints

$$\begin{aligned} F_a(s) &= (c_{d,0} + c_{d,1} \cdot \gamma(s)) \cdot \frac{2}{m} \cdot E_{\text{kin}}(s) \\ F_g(s) &= m \cdot g \cdot \sin(\theta(s)) \\ F_r(s) &= c_r \cdot m \cdot g \cdot \cos(\theta(s)) \\ F_p(s) &= c_{s,1} \cdot F_u(s)^2 \cdot \sqrt{\frac{2 \cdot E_{\text{kin}}(s)}{m}} + c_{s,2} \cdot F_u(s) . \end{aligned} \quad (3.53)$$



### 3.3 Numerical Results

In this section, the solution of the convex optimization problem constructed in Section 3.1 is presented. First, the discretization step is chosen as a trade-off between computational time and accuracy, and a benchmark solution is computed for the unlimited-consumption problem. Thereafter, the results for specific boundary conditions are shown and then compared to those obtained by inserting the optimal input trajectories into a third-party nonlinear simulator. This part is followed by a parameter study designed to understand how varying terminal constraints on battery charge and fuel consumption may affect the optimal solution.

#### Numerical Solution Method

The convex control problem was discretized using the standard Euler method of the general form

$$x_{k+1} = x_k + \Delta s \cdot f(x_k, u_k) , \quad (3.54)$$

where  $k = \{0, 1, \dots, N-1, N\}$ . The number of discrete steps is  $N = S/\Delta s$  where  $S$  is the length of the circuit. The problem was constructed with the linear matrix inequality parser YALMIP [84], whereby all variables were normalized in terms of units and magnitude (to avoid ill-conditioning of the problem) and solved using the dedicated second-order conic programs solver ECOS [85]. The length of the discretization step was chosen to be  $\Delta s = 10$  m, which strikes a reasonable balance between problem size and accuracy of the solution, as shown in Fig. 3.1. The loss of accuracy when choosing  $\Delta s = 10$  m compared to  $\Delta s = 2$  m is comparably small (0.1 s), while the rise in evaluation time is very large ( $> 300\%$ ). For the finest discretization ( $\Delta s = 2$  m), the lap time is slightly longer than for the coarser discretization, due to the step-size-dependent precision of the Euler forward integration method.

#### Nonlinear Benchmark Solution

Using dynamic programming and the convex approach presented, a benchmark solution was computed for the unlimited-consumption problem introduced in Section 3.2. The solutions shown in Fig. 3.2 coincide up to numerical errors, as well as the achieved lap times of 87.4895 s (DP) and 87.4894 s (Convex), which represent an operational lower bound for the energy management problem.

#### Solution with Fixed Terminal Conditions

First, the optimal state and input trajectories along one lap are analyzed in detail for specific boundary conditions on fuel and battery consumptions. Fig. 3.3-3.5 show the solution to a problem with a nominal fuel load of  $r_f = 100\%$  and a lower bound on the state of energy variation  $\Delta E_{b,\min} = 2$  MJ, which means that throughout the course of the lap the battery must be charged by 2 MJ. These results were obtained in less than one second on a 2.6 GHz processor. The corresponding lap time is 87.967 s. Fig. 3.3 shows the

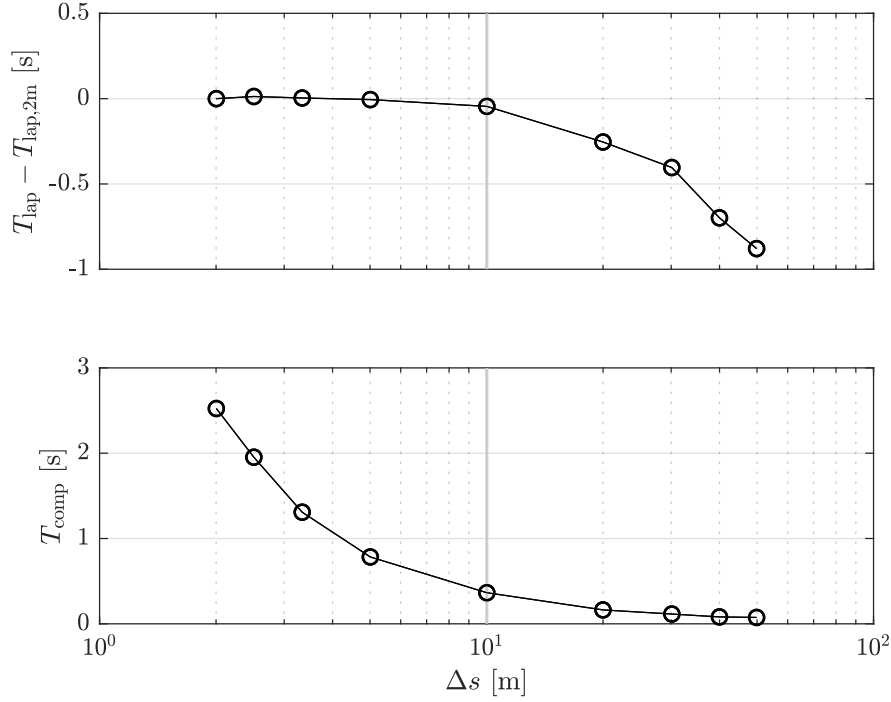


Figure 3.1: Lap time deviation and computation time for spatial discretizations from 2 m to 50 m on semi-logarithmic plots.

optimal velocity profile including the maximum speed attainable. Two types of operating regions are revealed, namely power-limited regions, where the maximum kinetic energy constraint is inactive and the speed limitations arise from the available amount of energy, and grip-limited curves, where the vehicle moves at maximum speed. Fig. 3.4 shows the resulting optimal power trajectories. These profiles suggest a bang-bang solution. The ICE is always in full-throttle in the power-limited regions. The MGU-K is operated at maximum power in the first part of the straights, where the lethargy can be reduced most effectively and then turned off, since in this scenario the battery must be charged by 2 MJ. Fig. 3.5 shows that the constraints on the maximum fuel load and on the minimum battery state of charge constraints are active, as well as the lower bound of  $-2$  MJ on the K2ES energy, whereas the maximal 4 MJ of ES2K are not reached by far. Such a finding suggests that in race scenarios the control of this energy variable can be neglected. The change in the battery state of energy of 2 MJ results from the difference between the regenerative braking energy K2ES and the boosting energy ES2K, combined with the MGU-H waste heat recovery. In Section 3.1 above, the constraints relating kinetic energy to speed and speed to time were relaxed, assuming that they would always be active. The validity of these assumptions can be verified in Fig. 3.6. These relaxation tests, where the left-hand side of each relaxed equality is compared to its right-hand side, can be performed in the post-processing phase to check whether the relaxed constraints actually hold with equality.

Table 3.1: Differences in lap time and terminal conditions for different battery consumptions.

$\Delta E_{b,\min}$	$\Delta T_{\text{lap}}$	Fuel	Battery
1 MJ	670 ms	-3.3%	-12.8%
0 MJ	667 ms	-3.4%	-9.9%
-1 MJ	591 ms	-4.5%	-17.7%

### Comparison with a High-fidelity Nonlinear Simulator

In this section, the optimal state and control input trajectories computed with the approximated model derived in Sections 2.1 and 3.1 and presented in Section 3.3 are compared to the results obtained by operating the third-party high-fidelity nonlinear simulator presented in Section 2.3 in accordance with the optimal solutions. The resulting state trajectories obtained are compared to the optimal trajectories depicted in Fig. 3.7. The main differences consist of a slightly larger lap time and a cumulative drift in the battery state of charge of 13%, whereas the fuel consumption, ES2K and K2ES show cumulative deviations of less than 4%.

Table 3.1 summarizes the errors in lap time, fuel consumption and battery charge for a set of battery terminal conditions. The values indicate the presence of a constant drift in lap time, fuel consumption and battery state of charge. Nevertheless, the relative

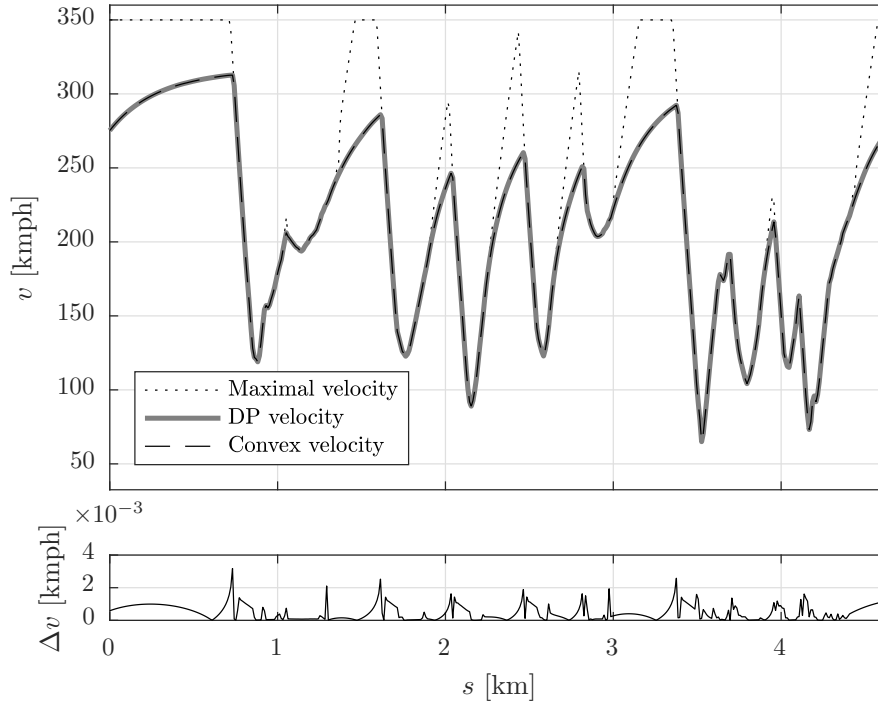


Figure 3.2: Optimal and maximal velocity profiles.

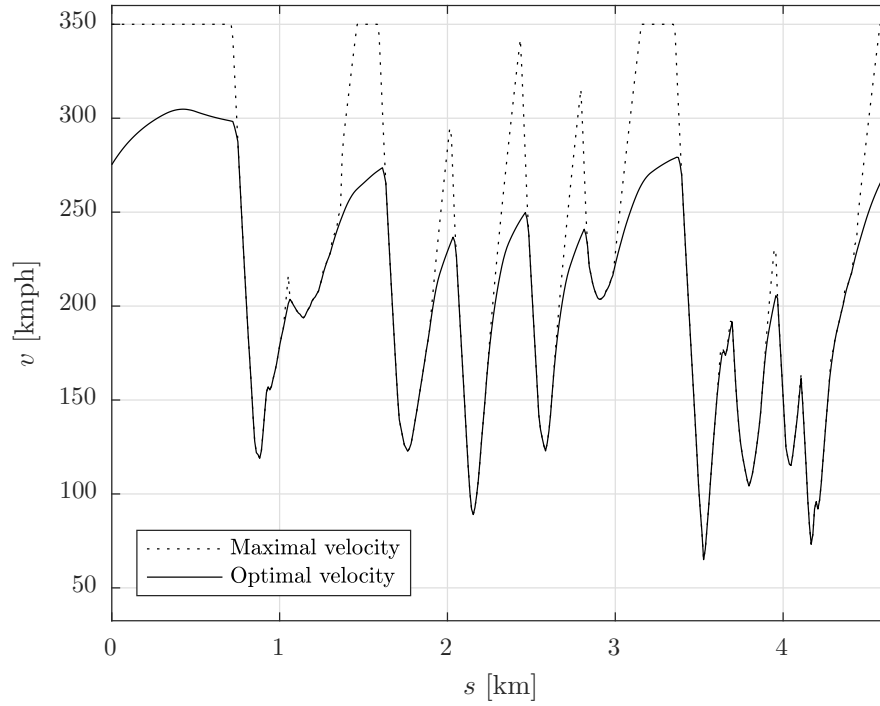


Figure 3.3: The optimal and the maximal velocity profile along the racetrack.

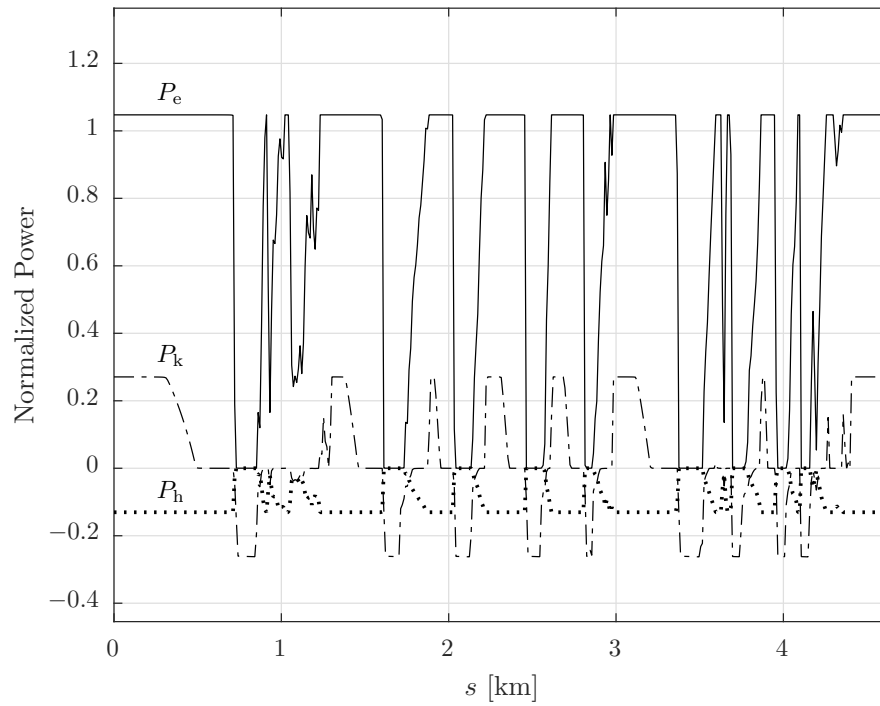


Figure 3.4: The optimal ICE, MGU-K and MGU-H power trajectories.

changes of the quantities, such as the dependency of lap time on the battery terminal condition are reproduced with high accuracy. Since the focus of this study is not on the

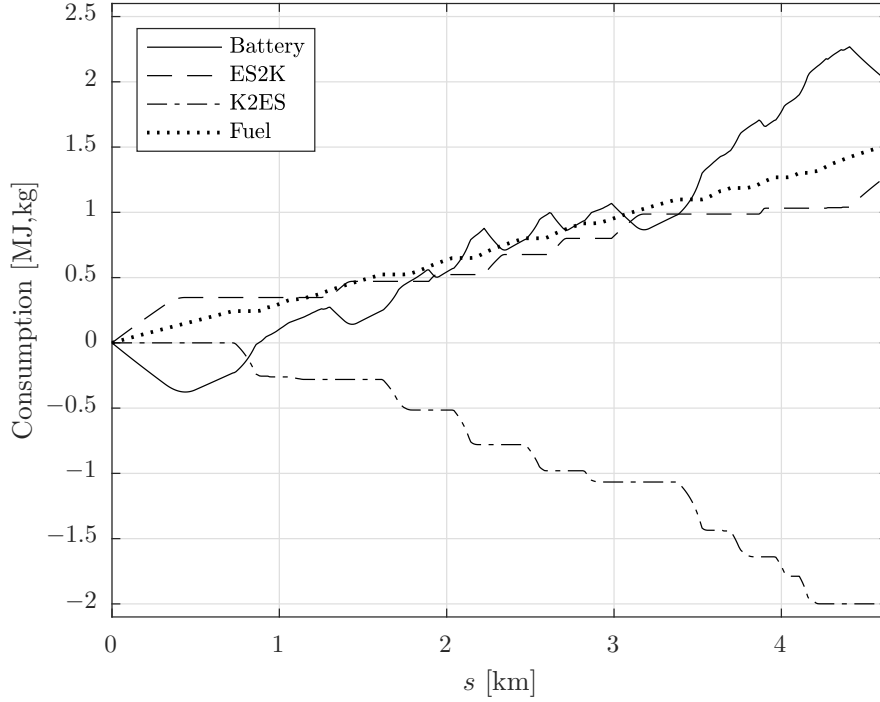


Figure 3.5: The optimal trajectories of the state variables.

absolute lap time, but rather on lap time variations with respect to changing boundary conditions, the simulation errors are acceptable.

### The Effect of Varying Terminal Conditions

The effectiveness of the proposed optimization methodology allows parameter studies to be carried out on several variables and yields new insights on their impact on lap time and optimal strategy. The boundary conditions on fuel load and battery discharge are varied between 95% and 105%, and between  $-4$  MJ and  $4$  MJ, respectively, to form a grid of 357 points for which the minimum lap time solutions are computed. The entire computation took about 6 minutes. As shown in Fig. 3.8, the plateau indicates that from a certain energy consumption allowance on upwards, no further reduction in lap time can be achieved. In fact, the lowest value attained corresponds to the operational lower bound from the nonlinear benchmark solution computed in Section 3.3, and therefore proves the optimality of the solution of the full convex problem.

Keeping the fuel load fixed at  $r_f = 100\%$  and varying the boundary conditions on  $\Delta E_{b,\min}$ , the major impacts are observed when the battery is charged, i.e., between  $0$  and  $4$  MJ. As Fig. 3.9 shows, the MGU-K cut-off occurs earlier in the straights as  $\Delta E_{b,\min}$  is increased. This leads to a lap time increase of up to more than  $1.5$  s, as Fig. 3.10 shows. On the other hand, below approximately  $0$  MJ no further lap time improvements are found for this particular track. This fact is depicted in Fig. 3.9, which shows that below  $0$  MJ the MGU-K behaviour does not change, as it remains at maximum power throughout all straights, where the vehicle has no lateral grip limitations. Thus, the speed profile

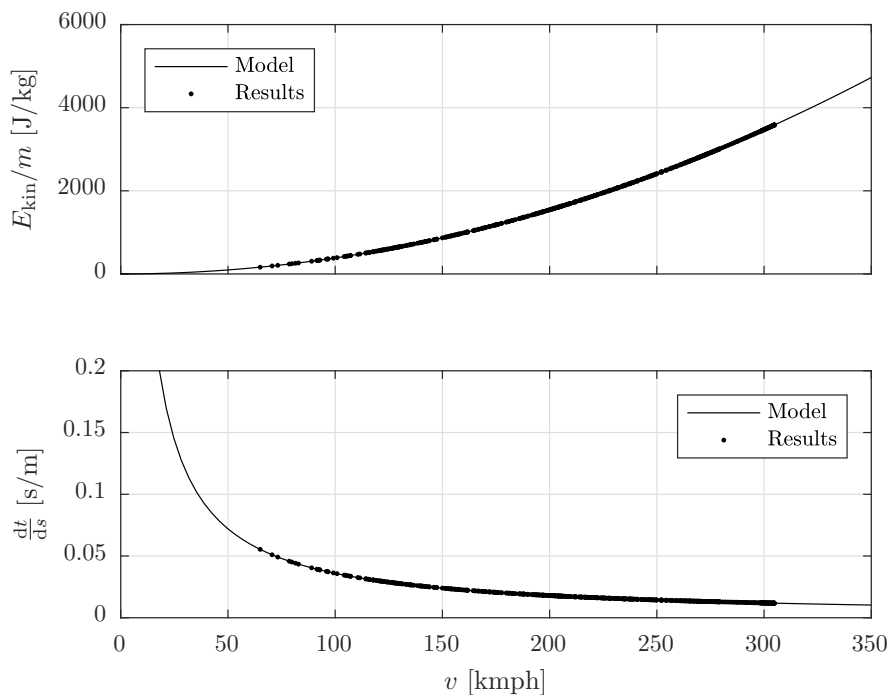


Figure 3.6: The conic constraints of the kinetic energy and of the speed are always active.

and, consequently, the lap time are not affected. Therefore, the optimal strategy is to keep a charge-sustained operation over several laps, since, in terms of lap time, energy recuperation appears to be more expensive than energy depletion.

If the fuel load is increased under charge-sustained battery operation, the maximum ICE power regions slightly enlarge, as depicted in Fig. 3.11, where otherwise hardly any differences can be noticed. Fig. 3.12 shows that changes in lap time are one order of magnitude smaller than those shown in Fig. 3.10. This is due to the fact that the nominal fuel load chosen by the FIA is such that the ICE can be operated at full-throttle in the power-limited regions<sup>1</sup> and that the variation on engine operation in the fuel load range shown in Fig. 3.11 is also one order of magnitude lower when compared with the MGU-K actuation for the various battery charge levels shown in Fig. 3.9. Of course, a larger sensitivity would be observed at even lower fuel loads. However, such a scenario is not representative for a race or qualifying lap and therefore not of interest. Once engine back-off is no longer employed, i.e.,  $r_f = 100\%$ , there is little reduction in lap time, which is primarily due to thermal recharge in part-load operation. If several laps are to be analyzed, it is optimal to keep a nominal fuel allowance. Any gains in lap time arising from a higher fuel consumption could not be compensated by laps where this excess fuel would be saved. This fact is mainly due to the presence of conversion efficiency and the quadratic relation between aerodynamic drag and vehicle speed.

<sup>1</sup> which is why such a limit was increased for the 2017 and 2018 seasons, as the aerodynamic drag and rolling friction were increased by the adoption of wider wings and broader tires.

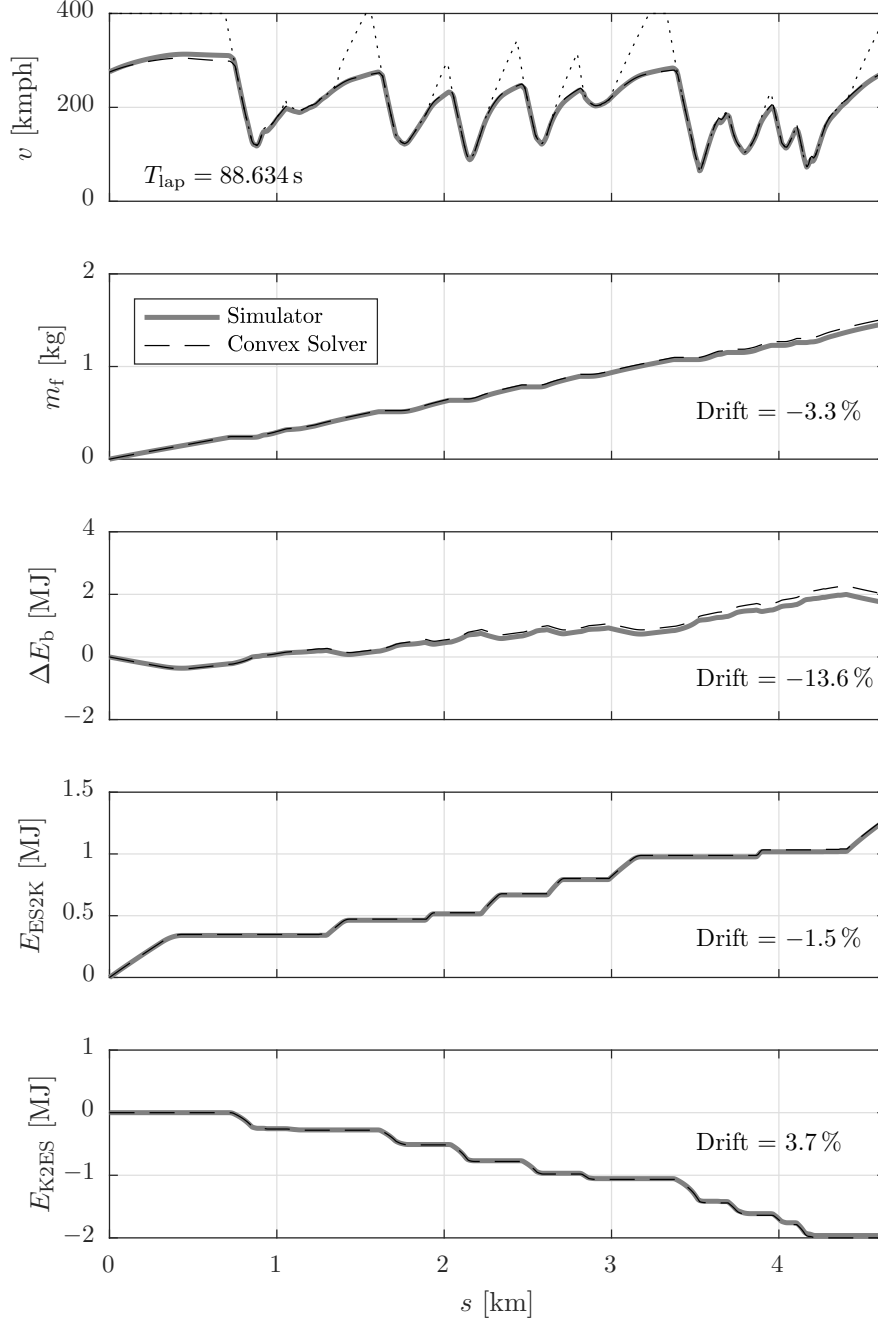


Figure 3.7: Speed and energy profiles from the high-fidelity nonlinear simulator and from the convex solver.

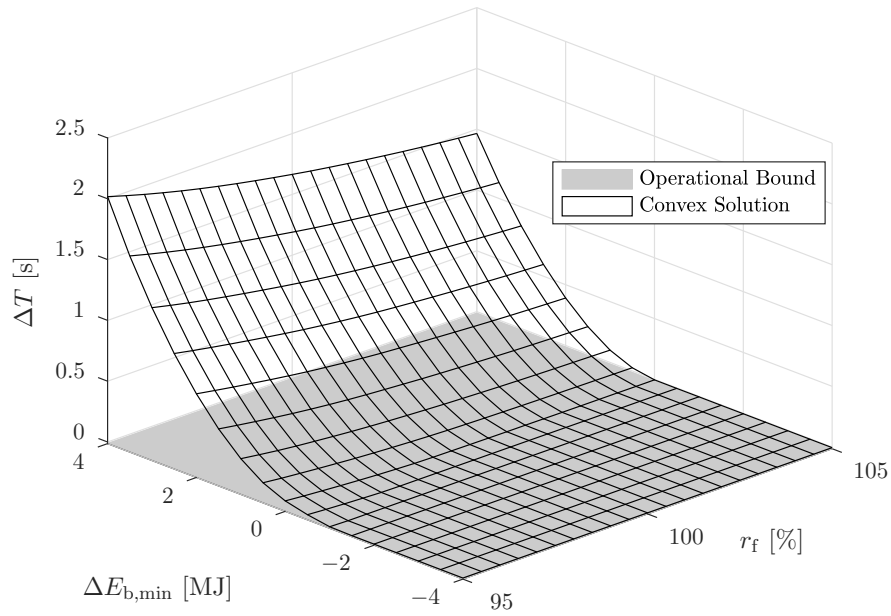


Figure 3.8: Minimum lap time variation as a function of fuel load and battery discharge, and the nonlinear benchmark solution, which represents an operational lower bound on the achievable lap time.

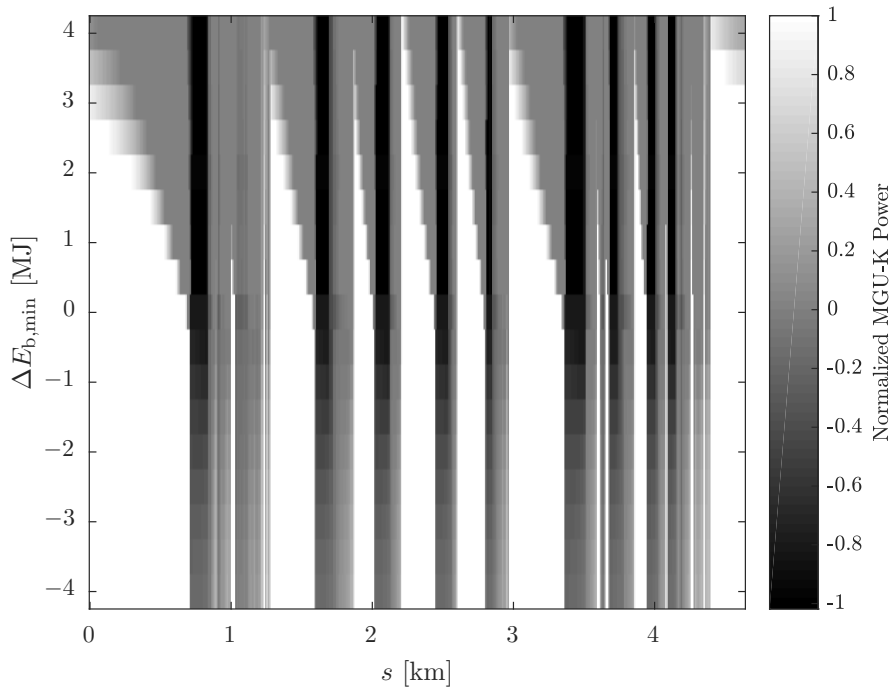
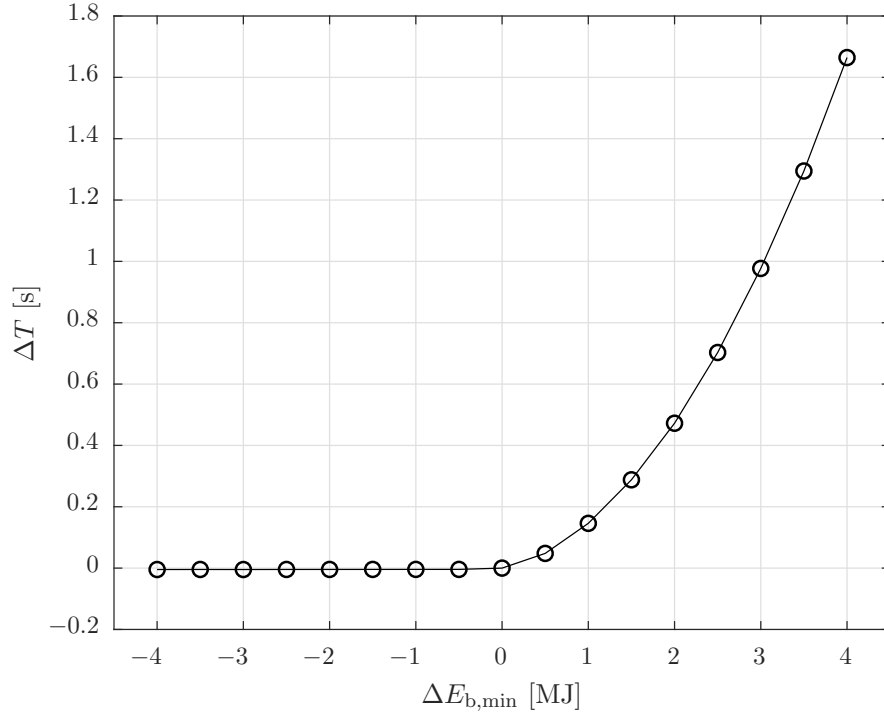
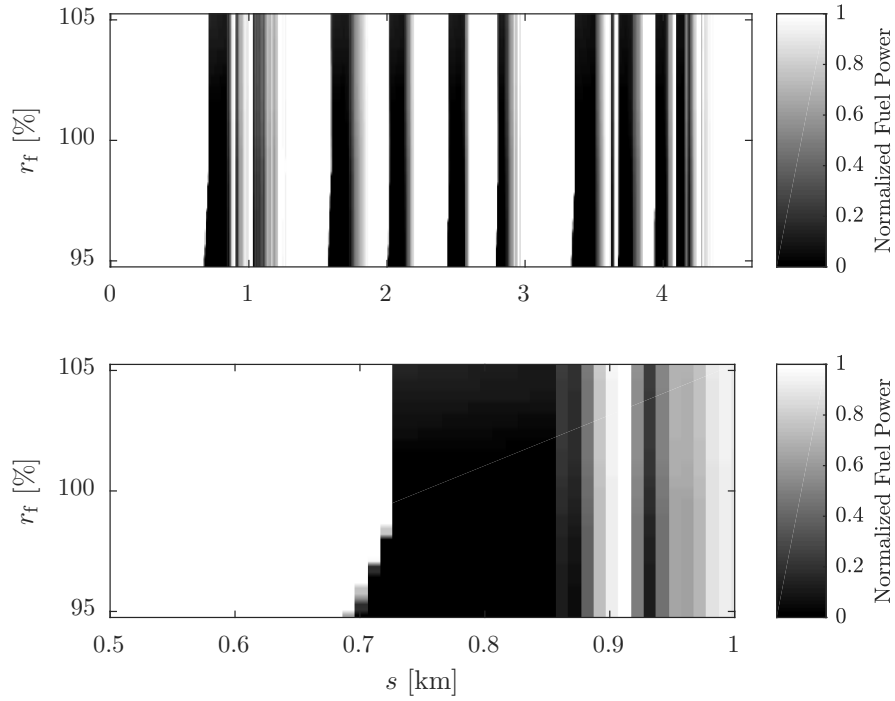


Figure 3.9: The optimal  $P_k(s)$  (normalized) over a range of  $\Delta E_{b,min}$  but for a fixed fuel allowance of 100 kg per race.



Figure 3.10: The impact of  $\Delta E_{b,\min}$  on lap time.Figure 3.11: The optimal fuel power  $P_f(s)$  (normalized) over a range of fuel allowances for a fixed  $\Delta E_{b,\min}$  of 0 MJ. The lower plot shows a zoom around the first corner.

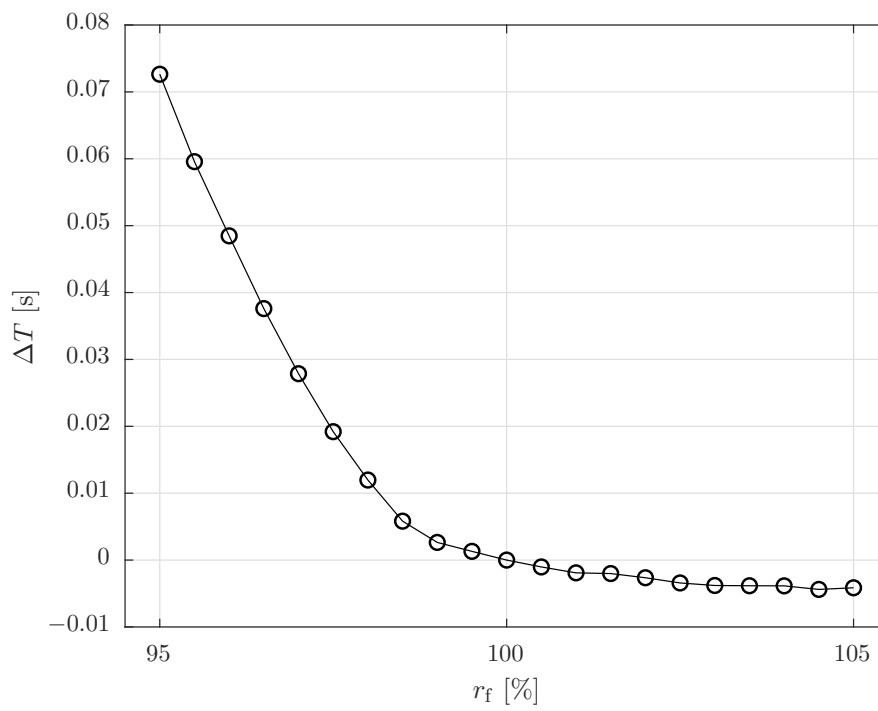


Figure 3.12: The impact of fuel allowance on lap time.

# 4

## Time-optimal Control Policy: The Analytical Solution

In this chapter, we compute the optimal control policy analytically. Leveraging a non-smooth version of PMP we derive a globally optimal feedforward implementation of the optimal control strategies that can be effectively loaded on the ECU, with look-up tables and in compliance with the sporting regulations. We test the optimal control policy on the benchmark and high-fidelity simulators introduced in Section 2.3. These results were presented in [2]. A minor extension is to be found in [5].

## 4.1 Optimal Control Problem in Time Domain

For the sake of simplicity, we will omit the dependence on time whenever it is clear from the context. Defining the state variables as kinetic, fuel, battery, ES2K and K2ES energy, and longitudinal position  $x = (E_{\text{kin}}, E_f, \Delta E_b, E_{\text{ES2K}}, E_{\text{K2ES}}, s)^\top$ , and choosing the input variables as fuel, MGU-K and braking power  $u = (P_f, P_k, P_{\text{brk}})^\top$ , the full optimal control problem presented in Chapter 2 is formulated as follows.

**Problem 1** (Constrained Lap Time Optimal Control)

$$\min_u \int_0^T dt \quad (4.1)$$

subject to the dynamics

$$\begin{aligned} \dot{E}_{\text{kin}} &= c_{s,1} \cdot P_u(P_f, P_k)^2 + c_{s,2} \cdot P_u(P_f, P_k) - P_d(E_{\text{kin}}, s) - P_{\text{brk}} \\ \dot{E}_f &= P_f \\ \Delta \dot{E}_b &= -(\alpha_b \cdot P_b(P_k, -\eta_h \cdot P_f)^2 + P_b(P_k, -\eta_h \cdot P_f)) \\ \dot{E}_{\text{ES2K}} &= \max \{0, P_{k,\text{dc}}(P_k) + P_{h,\text{dc}}(-\eta_h \cdot P_f)\} \\ \dot{E}_{\text{K2ES}} &= \min \{0, P_{k,\text{dc}}(P_k)\} \\ \dot{s} &= \sqrt{2 \cdot E_{\text{kin}}/m} \ , \end{aligned} \quad (4.2)$$

where

$$\begin{aligned} P_u(P_f, P_k) &= \eta_e \cdot P_f - P_{e,0} + P_k \\ P_b(P_k, P_h) &= P_{k,\text{dc}}(P_k) + P_{h,\text{dc}}(P_h) + P_{\text{aux}} \\ P_{x,\text{dc}}(P_x) &= \alpha_x \cdot P_x^2 + P_x \quad \text{for } x = k, h \ , \end{aligned} \quad (4.3)$$

and the state and input constraints

$$\begin{aligned} P_f(t) &\in [0, P_{f,\text{max}}] \\ P_k(t) &\in [P_{k,\text{min}}, P_{k,\text{max}}] \\ P_{\text{brk}}(t) &\in [0, P_{\text{brk},\text{max}}] \\ E_{\text{kin}}(t) &\leq E_{\text{kin},\text{max}}(s(t)) \\ E_{\text{kin}}(T) &\in \{E_{\text{kin}}(0)\} \\ E_f(T) &\leq E_{f,\text{max}} \\ \Delta E_b(T) &\geq \Delta E_{b,\text{min}} \\ E_{\text{ES2K}}(T) &\leq 4\text{MJ} \\ E_{\text{K2ES}}(T) &\geq -2\text{MJ} \\ s(T) &= S \ . \end{aligned} \quad (4.4)$$

We can reformulate Problem 1 to an unconstrained version by including the state and input constraints into the cost functions, using the indicator functions  $\Psi_{\mathcal{X}}(x)$  as described in Appendix A.2. We define the stage cost function as

$$g(x, u) = 1 + \Psi_{[-\infty, 0]}(E_{\text{kin}} - E_{\text{kin}, \max}(s)) + \Psi_{[0, P_{\text{f}, \max}]}(P_{\text{f}}) + \Psi_{[P_{\text{k}, \min}, P_{\text{k}, \max}]}(P_{\text{k}}) + \Psi_{[0, P_{\text{brk}, \max}]}(P_{\text{brk}}) , \quad (4.5)$$

and the terminal cost function as

$$h(x(T)) = \Psi_{\{E_{\text{kin}}(0)\}}(E_{\text{kin}}(T)) + \Psi_{[-\infty, E_{\text{f}, \max}]}(E_{\text{f}}(T)) + \Psi_{[\Delta E_{\text{b}, \min}, \infty]}(\Delta E_{\text{b}}(T)) + \Psi_{[-\infty, 4 \text{ MJ}]}(E_{\text{ES2K}}(T)) + \Psi_{[-2 \text{ MJ}, \infty]}(E_{\text{K2ES}}(T)) + \Psi_{\{S\}}(s(T)) . \quad (4.6)$$

This way we can reformulate Problem 1 to an equivalent unconstrained version as follows.

**Problem 2** (Unconstrained Lap Time Optimal Control)

$$\min_u \int_0^T g(x(t), u(t)) dt + h(x(T)) , \quad (4.7)$$

subject to Eq. (4.2) and (4.3).

We can find the optimal control policy for Problem 1 by applying PMP to Problem 2. The Hamiltonian of Problem 2 is

$$\begin{aligned} H(x, u, \lambda) = & 1 \\ & + \lambda_{\text{kin}} \cdot (c_{\text{s}, 1} \cdot P_{\text{u}}(P_{\text{f}}, P_{\text{k}})^2 + c_{\text{s}, 2} \cdot P_{\text{u}}(P_{\text{f}}, P_{\text{k}}) - P_{\text{brk}} - P_{\text{d}}(E_{\text{kin}}, s)) \\ & + \lambda_{\text{f}} \cdot P_{\text{f}} - \lambda_{\text{b}} \cdot (\alpha_{\text{b}} \cdot P_{\text{b}}(P_{\text{k}}, -\eta_{\text{h}} \cdot P_{\text{f}})^2 + P_{\text{b}}(P_{\text{k}}, -\eta_{\text{h}} \cdot P_{\text{f}})) \\ & + \lambda_{\text{ES2K}} \cdot \max \{0, P_{\text{k}, \text{dc}}(P_{\text{k}}) + P_{\text{h}, \text{dc}}(-\eta_{\text{h}} \cdot P_{\text{f}})\} \\ & + \lambda_{\text{K2ES}} \cdot \min \{0, P_{\text{k}, \text{dc}}(P_{\text{k}})\} + \lambda_{\text{space}} \cdot \sqrt{2 \cdot E_{\text{kin}}/m} \\ & + \Psi_{[-\infty, 0]}(E_{\text{kin}} - E_{\text{kin}, \max}(s)) + \Psi_{[0, P_{\text{f}, \max}]}(P_{\text{f}}) \\ & + \Psi_{[P_{\text{k}, \min}, P_{\text{k}, \max}]}(P_{\text{k}}) + \Psi_{[0, P_{\text{brk}, \max}]}(P_{\text{brk}}) , \end{aligned} \quad (4.8)$$

where  $\lambda \in \mathbb{R}^6$  are the costate variables. Despite the fact that the Hamiltonian is non-smooth due to the piecewise affinity of the ES2K and K2ES dynamics and to the presence of the indicator functions, it is a convex function with respect to the input variables. Therefore, PMP is necessary and sufficient to guarantee global optimality. To derive the optimal control policy, we need to include zero into the subdifferential of the Hamiltonian with respect to the input  $u$  as  $0 \in \partial_u H(x, u, \lambda)$ . The resulting control policy can be shown to be a sole function of the costate variables  $\lambda$ . Using a numerical solver like the one

presented in Chapter 3, the values of  $\lambda$  can be calculated offline prior to a race for a specific scenario.

### Costate Variables

The dynamics of the costate variables are derived as described in Appendix A.2 as

$$\begin{aligned}
 \dot{\lambda}_{\text{kin}} &\in \frac{\partial P_d}{\partial E_{\text{kin}}}(E_{\text{kin}}^*, s^*) \cdot \lambda_{\text{kin}} - \frac{\lambda_{\text{space}}}{\sqrt{2 \cdot m \cdot E_{\text{kin}}^*}} - N_{[0, E_{\text{kin}, \max}(s)]}(E_{\text{kin}}^*) \\
 \dot{\lambda}_{\text{f}} &= 0 \\
 \dot{\lambda}_{\text{b}} &= 0 \\
 \dot{\lambda}_{\text{ES2K}} &= 0 \\
 \dot{\lambda}_{\text{K2ES}} &= 0 \\
 \dot{\lambda}_{\text{space}} &\in \frac{\partial P_d}{\partial s}(E_{\text{kin}}^*, s^*) \cdot \lambda_{\text{kin}} - N_{[E_{\text{kin}}^*, \infty]}(E_{\text{kin}, \max}(s^*)) \cdot \frac{\partial E_{\text{kin}, \max}}{\partial s}(s^*) ,
 \end{aligned} \tag{4.9}$$

where the notation  $(\cdot)^*$  denotes optimality and the set-valued function normal cone  $N_{\mathcal{X}}(x)$  is defined in Appendix A.2. The terminal conditions are

$$\begin{aligned}
 \lambda_{\text{kin}}(T) &\in N_{\{E_{\text{kin}}(0)\}}(E_{\text{kin}}^*(T)) \\
 \lambda_{\text{f}}(T) &\in N_{[-\infty, E_{\text{f}, \max}]}(E_{\text{f}}^*(T)) \\
 \lambda_{\text{b}}(T) &\in N_{[\Delta E_{\text{b}, \min}, \infty]}(\Delta E_{\text{b}}^*(T)) \\
 \lambda_{\text{ES2K}}(T) &\in N_{[-\infty, 4\text{MJ}]}(E_{\text{ES2K}}^*(T)) \\
 \lambda_{\text{K2ES}}(T) &\in N_{[-2\text{MJ}, \infty]}(E_{\text{K2ES}}^*(T)) \\
 \lambda_{\text{space}}(T) &\in N_{\{s\}}(s^*(T)) .
 \end{aligned} \tag{4.10}$$

Based on these conditions, we get

$$\begin{aligned}
 \lambda_{\text{f}} &\geq 0 \\
 \lambda_{\text{b}} &\leq 0 \\
 \lambda_{\text{ES2K}} &\geq 0 \\
 \lambda_{\text{K2ES}} &\leq 0 ,
 \end{aligned} \tag{4.11}$$

whereby the costate variables  $\lambda_{\text{f}}$ ,  $\lambda_{\text{b}}$ ,  $\lambda_{\text{ES2K}}$  and  $\lambda_{\text{K2ES}}$  related to the consumption are constant and represent the sensitivity of the achievable lap time with respect to the corresponding state variables. Moreover, (4.10) shows that these costate variables are

non-zero only if the corresponding terminal state constraint is active, i.e.,

$$\begin{aligned}
 \lambda_f & \begin{cases} \geq 0 & \text{if } E_f^*(T) = E_{f,\max} \\ = 0 & \text{if } E_f^*(T) < E_{f,\max} \end{cases} \\
 \lambda_b & \begin{cases} \leq 0 & \text{if } \Delta E_b^*(T) = \Delta E_{b,\min} \\ = 0 & \text{if } \Delta E_b^*(T) > \Delta E_{b,\min} \end{cases} \\
 \lambda_{\text{ES2K}} & \begin{cases} \geq 0 & \text{if } E_{\text{ES2K}}^*(T) = 4 \text{ MJ} \\ = 0 & \text{if } E_{\text{ES2K}}^*(T) < 4 \text{ MJ} \end{cases} \\
 \lambda_{\text{K2ES}} & \begin{cases} \leq 0 & \text{if } E_{\text{K2ES}}^*(T) = -2 \text{ MJ} \\ = 0 & \text{if } E_{\text{K2ES}}^*(T) > -2 \text{ MJ} \end{cases} .
 \end{aligned} \tag{4.12}$$

The optimal control policy is not a function of  $\lambda_{\text{space}}(t)$ , since in (4.8) this last costate variable is not multiplied by any function of the input variables, and therefore its value is not needed. The first costate variable  $\lambda_{\text{kin}}(t)$  is the only time-varying variable in the optimal control policy. This variable represents how much a change in kinetic energy, and therefore of speed, on any specific point on the track would affect optimality, i.e., reduce or increase lap time. Fig. 4.1 shows a typical trajectory of this variable on the circuit of Barcelona. The local minima correspond to the beginning of the straights, where the maximum speed constraint becomes inactive. These are the locations where an increase

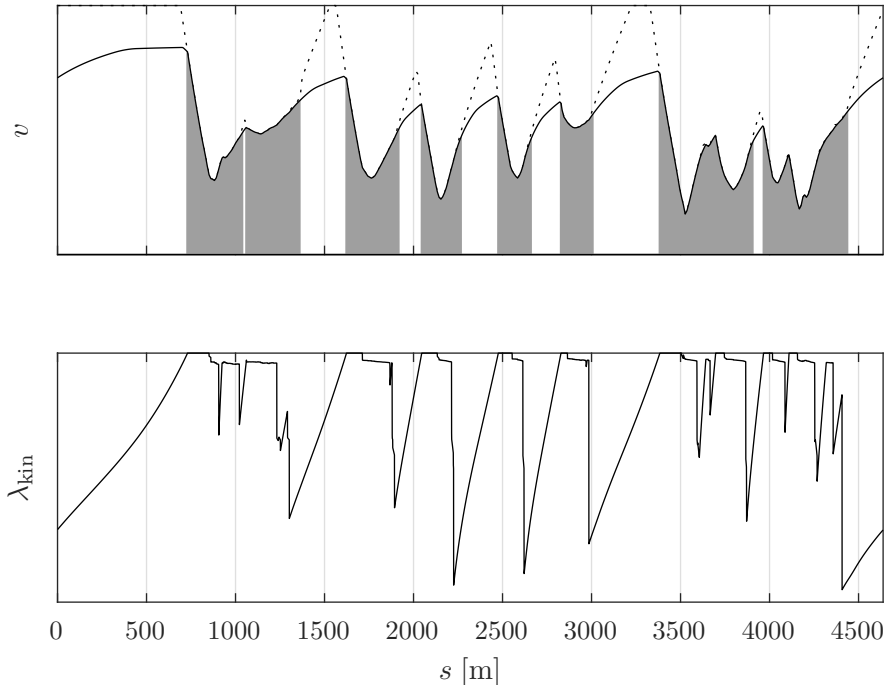


Figure 4.1: Maximum (dashed) and optimal speed profile together with the kinetic costate variable  $\lambda_{\text{kin}}$ . In the upper plot, grip-limited regions are highlighted in grey.

in speed would most effectively reduce lap time. In fact, a larger (or lower) velocity at the beginning of a straight would be beneficial (or disadvantageous) throughout the whole straight, as the lap time is the integral of  $1/v$  in space, and speed would be overall higher (or lower). On the other hand, in the braking points,  $\lambda_{\text{kin}}$  reaches 0 and, accordingly, any changes in kinetic energy would not affect optimality. Moreover, in the upper plot, two regions may be distinguished: First, a so-called grip-limited region, where the driver follows the maximum speed profile attainable in the curves by requiring a specific amount of thrust, which must be delivered with precision. Second, a power-limited region denoted by an inactive maximum speed constraint, where the driver requires 100% propulsive power. In this region, a thrust controller is to be implemented in addition to the power split, which means that the ICE and MGU-K power can be chosen independently.



## 4.2 Optimal Control Policy

The optimal control policy can be computed by evaluating the subdifferential (see Appendix A.2) of the Hamiltonian (4.8) with respect to the input  $u$  as

$$\begin{aligned}
0 \in \partial_{P_f} H(x^*, u^*, \lambda) &= \lambda_{\text{kin}} \cdot \eta_e \cdot (2 \cdot c_{s,1} \cdot (\eta_e \cdot P_f^* - P_{e,0} + P_k^*) + c_{s,2}) + \lambda_f \\
&\quad + \left( -\lambda_b \cdot (2 \cdot \alpha_b \cdot P_b(P_k^*, -\eta_h \cdot P_f^*) + 1) \right. \\
&\quad \left. + \lambda_{\text{ES2K}} \cdot \sigma(P_{k,\text{dc}}(P_k^*) + P_{h,\text{dc}}(-\eta_h \cdot P_f^*)) \right) \cdot (2 \cdot \alpha_h \cdot \eta_h^2 \cdot P_f^* - \eta_h) \\
&\quad + N_{[0, P_{f,\text{max}}]}(P_f^*) \\
0 \in \partial_{P_k} H(x^*, u^*, \lambda) &= \lambda_{\text{kin}} \cdot (2 \cdot c_{s,1} \cdot (\eta_e \cdot P_f^* - P_{e,0} + P_k^*) + c_{s,2}) \\
&\quad + \left( -\lambda_b \cdot (2 \cdot \alpha_b \cdot P_b(P_k^*, -\eta_h \cdot P_f^*) + 1) \right. \\
&\quad + \lambda_{\text{ES2K}} \cdot \sigma(P_{k,\text{dc}}(P_k^*) + P_{h,\text{dc}}(-\eta_h \cdot P_f^*)) \\
&\quad \left. + \lambda_{\text{K2ES}} \cdot \underbrace{\sigma(-P_{k,\text{dc}}(P_k^*))}_{\sigma(-P_k^*)} \right) \cdot (2 \cdot \alpha_k \cdot P_k^* + 1) \\
&\quad + N_{[P_{k,\text{min}}, P_{k,\text{max}}]}(P_k^*) \\
0 \in \partial_{P_{\text{brk}}} H(x^*, u^*, \lambda) &= -\lambda_{\text{kin}} + N_{[0, P_{\text{brk,max}}]}(P_{\text{brk}}^*) ,
\end{aligned} \tag{4.13}$$

where the set-valued Heaviside function  $\sigma(x)$  is the subdifferential of  $\max\{0, x\}$  and is defined as

$$\partial_x \max\{0, x\} = \sigma(x) := \begin{cases} 0 & \text{if } x < 0 \\ [0, 1] & \text{if } x = 0 \\ 1 & \text{if } x > 0 \end{cases} , \tag{4.14}$$

whereas  $\partial_x (-\min\{0, x\}) = -\sigma(-x)$ .

From the third inclusion of (4.13) we can derive that if  $\lambda_{\text{kin}}$  is positive, the normal cone must also be positive, which is only possible on the right-hand side of the cone, and therefore  $P_{\text{brk}}^* = P_{\text{brk,max}}$ . If  $\lambda_{\text{kin}}$  is negative, then the normal cone must also be negative and therefore  $P_{\text{brk}}^* = 0$ . For  $\lambda_{\text{kin}} = 0$  we obtain that  $P_{\text{brk}}^* \in [0, P_{\text{brk,max}}]$ . This result can be expressed as

$$P_{\text{brk}}^* \in P_{\text{brk,max}} \cdot \sigma(\lambda_{\text{kin}}) . \tag{4.15}$$

For the computation of the optimal input variables  $P_f^*$  and  $P_k^*$ , we can use the same reasoning. A detailed derivation can be found in Appendix A.3. The costate variables  $\lambda_f$ ,  $\lambda_b$ ,  $\lambda_{\text{ES2K}}$  and  $\lambda_{\text{K2ES}}$  are constant over one entire lap and depend on the boundary conditions on fuel load and battery deployment. Therefore, they can be treated as given parameters in the computation of the optimal control policy, whereas the position-

Table 4.1: Switch-points of  $\lambda_{\text{kin}}$  with associated values of  $P_e^*$ ,  $P_k^*$  and  $P_u^*$ . The values listed represent the maximum and minimum ICE power thresholds, the maximum MGU-K power threshold, the interval where the MGU-K is operated only with the energy extracted from the MGU-H, and the interval where the MGU-K is shut off, as well as the minimum MGU-K power threshold.

$\lambda_{\text{kin}}$	$P_e^*$	$P_k^*$	$P_u^* = P_e^* + P_k^*$
$\lambda_{e,\text{max}}$	$P_{e,\text{max}}$	$P_{k,\text{emax}}$	$P_{e,\text{max}} + P_{k,\text{emax}}$
$\lambda_{e,0}$	$-P_{e,0}$	$P_{k,e0}$	$-P_{e,0} + P_{k,e0}$
$\lambda_{k,\text{max}}$	$P_{e,k\text{max}}$	$P_{k,\text{max}}$	$P_{e,k\text{max}} + P_{k,\text{max}}$
$\lambda_{k,h+}$	$P_{e,kh+}$	$P_{k,h}(-\eta_h \cdot P_{f,kh+})$	$P_{e,kh+} + P_{k,h}(-\eta_h \cdot P_{f,kh+})$
$\lambda_{k,h-}$	$P_{e,kh-}$	$P_{k,h}(-\eta_h \cdot P_{f,kh-})$	$P_{e,kh-} + P_{k,h}(-\eta_h \cdot P_{f,kh-})$
$\lambda_{k,0+}$	$P_{e,k0+}$	0	$P_{e,k0+}$
$\lambda_{k,0-}$	$P_{e,k0-}$	0	$P_{e,k0-}$
$\lambda_{k,\text{min}}$	$P_{e,k\text{min}}$	$P_{k,\text{min}}$	$P_{e,k\text{min}} + P_{k,\text{min}}$

dependent kinetic costate variable  $\lambda_{\text{kin}}$  is used as a decision variable, yielding

$$\begin{aligned}
 &P_f^*(\lambda_{\text{kin}}), P_k^*(\lambda_{\text{kin}}), P_{\text{brk}}^*(\lambda_{\text{kin}}) \\
 &P_e^*(\lambda_{\text{kin}}) = \eta_e \cdot P_f^*(\lambda_{\text{kin}}) - P_{e,0} \\
 &P_u^*(\lambda_{\text{kin}}) = P_e^*(\lambda_{\text{kin}}) + P_k^*(\lambda_{\text{kin}}) .
 \end{aligned} \tag{4.16}$$

These optimal inputs are piecewise affine functions and can therefore be obtained using a first-order interpolation on the values listed in Table 4.1, where the following notation is used: The thresholds  $P_{k,i}$  with  $i = \text{emax}, e0$  represent the optimal values of  $P_k$  at the switch-points of  $P_e$ , whereas the thresholds  $P_{f,j}$  with  $j = k\text{max}, kh+, kh-, k0+, k0-, k\text{min}$  are the values of  $P_e$  at the switch-points of  $P_k$ . Moreover, the set  $\Lambda_{k,h} = [\lambda_{k,h+}, \lambda_{k,h-}]$  is the interval in  $\lambda_{\text{kin}}$  in which the MGU-K is operated exclusively with the power extracted from the MGU-H, whereas the interval  $\Lambda_{k,0} = [\lambda_{k,0+}, \lambda_{k,0-}]$  represents the case where the MGU-K is turned off. These intervals can be shown to exist only if the corresponding terminal constraint is active on either the ES2K or the K2ES energy. The table must be sorted as a function of the kinetic costate variable  $\lambda_{\text{kin}}$ , since the order of the thresholds may change, given different vehicle and track parameters or energy budgets. Given the value of  $\lambda_{\text{kin}}$  on any specific point on the track, the optimal control inputs can be inferred using the results listed in Table 4.1. Fig. 4.2 shows the piecewise affine control policy for the ICE and the MGU-K. The optimal total power to be delivered by the power unit results from the sum of the ICE and MGU-K power and is shown in Fig. 4.3.

Due to the FIA regulations, the optimal control policy based on the kinetic costate variable  $\lambda_{\text{kin}}$  cannot be used in the so-called grip-limited region where the power request of the driver  $P_{\text{req}}$  is less than 100% of the maximum power. In this case, it is only allowed to decide how to split the demand between the ICE and the MGU-K. The optimal power

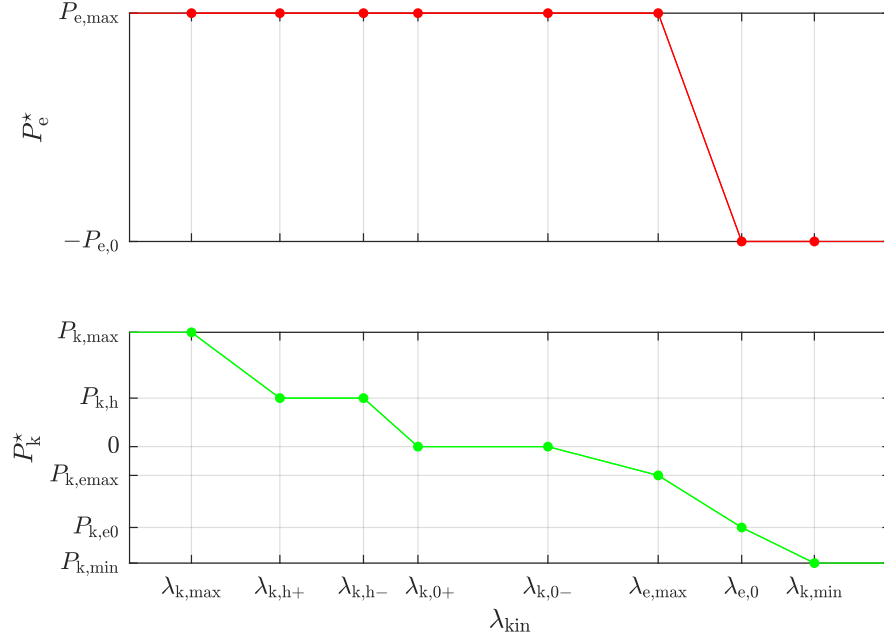


Figure 4.2: Optimal ICE and MGU-K power as a function of the kinetic costate variable.

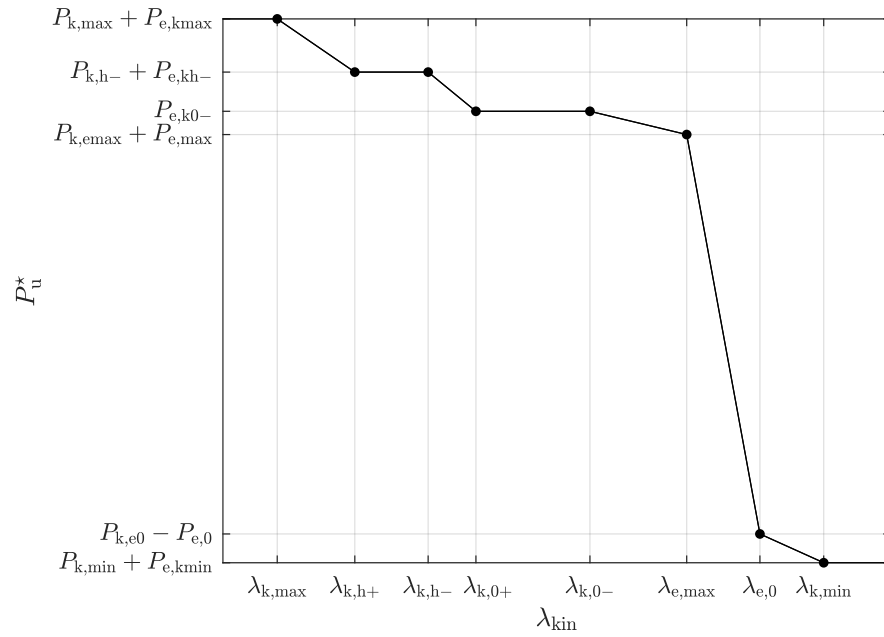


Figure 4.3: Optimal total power of the power unit as a function of the kinetic costate variable.

split  $[P_e, P_k] = \text{PS}^*(P_u)$  can be obtained by representing the optimal total power of the power unit together with the ICE and the MGU-K power as shown in Fig. 4.4. It is worth noticing that, since the consumption costate variables  $\lambda_f$ ,  $\lambda_b$ ,  $\lambda_{\text{ES2K}}$  and  $\lambda_{\text{K2ES}}$  are constant, the optimal power split does not change throughout the lap. In the power-limited region, where the power request is 100%, such a request can be overwritten: The

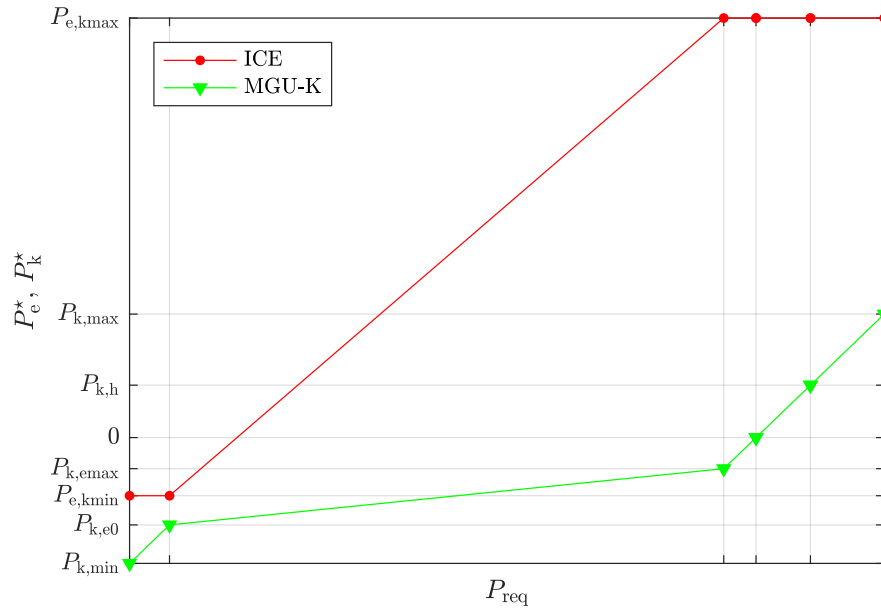


Figure 4.4: Optimal power split: optimal ICE and MGU-K power as a function of the total power unit power.

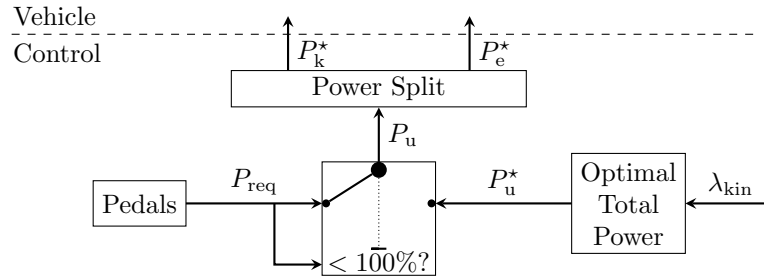


Figure 4.5: Optimal control policy implementation.

optimal total power can be inferred from the interpolation of the kinetic costate variable  $\lambda_{\text{kin}}$  as shown in Fig. 4.3 and then split between the actuators with the optimal power split. The optimal control policy can thus be implemented in accordance with the FIA regulations, as shown schematically in Fig. 4.5.

### 4.3 Numerical Results

The practical implementation of the theoretical outcomes consists of the following steps: First, the optimal control policy is compared with the numerical results obtained with the numerical solver presented in Chapter 3 from which the costate variables are taken. Second, the proposed control strategy is implemented in the benchmark simulator presented in Section 2.3, and the state and input trajectories, together with the lap-time, are compared to the optimal ones. A race lap on the circuit of Barcelona with a 100% fuel load is considered, where the battery has to be charged by 2.0 MJ. Finally, the optimal control policy is implemented in a high-fidelity nonlinear simulator. For confidentiality reasons, all the sensitive data have been normalized.

#### Optimal Control Policy

The optimal control policy derived in Section 4.2 depends on the system parameters and, in addition to the kinetic costate variable  $\lambda_{\text{kin}}$ , on the values of  $\lambda_f$ ,  $\lambda_b$ ,  $\lambda_{\text{ES2K}}$  and  $\lambda_{\text{K2ES}}$ . The numerical values obtained from the numerical solver fulfill the conditions defined in (4.12). In Fig. 4.6 and 4.7, the numerically optimal values of  $(\lambda_{\text{kin}}, P_u^*)$  are plotted together with the analytical results listed in Table 4.1. Fig. 4.8 presents a plot of the optimal power split. The good coherence between numerical and analytic results confirms the validity of both approaches as well as the validity of using linear interpolations among the values of Table 4.1.

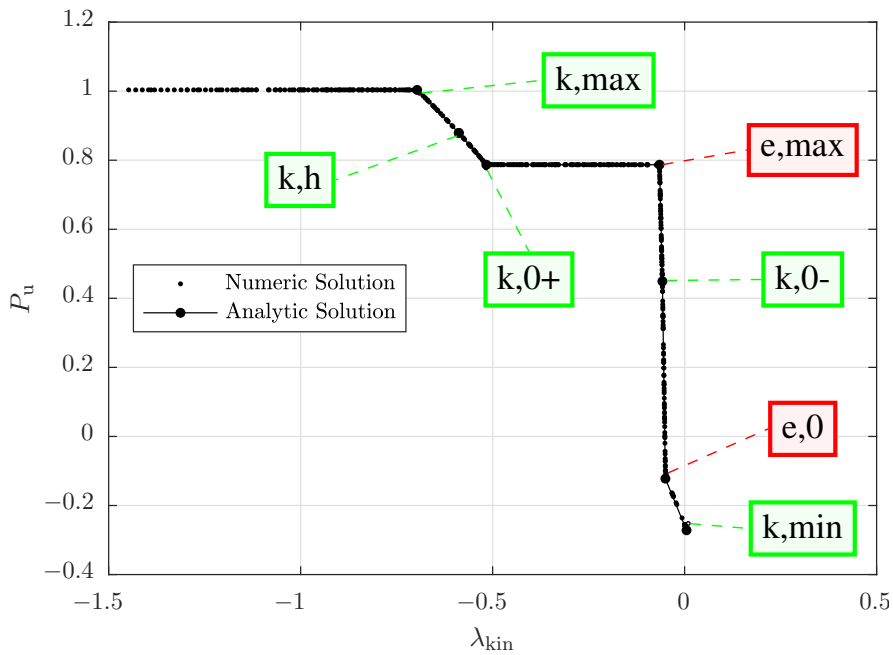


Figure 4.6: Normalized  $P_u$  modes as a function of  $\lambda_{\text{kin}}$ .

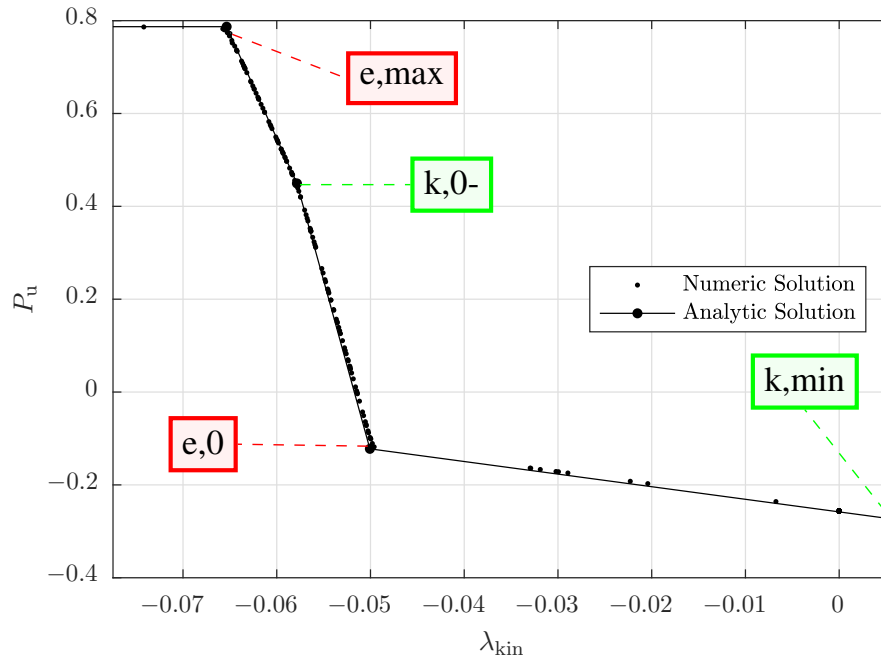


Figure 4.7: Zoom between maximum regenerative braking and maximum ICE power for the normalized  $P_u$  modes as a function of  $\lambda_{kin}$ .

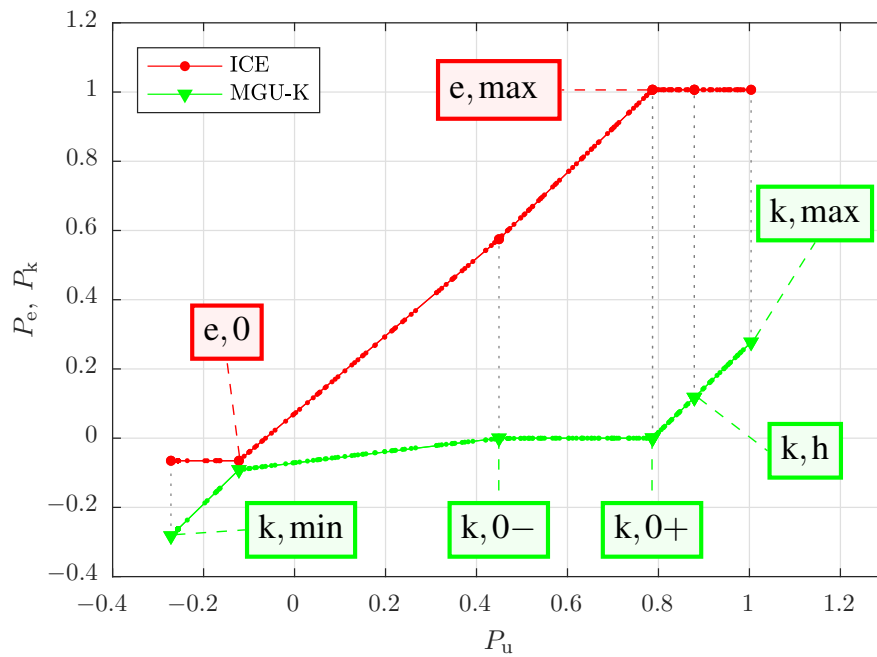


Figure 4.8: Normalized power split as a function of  $P_u$ .

### Benchmark Simulator

In this section, the piecewise affine control policy is implemented in the benchmark simulator introduced in Section 2.3 and the resulting state trajectories are compared with the optimal ones obtained by means of convex optimization. In order to generate the

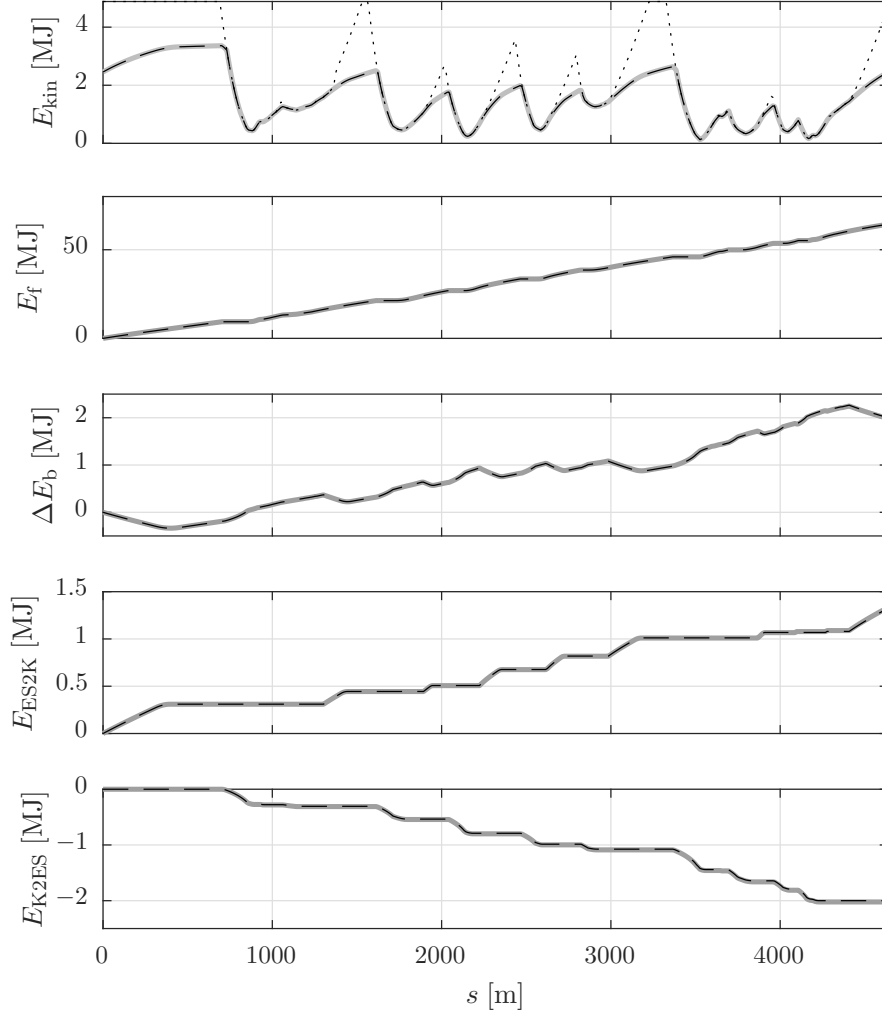


Figure 4.9: Optimal (dashed) and forward (solid) state trajectories along one lap. In the top plot, the maximum kinetic energy curve (dotted) is shown as well.

optimal power modes displayed in Fig. 4.2 and 4.3, and the optimal power split depicted in Fig. 4.4, the constant costate values of  $\lambda_f$ ,  $\lambda_b$ ,  $\lambda_{ES2K}$  and  $\lambda_{K2ES}$  are employed. The position-dependent kinetic costate variable  $\lambda_{kin}(s)$  is utilized as a decision variable to obtain the optimal power unit power as  $P_u^{ECU}(s, x) = P_u^*(\lambda_{kin}(s))$  when the vehicle is in a power-limited region. In the grip-limited regions the power to be delivered by the power unit  $P_u$  is imposed by the need of the driver to follow the maximum kinetic energy curve. We implement the power split between ICE and MGU-K as  $PS^{ECU}(s, x, P_u) = PS^*(P_u)$ , shown in Fig. 4.4. For every combination of fuel load and battery deployment the optimal solution is computed offline, whereby the arising costate variables are used to create the optimal control policy presented in Section 4.2 to be stored on the ECU. In Fig. 4.9 the optimal state trajectories obtained with the numerical solver are shown, along with the trajectories resulting from the implementation of the optimal control policy in the benchmark simulator. At the end of the lap, the largest gap lies below 1%. The optimal control

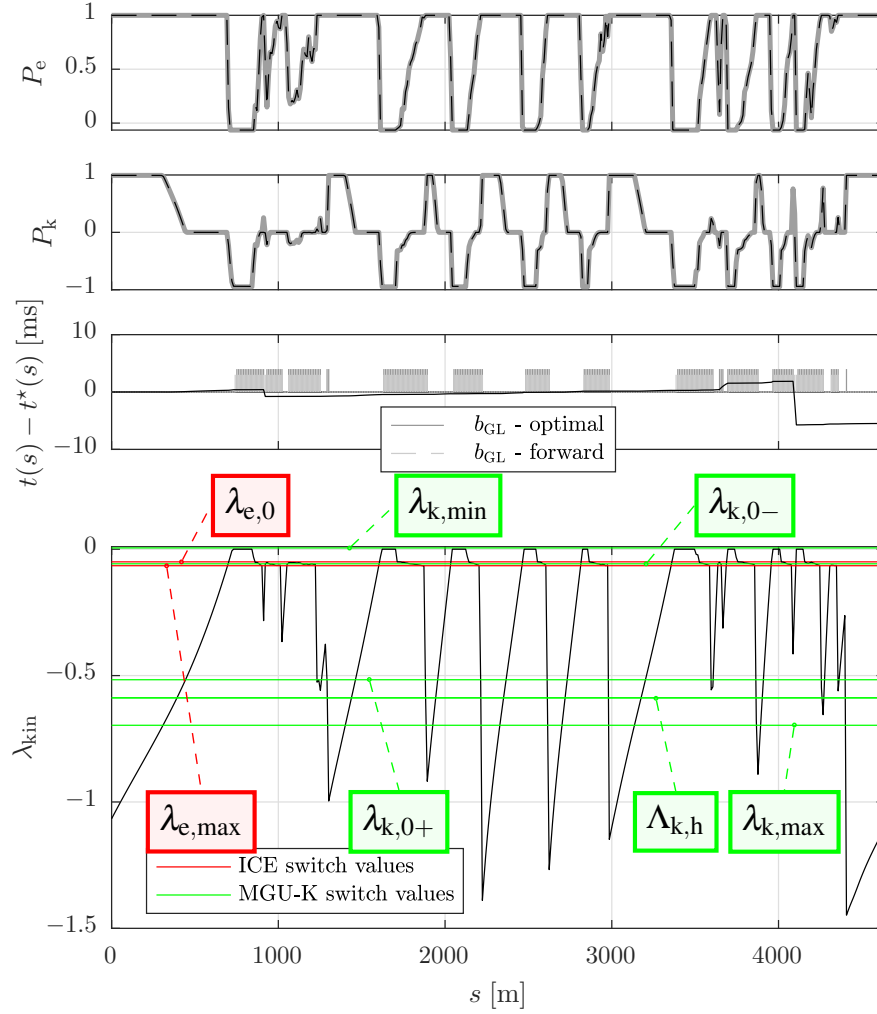


Figure 4.10: Optimal (dashed) and forward (solid) normalized input trajectories along one lap, lap-time difference with grip-limited regions for the optimal and the forward solution, and  $\lambda_{\text{kin}}(s)$  together with the switch values of Table 4.1.

inputs and those obtained by interpolating  $\lambda_{\text{kin}}(s)$  or  $P_u$  in power-limited or grip-limited regions, respectively, are shown in Fig. 4.10, where the behaviour of the kinetic costate variable  $\lambda_{\text{kin}}$  is depicted as well, together with the switch-points of the ICE and MGU-K optimal control policies. The very small differences observed arise when the optimal solution lies in a grip-limited region and the forward solution lies in a power-limited region or vice-versa, resulting in a lap time gap that is smaller than ten milliseconds, which can be ascribed to numerical errors and can therefore be neglected. These results show that, when implemented on the same model, the optimal control policy reflects the optimal control strategies, while guaranteeing compliance with the FIA regulations.

### High-fidelity Simulator

Fig. 4.11 shows the results obtained by implementing the optimal control policy on the high-fidelity nonlinear simulator presented in Section 2.3, describing an aggressive driv-



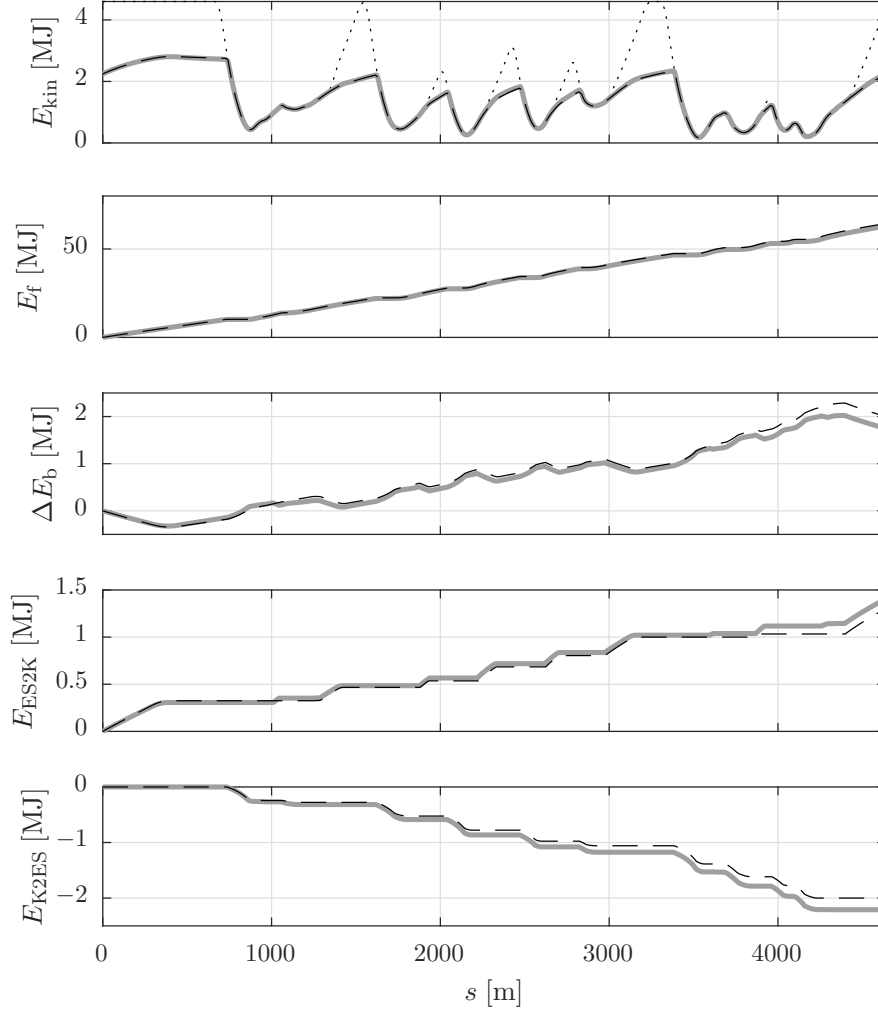


Figure 4.11: Optimal (dashed) and high-fidelity nonlinear simulator (solid) state trajectories along one lap. In the top plot, the maximum kinetic energy curve (dotted) is shown as well.

ing behaviour. Despite the limited significance of these results, they demonstrate that the optimal control policy presented works effectively and in accordance with the FIA regulations and that the optimal speed profile can be tracked accurately. The cumulative drifts in the consumption data represent a situation where the K2ES limitation is not active. They are used to illustrate how much the state variables deviate from the nominal solution. In a real race scenario, the direct energy transfer from the MGU-K to the battery would be blocked once the K2ES energy reaches -2 MJ, resulting in a slightly lower battery state of charge at the end of the lap. The drifts observed could be avoided by iteratively tuning the constant costate variables as in [5] or by controlling them online in an ECMS fashion, as shown in Chapter 6.



# 5

## A Two-level MPC Scheme

In this chapter, we present feedback control algorithms for the real-time energy management of the F1 power unit. First, we design a two-level MPC scheme, whereby the higher level periodically updates the optimal control strategies and the lower level tracks them in a lap time optimal fashion. These results can be found in [3].

As shown in the lower part of Fig. 1.1, the energy management system of the F1 car depends on the pedal operation. If the driver is not requesting full power, the car is in a grip-limited region, i.e., it is not further accelerated because the driver feels that a higher speed would exceed the grip limitations of the vehicle, resulting in a dangerous drift. In such a situation, the energy management system must deliver the amount of power requested and the energy management system can only choose how to split it between the ICE and the MGU-K, as in a conventional hybrid electric vehicle. On the other hand, if the driver is requesting maximum thrust, the car is in a power-limited region, since its acceleration is limited by the amount of power that can be delivered by the powertrain. The regulations allow overwriting a full-power request and the energy management system can decide the amount of thrust to provide and the split between the actuators [16].

In Chapters 3 and 4, the optimal control strategies were computed and a feedforward controller was designed and implemented for the energy management in a lap time optimal way and compatibly with the FIA regulations. Nevertheless, a feedback controller is still necessary to react to potential disturbances such as a model mismatch or an unexpected event. In this chapter, we modify the approach presented in Chapter 3 and exploit the optimal control policy derived in Chapter 4 to repeatedly update the power split and the thrust control, based on the measured state variables, by solving the energy management problem for one lap ahead. Subsequently, we formulate an optimality tracking zone MPC scheme for the power-limited region in the form of a LP that can be efficiently solved within the sampling window available. Since the computational time required to solve the high-level optimization problem is not short enough to be implemented as a feedback controller, a low-level MPC algorithm is designed to minimize excesses in fuel and battery consumption and to respond in a lap time optimal way. To this end, a zone MPC [86]–[88] is employed. This control scheme is an extension of trajectory tracking MPC, whereby the objective is to converge into a set instead of a trajectory. Thus far, this approach has

been effectively applied to glycemia regulation in type I diabetic patients [89]–[91] and to room temperature control [92].

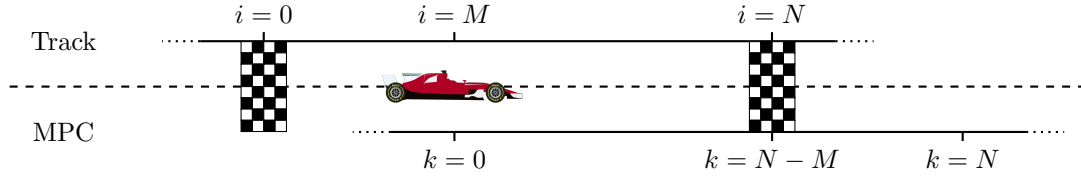


Figure 5.1: The discrete space-reference frame on the track and in the MPC formulation.

## 5.1 High-level MPC Optimization Problem

The optimal control problem presented in Sections 2.1 and 2.2 above is reformulated here in such a way that the energy management problem for one race lap can be solved from any point on the track and thus be implemented as a look-ahead controller. The following notation is introduced: The symbol  $\hat{x}(t)$  denotes the vector of measured values of the vector  $x$  at time  $t$ , whilst the superscript  $(\cdot)^*$  represents optimality. The notation  $x[k]$  represents the value of the vector  $x$  at the discrete step  $k$ . The variable  $\bar{x}^*[i = 0 : N]$  represents the optimal trajectory of the vector  $x$  along a nominal lap. The high-level MPC optimization problem presented is adapted from Chapter 3, formulated as a second-order conic program in space domain and discretized using the explicit Euler integration scheme with a discrete lap length of  $N \in \mathbb{N}$ . Assuming that the MPC is computed at some measured position  $\hat{s}(t)$  on the track, the corresponding index in the given discretization is found as

$$M = \max \{i \in \mathbb{N} | \Delta s \cdot i \leq \hat{s}(t)\} \quad (5.1)$$

and is shown in Fig. 5.1. The state variables of the MPC optimization problem are  $x = (E_{\text{kin}}, E_{\text{f}}, E_{\text{b}}, E_{\text{ES2K}}, E_{\text{K2ES}})^{\top}$ , whereas the input variables are  $u = (F_{\text{f}}, F_{\text{k}})^{\top}$ , which are expressed as forces, since the system dynamics here are formulated in the space domain. The time-optimal energy management problem is

$$\min \sum_{k=0}^{N-1} \frac{dt}{ds}[k] \cdot \Delta s \quad (5.2)$$

subject to the dynamics

$$\begin{aligned} E_{\text{kin}}[k+1] - E_{\text{kin}}[k] &= (F_{\text{p}}[k] - F_{\text{d}}(k, E_{\text{kin}}[k])) \cdot \Delta s \\ E_{\text{f}}[k+1] - E_{\text{f}}[k] &= F_{\text{f}}[k] \cdot \Delta s \\ E_{\text{b}}[k+1] - E_{\text{b}}[k] &= -F_{\text{i}}[k] \cdot \Delta s, \end{aligned} \quad (5.3)$$

$$\begin{cases} E_{\text{ES2K}}[k+1] - E_{\text{ES2K}}[k] \geq 0 \\ E_{\text{ES2K}}[k+1] - E_{\text{ES2K}}[k] \geq (F_{\text{k,dc}}[k] + F_{\text{h,dc}}[k]) \cdot \Delta s \\ E_{\text{K2ES}}[k+1] - E_{\text{K2ES}}[k] \leq 0 \\ E_{\text{K2ES}}[k+1] - E_{\text{K2ES}}[k] \leq F_{\text{k,dc}}[k] \cdot \Delta s \end{cases} \quad \forall k \neq N-M, \quad (5.4)$$

and

$$\begin{cases} E_{\text{ES2K}}[N-M+1] \geq 0 \\ E_{\text{ES2K}}[N-M+1] \geq (F_{\text{k,dc}}[N-M] + F_{\text{h,dc}}[N-M]) \cdot \Delta s \\ E_{\text{K2ES}}[N-M+1] \leq 0 \\ E_{\text{K2ES}}[N-M+1] \leq F_{\text{k,dc}}[N-M] \cdot \Delta s \end{cases}, \quad (5.5)$$

where at the time-step  $k = N - M$  the car is at the end of the lap, and therefore the ES2K and K2ES energy trajectories are reset to 0 at the following step  $k = N - M + 1$ . The initial conditions are the ones measured:

$$\begin{aligned} E_{\text{kin}}[0] &= \hat{E}_{\text{kin}}(t) \\ E_{\text{f}}[0] &= \hat{E}_{\text{f}}(t) \\ E_{\text{b}}[0] &= \hat{E}_{\text{b}}(t) \\ E_{\text{ES2K}}[0] &= \hat{E}_{\text{ES2K}}(t) \\ E_{\text{K2ES}}[0] &= \hat{E}_{\text{K2ES}}(t) \end{aligned} \quad (5.6)$$

The state and input constraints along the lap are given by

$$\begin{aligned} F_{\text{f}}[k] &\in [0, P_{\text{f,max}}] \cdot \frac{dt}{ds}[k] \\ F_{\text{k}}[k] &\in [P_{\text{k,min}}, P_{\text{k,max}}] \cdot \frac{dt}{ds}[k] \\ E_{\text{kin}}[k] &\leq E_{\text{kin,max}}[\text{mod}_N(k+M)] \end{aligned} \quad (5.7)$$

The modulo operator is used to relate the index in the prediction horizon to the position on the track, and is defined as  $\text{mod}_n(m) = m - n \cdot \lfloor m/n \rfloor$ ,  $n, m \in \mathbb{N}$ , whereby the floor operator is defined as  $\forall z \in \mathbb{R}_+$ ,  $\lfloor z \rfloor = \max\{n \in \mathbb{N} | z \geq n\}$ . The terminal constraints at the finish line are

$$\begin{aligned} E_{\text{f}}[N-M] &\leq N_{\text{lap}} \cdot \Delta E_{\text{f},0} \\ E_{\text{b}}[N-M] &\geq N_{\text{lap}} \cdot \Delta E_{\text{b},0} \\ E_{\text{ES2K}}[N-M] &\leq 4\text{MJ} \\ E_{\text{K2ES}}[N-M] &\geq -2\text{MJ} \end{aligned} \quad (5.8)$$

and the terminal constraints at the end of the prediction horizon of one lap are

$$\begin{aligned}
 E_{\text{kin}}[N] &\geq \bar{E}_{\text{kin}}^*[M] \\
 E_{\text{f}}[N] &\leq \bar{E}_{\text{f}}^*[M] + N_{\text{lap}} \cdot \Delta E_{\text{f},0} \\
 E_{\text{b}}[N] &\geq \bar{E}_{\text{b}}^*[M] + N_{\text{lap}} \cdot \Delta E_{\text{b},0} \\
 E_{\text{ES2K}}[N] &\leq \bar{E}_{\text{ES2K}}^*[M] \\
 E_{\text{K2ES}}[N] &\geq \bar{E}_{\text{K2ES}}^*[M] ,
 \end{aligned} \tag{5.9}$$

whereby  $N_{\text{lap}}$  is the current lap number and the optimal state trajectory of a lap under nominal conditions is used as a terminal state constraint. The physical constraints are

$$\begin{aligned}
 \frac{dt}{ds}[k] \cdot v_0 + v[k] \cdot \frac{1}{v_0} &\geq \left\| \frac{2}{\frac{dt}{ds}[k] \cdot v_0 - v[k] \cdot \frac{1}{v_0}} \right\|_2 \\
 E_{\text{kin}}[k] &\geq \frac{1}{2} \cdot m \cdot v[k]^2 \\
 F_{\text{d}}[k] &= F_{\text{a}}[k] + F_{\text{g}}[k] + F_{\text{r}}[k] \\
 F_{\text{a}}[k] &= (c_{\text{d},0} + c_{\text{d},1} \cdot \gamma[\text{mod}_N(k+M)]) \cdot \frac{2}{m} \cdot E_{\text{kin}}[k] \\
 F_{\text{g}}[k] &= m \cdot g \cdot \sin(\theta[\text{mod}_N(k+M)]) \\
 F_{\text{r}}[k] &= c_{\text{r}} \cdot m \cdot g \cdot \cos(\theta[\text{mod}_N(k+M)]) \\
 \frac{dt}{ds}[k] \cdot v_0 + (c_{\text{s},2} \cdot F_{\text{u}}[k] - F_{\text{p}}[k]) \cdot \frac{1}{F_0} &\geq \left\| \frac{2 \cdot \sqrt{-c_{\text{s},1}} \cdot F_{\text{u}}[k] \cdot \sqrt{\frac{v_0}{F_0}}}{\frac{dt}{ds}[k] \cdot v_0 - (c_{\text{s},2} \cdot F_{\text{u}}[k] - F_{\text{p}}[k]) \cdot \frac{1}{F_0}} \right\|_2 \\
 F_{\text{u}}[k] &= F_{\text{e}}[k] + F_{\text{k}}[k] \\
 F_{\text{e}}[k] &= \eta_{\text{e}} \cdot F_{\text{f}}[k] - P_{\text{e},0} \frac{dt}{ds}[k] \\
 F_{\text{h}}[k] &= -\eta_{\text{h}} \cdot F_{\text{f}}[k] \\
 \frac{dt}{ds}[k] \cdot v_0 + (F_{\text{k},\text{dc}}[k] - F_{\text{k}}[k]) \cdot \frac{1}{F_0} &\geq \left\| \frac{2 \cdot \sqrt{\alpha_{\text{k}}} \cdot F_{\text{k}}[k] \cdot \sqrt{\frac{v_0}{F_0}}}{\frac{dt}{ds}[k] \cdot v_0 - (F_{\text{k},\text{dc}}[k] - F_{\text{k}}[k]) \cdot \frac{1}{F_0}} \right\|_2 \\
 \frac{dt}{ds}[k] \cdot v_0 + (F_{\text{h},\text{dc}}[k] - F_{\text{h}}[k]) \cdot \frac{1}{F_0} &\geq \left\| \frac{2 \cdot \sqrt{\alpha_{\text{h}}} \cdot F_{\text{h}}[k] \cdot \sqrt{\frac{v_0}{F_0}}}{\frac{dt}{ds}[k] \cdot v_0 - (F_{\text{h},\text{dc}}[k] - F_{\text{h}}[k]) \cdot \frac{1}{F_0}} \right\|_2 \\
 F_{\text{b}}[k] &= F_{\text{k},\text{dc}}[k] + F_{\text{h},\text{dc}}[k] + P_{\text{aux}} \cdot \frac{dt}{ds}[k] \\
 \frac{dt}{ds}[k] \cdot v_0 + (F_{\text{i}}[k] - F_{\text{b}}[k]) \cdot \frac{1}{F_0} &\geq \left\| \frac{2 \cdot \sqrt{\alpha_{\text{b}}} \cdot F_{\text{b}}[k] \cdot \sqrt{\frac{v_0}{F_0}}}{\frac{dt}{ds}[k] \cdot v_0 - (F_{\text{i}}[k] - F_{\text{b}}[k]) \cdot \frac{1}{F_0}} \right\|_2 ,
 \end{aligned} \tag{5.10}$$

where  $v_0 = 1 \text{ m/s}$  and  $F_0 = 1 \text{ N}$  are normalization constants.

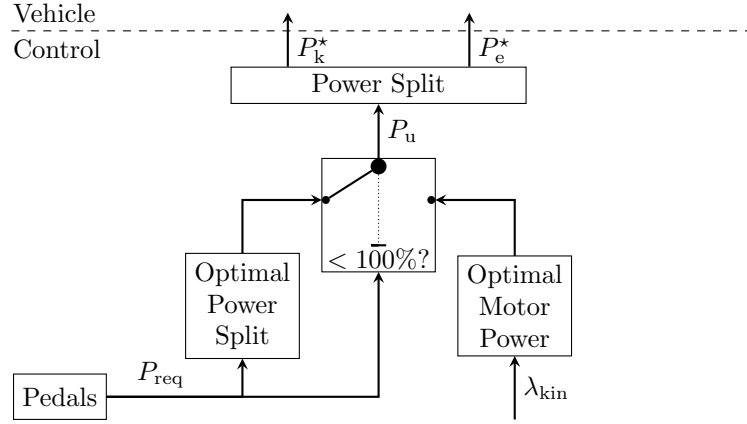


Figure 5.2: Optimal control policy implementation.

## 5.2 High-level MPC Implementation

For the implementation of the control strategies obtained numerically, we rely on the approach presented in Chapter 4, where the time-optimal control policy for the input  $u$  was derived using PMP and was shown to be a sole function of the costate variables  $\lambda$ . These variables represent the sensitivity of lap time towards a perturbation of the corresponding state variables and can be extracted from the numerical solution. The variables  $\lambda_f$ ,  $\lambda_b$ ,  $\lambda_{ES2K}$  and  $\lambda_{K2ES}$  represent the sensitivity of the cost function towards a change in the consumption of fuel, battery, ES2K and K2ES energy, respectively. They are shown to be constant over one entire prediction horizon, since their corresponding state variables, which represent the energy consumption, are not present in the stage cost function, nor in the system dynamics. The first costate variable  $\lambda_{kin}(s)$  is related to the kinetic energy and represents the sensitivity of lap time towards a change in speed at a specific point on the track. It is the only non-constant variable in the optimal control policy and it indicates where to most conveniently deploy propulsive energy. A typical trajectory of this variable is shown in Fig. 4.1 for the circuit of Barcelona. The last four constant costate variables can be treated as given parameters of the optimal control policy. They are used to obtain the optimal ICE and MGU-K power as functions of the kinetic costate variable  $\lambda_{kin}$  as explained in Section 4.2. These optimal functions shown in Fig. 4.2 are piecewise affine and can thus be evaluated using first-order interpolations on the switch values. For the grip-limited region, where the power request must be fulfilled, the piecewise affine optimal power split shown in Fig. 4.4 can be used. This way, the optimal control policy can be implemented on the ECU in compliance with the FIA regulations, for both the power-limited and the grip-limited region, as schematically represented in Fig. 5.2.



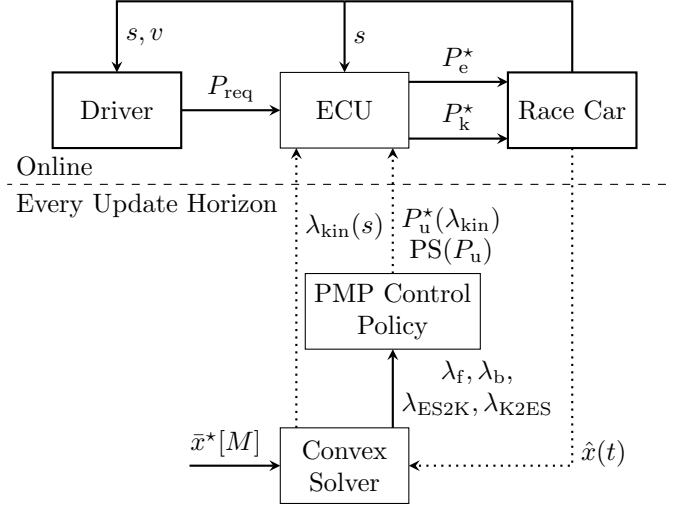


Figure 5.3: Structure of the high-level MPC scheme.

The high-level MPC scheme presented in this chapter updates the control policy on the car in every predefined section of the lap. Analogously to Chapter 3, the numerical optimal control problem presented in Section 5.1 is solved by employing a dedicated second-order conic program solver in about one second. The costate variables  $\lambda$  obtained are then stored, whereby the kinetic costate variable  $\lambda_{\text{kin}}(s)$  is used as a decision variable in the power-limited region, and the constant costate values of  $\lambda_f$  to  $\lambda_{\text{K2ES}}$  serve to evaluate the optimal motor power and the optimal power split to be used in real-time. A schematic representation of the high-level MPC scheme is supplied in Fig. 5.3.

### 5.3 Low-level Optimality Tracking Zone MPC

The high-level MPC scheme presented in the Sections 5.1 and 5.2 above can be used to periodically update the energy management strategies. Specifically, in the so-called grip-limited region, where the power requested by the driver must be provided, the power split is used to trade fuel with electrical energy and the driver is responsible for following the lap time optimal speed trajectory, which corresponds to the maximum speed profile. Therefore, in the grip-limited region, an occasional update of the power split – for instance, every sector of the track – is enough to balance any deviations in terms of consumption. In the power-limited region, where the 100% power request of the driver can be overwritten, the energy management system can act as a thrust controller and trade speed and lap time against energy consumption. Therefore, in the power-limited region, the feedback control system is responsible for tracking the lap time optimal strategies and must be able to react quickly to external disturbances. The necessary update frequency to comply with such a requirement cannot be achieved with the high-level MPC, due to its mathematical complexity. In order to comply with the 100 Hz feedback sampling frequency allowed by the FIA, a MPC algorithm that can be efficiently solved one magnitude faster is to be designed for the power-limited region, where the power delivered by the ICE and the MGU-K can be chosen independently. Considering race conditions, the following assumptions are made: The terminal constraint on the ES2K energy is always inactive and the K2ES energy does not change significantly in the power-limited regions. This way, the only relevant state variables to be controlled on the straights are the kinetic, the fuel, and the battery energy, i.e.,  $x = (E_{\text{kin}}, E_{\text{f}}, E_{\text{b}})^{\top}$ . Once again, the problem is formulated in the space domain, whereby the input variables are the ICE and the MGU-K force, i.e.,  $u = (F_{\text{e}}, F_{\text{k}})^{\top}$ . The system is linearized around the optimal trajectories  $(x^*, u^*)$ , whereby the state-space matrices are kept constant at their mean value, as they can be shown not to vary significantly. The deviations from the optimal trajectories obtained with the high-level MPC scheme are defined as

$$\begin{aligned}\delta x &:= x - x^* \\ \delta u &:= u - u^* .\end{aligned}\tag{5.11}$$

The linearized dynamics are obtained as

$$\delta x[k+1] = A\delta x[k] + B\delta u[k] ,\tag{5.12}$$

whereby the computation of the matrices  $A$  and  $B$  can be found in Appendix A.4. The objective is to track the optimal state trajectories generated by the high-level MPC, but from a unilateral side, since positive deviations, such as a lower fuel consumption and a higher battery state of energy, do not have to be penalized and corrected if such an action is not optimal for the lap time. Therefore, a zone MPC scheme is designed, in which

instead of points time-varying sets are tracked. The weights of the stage cost function of the MPC algorithm are based on the following rationale: The use of constant weights would result in a controller that would trade speed for consumptions, independent of the position, and therefore ignore the impact of such actions on lap time. For a general optimal control problem, the costate variables represent the sensitivity of the cost-to-go function with respect to a deviation in the corresponding state variables [21], [93], i.e., they can be used to approximate how a perturbation  $\delta x$  in the state variables would change the cost-to-go value  $J$  in the best-case-scenario as

$$J^*(s, \delta x(s) + x^*(s)) - J^*(s, x^*(s)) \approx \lambda^*(s)^\top \delta x(s) . \quad (5.13)$$

Therefore, in order to track minimum lap time strategies, the costate variables of the optimization problem (2.17) can be used as weights in the stage cost function as

$$l(\delta x(s), \delta u(s)) = \lambda^*(s)^\top \delta x(s) . \quad (5.14)$$

Combining the fact that this approximation is valid for small deviations with the willingness of not penalizing a lower fuel or battery consumption, we define the following MPC optimization problem:

$$\begin{aligned} \min_{\delta u} \quad & \sum_{k=1}^n \tilde{\lambda}_{\text{kin}}^*[k] \cdot \delta E_{\text{kin}}[k] + \lambda_{\text{f}}^* \cdot \varepsilon_{\text{f}}[k] - \lambda_{\text{b}}^* \cdot \varepsilon_{\text{b}}[k] \\ \text{s.t.} \quad & \varepsilon_{\text{f}}[k] \geq \delta E_{\text{f}}[k], \quad \varepsilon_{\text{f}}[k] \geq 0 \\ & \varepsilon_{\text{b}}[k] \geq -\delta E_{\text{b}}[k], \quad \varepsilon_{\text{b}}[k] \geq 0 \\ & \delta x[k+1] = A \cdot \delta x[k] + B \cdot \delta u[k] \\ & \delta x[k] + \tilde{x}^*[k] \in \mathcal{X}, \quad \delta u[k] + \tilde{u}^*[k] \in \mathcal{U} \\ & \delta x[0] = \hat{x}(t) - \tilde{x}^*[0] , \end{aligned} \quad (5.15)$$

where the slack variables  $\varepsilon$  are employed for the unilateral tracking of the optimal consumption trajectories, the notation

$$\tilde{p}[k] = p[M+k] + (p[M+k+1] - p[M+k]) \cdot \frac{\hat{s}(t) - M \cdot \Delta s}{\Delta s} \quad (5.16)$$

denotes the trajectory of  $p$  shifted in order to start at the measured position  $\hat{s}(t)$ , and  $M$  is defined as in (5.1). The implementation of this MPC algorithm in the control loop is shown in Fig. 5.4.

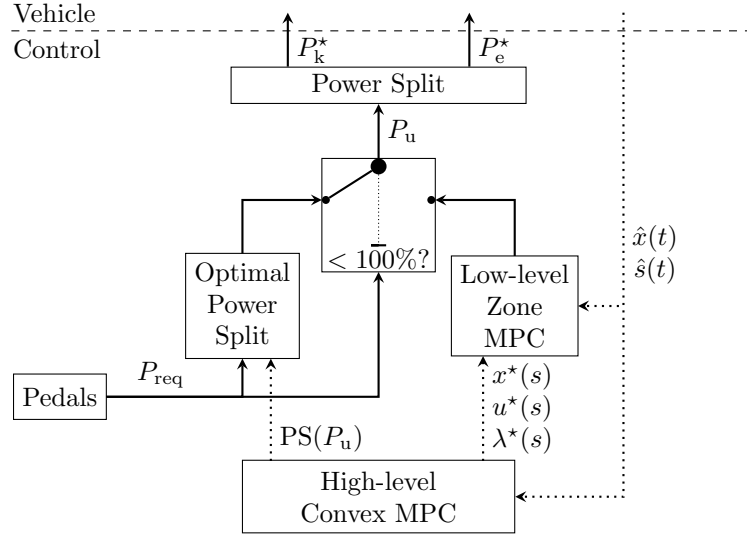


Figure 5.4: Structure of the two-level MPC scheme.

## 5.4 Numerical Results

This section presents the results obtained by implementing the two-level MPC scheme on the two simulators from Section 2.3. First, two different disturbances that will be used to test the feedback behaviour are introduced. Thereafter, the behaviour of the two-level MPC is compared on a benchmark simulator with the feedforward controller presented in Chapter 4. Finally, the results obtained on a third-party high-fidelity simulator are shown over a single lap as well as over multiple laps. All simulations are carried out using the circuit of Barcelona, with a nominal fuel load  $r_f = 100\%$ , i.e.,  $\Delta E_{f,0}$  defined as in (2.19) each lap, and in charge-sustained operation, i.e.,  $\Delta E_{b,0} = 0$  MJ, as this was shown in Section 3.3 to be the lap time optimal strategy over multiple laps. The high-level MPC optimization problem was solved with the solver ECOS [85] at the beginning of every sector of the track, i.e., every third of the track. The low-level MPC algorithm was implemented using FORCES Pro [94] with a sampling rate of 100 Hz.

### Disturbances

Two different types of disturbance that can occur during a race are considered: an unexpected braking event and a fresh tires scenario. For the unexpected braking event, the maximum kinetic energy curve is the same as the nominal one, except on a straight in the middle of the lap, where the car is forced to brake suddenly and is able to fully re-accelerate after a short stretch. This change in the maximum kinetic energy line is shown in Fig. 5.5. In the fresh tires scenario, the enhanced grip of the tires mounted allow the

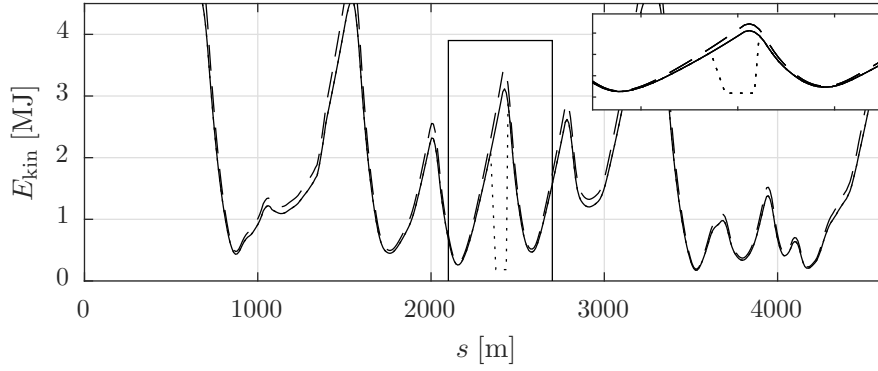


Figure 5.5: Maximal kinetic energy curve for the nominal case (solid), the unexpected braking event (dotted) and the fresh tires scenario (dashed).

car to corner at a higher speed. This scenario is shown in Fig. 5.5 and is simulated by setting the maximum kinetic energy line 10% higher than the nominal one.

### Benchmark Simulator

In this subsection the two-level MPC presented is tested on the benchmark simulator described in Section 2.3 in the presence of an unexpected braking event. This test allows a direct comparison of the behaviour of the feedback controller with the globally optimal solution computed for the specific disturbance scenario, using the approach presented in Chapter 3. As shown in Fig. 5.6 and 5.7, the state and input trajectories achieved with the feedback controller are closer to the optimal ones, especially in the region of acceleration right after the unexpected braking phase: The feedforward controller cuts the engine and MGU-K power, since it expects to be at the end of the straight, while the two-level MPC delivers maximal power due to the velocity gap. Accordingly, the fuel and battery drifts at the end of the lap, as well as the lap time difference, are negligible if the two-level MPC is used.

### High-fidelity Nonlinear Simulator

The benchmark simulator presented in Section 2.3 uses the same model for optimization and simulation and thus allows to benchmark the solutions obtained against the global optimum, but it does not allow the achievable performance to be measured. In order to test the proposed algorithms in a more realistic scenario, the two-level MPC controller is now implemented on a third-party high-fidelity nonlinear simulator. Figs. 5.8 and 5.9 compare the results obtained from using the two-level MPC controller together with the nonlinear simulator against the global optimal benchmark solution for the unexpected braking event and fresh tires scenarios, respectively. The two-level MPC controller is able to reject the disturbances reasonably well, whereby the drift observable in the battery energy trajectory is mainly due to model mismatch. Fig. 5.10 and 5.11 compare the performance of four types of controllers evaluated on the high-fidelity nonlinear simulator over several laps for both disturbance scenarios. In the case of the unexpected braking

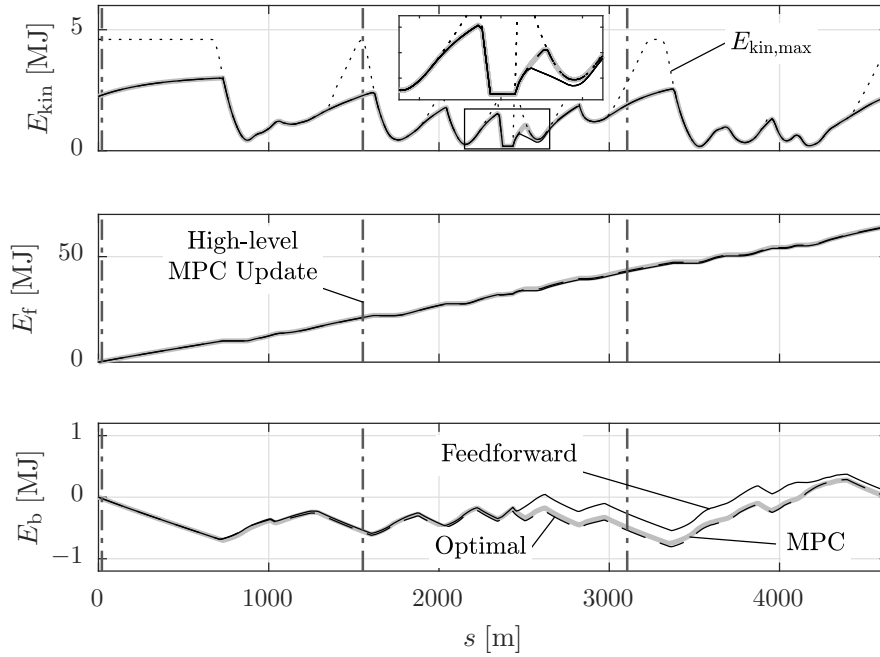


Figure 5.6: State trajectories over one lap for the unexpected braking event on the benchmark simulator.

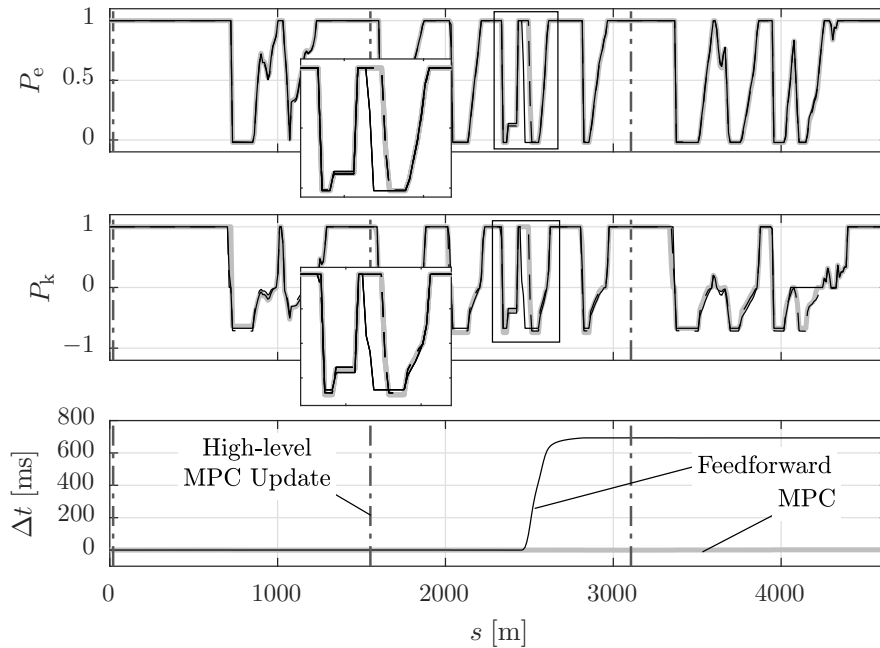


Figure 5.7: Normalized input trajectories and lap time difference over one lap for the unexpected braking event on the benchmark simulator.

event scenario, the disturbance occurs in the first lap only, whereas in the fresh tires scenario the disturbance occurs during every lap. The lower lap time observed in the first lap of the latter scenario is due to the fact that the initial speed is set equal to the one

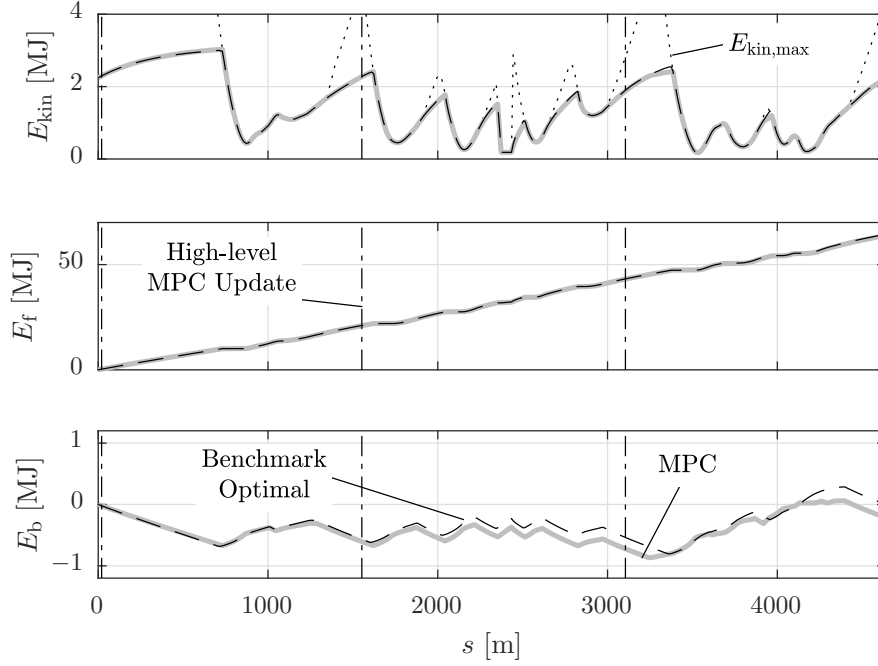


Figure 5.8: State trajectories over one lap for the unexpected braking event on the high-fidelity nonlinear simulator.

of the optimal solution for the benchmark simulator, which does not coincide with the slower velocity achieved at the finish line in the subsequent laps. The pure feedforward controller is not able to reject the disturbances and therefore yields a sub-optimal lap time during the first lap and significant drifts in terms of fuel and battery energy over the remaining laps. Using either the high-level MPC or the low-level MPC leads to a slight improvement over the pure feedforward solution, but there are still significant lap time losses or drifts in the consumptions. In fact, if the high-level MPC algorithm is not able to cope with unexpected disturbances, as shown in Fig. 5.10 by the slower lap time achieved in the first lap due to the braking event, the low-level MPC scheme cannot properly adapt the energy management, such as in the case of a higher maximum speed profile arising from the fresh tires, as shown in Fig. 5.11 by the larger deviations in the consumptions. Only the combination of the high- and the low-level MPC in the proposed two-level MPC structure yields satisfactory results in terms of lap time and disturbance rejection.

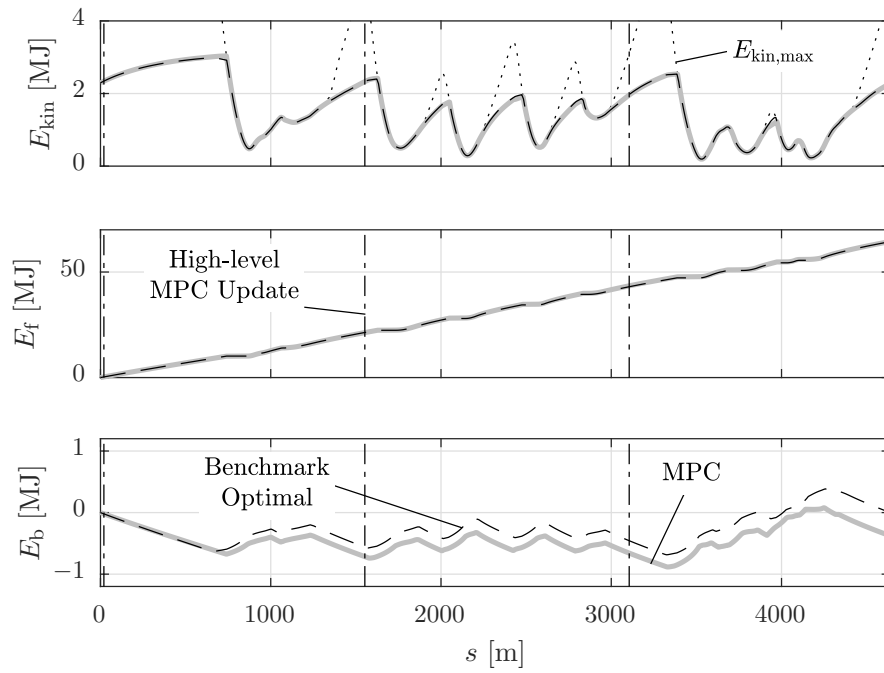


Figure 5.9: State trajectories over one lap for the fresh tires scenario on the high-fidelity nonlinear simulator.

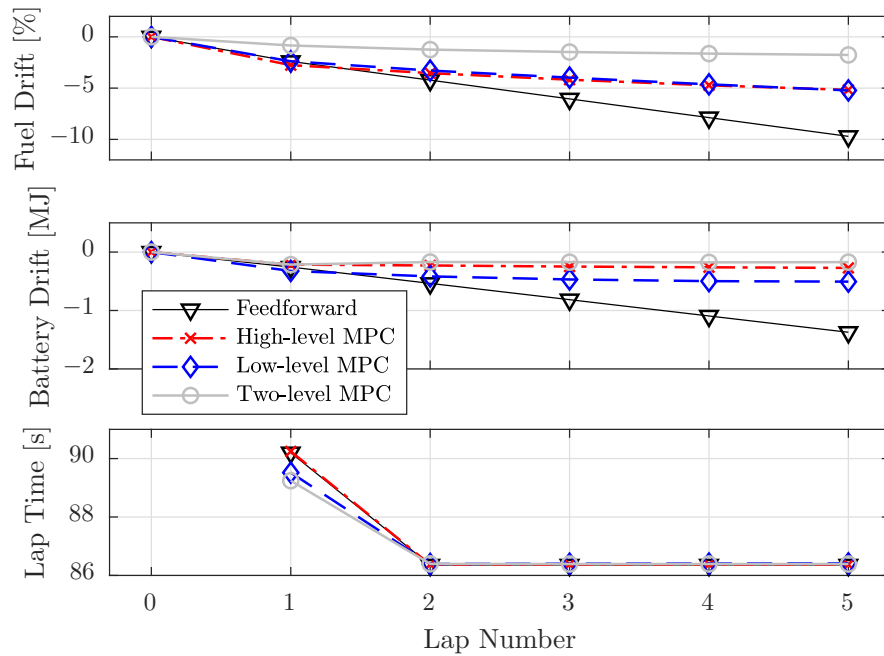


Figure 5.10: Lap time and fuel and battery drifts measured over multiple laps for the unexpected braking event (occurring only in the first lap) on the high-fidelity nonlinear simulator.



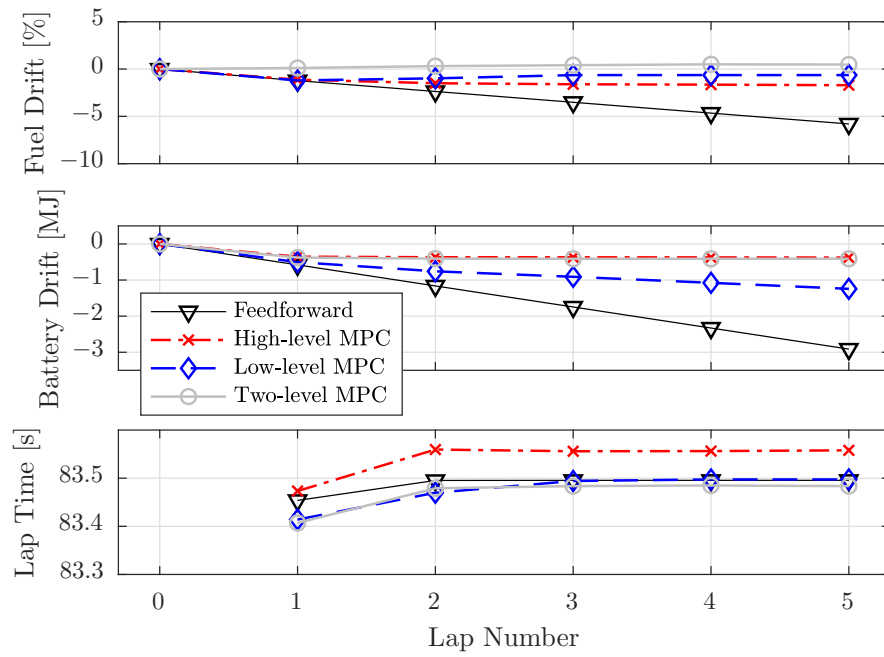


Figure 5.11: Lap time and fuel and battery drifts measured over multiple laps for the fresh tires scenario on the high-fidelity nonlinear simulator.



# 6

## Equivalent Lap Time Minimization Strategies

In this chapter we synthesize control strategies inspired to ECMS [19], namely, Equivalent Lap Time Minimization Strategies (ELTMS), whereby we adjust the optimal control policy derived in Chapter 4 using three PID controllers acting on an equivalent reformulation of the consumption costate variables of the problem. Once again, the notation  $(\bar{\cdot})^*$  denotes the optimal trajectory under nominal conditions. These results can be found in [4].

## 6.1 Controller Structure

The optimal trajectory of the kinetic costate variable  $\lambda_{\text{kin}}(s)$  is not significantly affected by changes in energy budgets, i.e., the values  $\Delta E_{f,0}$  and  $\Delta E_{b,0}$  chosen for a specific lap [5]. Therefore, we do not control its trajectory but use it as a given exogenous variable. Nevertheless, a robustification is necessary. If, exiting a corner, the driver would go at full throttle earlier than expected, the car would be in a power-limited region where the kinetic costate variable is almost zero. Accordingly, very little power would be deployed at the beginning of the subsequent straight with a consequent non-negligible lap time loss. Driven by this rationale, we modify the trajectory of the kinetic costate variable in the nominal grip-limited regions as follows: As Fig. 6.1 shows, between the apex of a corner, coinciding with the local minimum of the speed profile, and the end of the grip-limited region containing it, the value of the kinetic costate variable is set equal to its value at the beginning of the next power-limited region. This way, if the driver was to require maximum power earlier than expected, the powertrain would deploy the same amount of power as at the beginning of the power-limited region under nominal conditions. Conversely, no effect would be noticed if the driver required less than 100% power, since in that case such a power request would be met, ignoring the value of the kinetic costate variable  $\lambda_{\text{kin}}$ . Since we are focusing on race scenarios, the ES2K terminal constraint is inactive, as shown in Section 3.3 and, due to (4.12), we have  $\lambda_{\text{ES2K}} = 0$ .

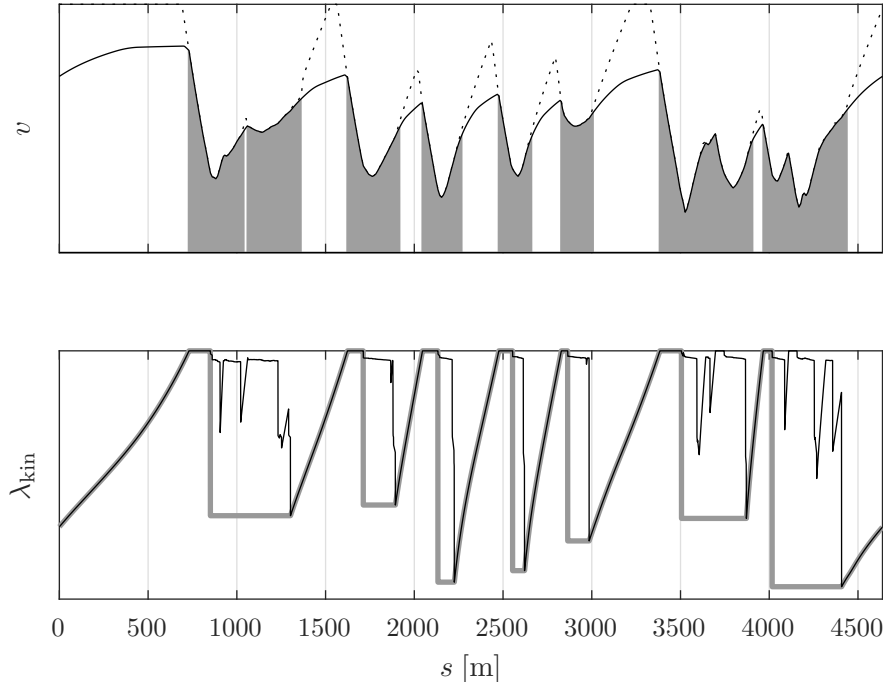


Figure 6.1: Maximum (dotted) and optimal speed profile together with the power-limited (white) and the grip-limited (grey) regions. Nominal (black) and robustified (grey) kinetic costate variable  $\lambda_{\text{kin}}$ .

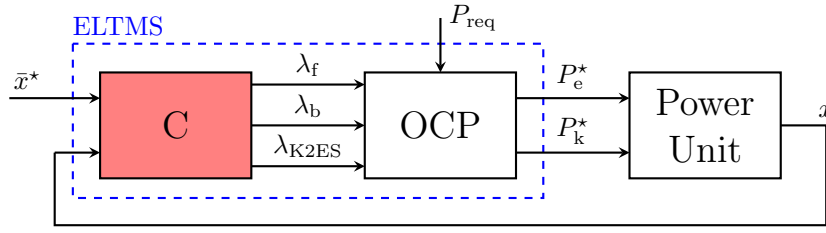


Figure 6.2: Structure of the equivalent lap time minimization strategies (ELTMS). A controller is responsible for tracking the nominal state trajectories  $\bar{x}^*$  by adapting the costate variables, which determine the optimal control policy (OCP) shown in Fig. 4.5.

## 6.2 Controller Design

As in Chapter 4, the input is given by  $u = (P_f, P_k, P_{brk})^\top$  and the input constraint set is  $\mathcal{U} = [0, P_{f,\max}] \times [P_{k,\min}, P_{k,\max}] \times [0, P_{brk,\max}]$ . We define the control Hamiltonian  $\tilde{H}(u, \lambda)$ , whereby only the input-dependent components of the Hamiltonian (4.8) are given and  $\lambda_{\text{ES2K}} = 0$ , as

$$\tilde{H}(u, \lambda) := \lambda_{\text{kin}} \cdot P_p(u) + \lambda_f \cdot P_f(u) - \lambda_b \cdot P_1(u) + \lambda_{\text{K2ES}} \cdot P_{\text{K2ES}}(u) + \Psi_{\mathcal{U}}(u) . \quad (6.1)$$

Considering the kinetic costate trajectory as given, the only parameters affecting the optimal control policy shown in Fig. 4.5 are the constant costate variables related to fuel, battery, and K2ES consumption  $\lambda_f$ ,  $\lambda_b$  and  $\lambda_{\text{K2ES}}$ , respectively. Therefore, we design ELTMS to adapt these costate variables in order to track precomputed nominal state trajectories  $\bar{x}^*$ , as shown in Fig. 6.2. An intuitive approach would be to build three SISO control loops or a unique MIMO controller which would relate each costate to its corresponding state variable. However, such an approach lacks in performance, owing to the non-smooth nature of the energy management: In the grip-limited region, there is only one degree of freedom, namely the power split, and the sporting regulations allow the energy management system to decide how to trade fuel with battery charge. In the power-limited region, the additional degree of freedom granted by the thrust control allows lap time to be traded for energy consumption.

Motivated by such a rationale, and similarly to multivariable ECMS [45], we reformulate the costate variables. First, we define a lap time equivalence factor  $q_t \geq 0$ , and the fuel-to-electricity weight  $q_f \in [0, 1]$  as well as the K2ES-to-battery weight  $q_{\text{K2ES}} \in [0, 1]$ . Then, we express the fuel, battery, and K2ES costate variables as

$$\begin{aligned} \lambda_f &= q_t \cdot q_f \\ \lambda_b &= -q_t \cdot (1 - q_f) \cdot (1 - q_{\text{K2ES}}) \\ \lambda_{\text{K2ES}} &= -q_t \cdot (1 - q_f) \cdot q_{\text{K2ES}} , \end{aligned} \quad (6.2)$$

and substitute them in the control Hamiltonian (6.1) as

$$\begin{aligned} \tilde{H}(u, \lambda) := & \lambda_{\text{kin}} \cdot P_p(u) + q_t \cdot (q_f \cdot P_f(u) + (1 - q_f) \cdot ((1 - q_{\text{K2ES}}) \cdot P_i(u) - q_{\text{K2ES}} \cdot P_{\text{K2ES}}(u))) \\ & + \Psi_{\mathcal{U}}(u) . \end{aligned} \quad (6.3)$$

Defining the weighted consumption power as

$$P_c(u, q_f, q_{\text{K2ES}}) = q_f \cdot P_f(u) + (1 - q_f) \cdot ((1 - q_{\text{K2ES}}) \cdot P_i(u) - q_{\text{K2ES}} \cdot P_{\text{K2ES}}(u)) , \quad (6.4)$$

the control Hamiltonian (6.3) can be expressed as

$$\tilde{H}(u, \lambda) = \lambda_{\text{kin}} \cdot P_p(u) + q_t \cdot P_c(u, q_f, q_{\text{K2ES}}) + \Psi_{\mathcal{U}}(u) . \quad (6.5)$$

Some comments are in order. First, the control Hamiltonian (6.5) shows that the equivalence factor  $q_t$  defines the trade-off between lap time and consumption. In fact, it affects only the power-limited regions where the kinetic costate variable  $\lambda_{\text{kin}}$  is used to determine how much power to provide with both the ICE and the MGU-K as shown in Fig. 4.2. In the grip-limited regions, the amount of power to be delivered is determined by the driver and the equivalence factor  $q_t$  has no impact on the power split displayed in Fig. 4.4: The trade-off between fuel and electric energy consumption is solely determined by the weights  $q_f$  and  $q_{\text{K2ES}}$ . Second, deviations in fuel and K2ES energy profiles are to be expected only in the grip-limited regions, since on the straights the ICE is almost always operated at full power and the MGU-K is not used in generator mode, i.e., by braking the ICE. These observations allow us to define the control loops as follows: We use the equivalence factor  $q_t$  in the power-limited regions to control the weighted energy consumption

$$E_c(E_f, E_b, E_{\text{K2ES}}, q_f, q_{\text{K2ES}}) = q_f \cdot E_f - (1 - q_f) \cdot ((1 - q_{\text{K2ES}}) \cdot E_b + q_{\text{K2ES}} \cdot E_{\text{K2ES}}) \quad (6.6)$$

such that it tracks its nominal trajectory

$$\bar{E}_c^* = E_c(\bar{E}_f^*, \bar{E}_b^*, \bar{E}_{\text{K2ES}}^*, q_f, q_{\text{K2ES}}) . \quad (6.7)$$

In the grip-limited region, we use the weights  $q_f$  and  $q_{\text{K2ES}}$  to control the fuel and the K2ES energy  $E_f$  and  $E_{\text{K2ES}}$ . These three SISO control loops can be handled with standard PID controllers that are active only in the power-limited or grip-limited regions, as illustrated in Fig. 6.3. To summarize, a PID controller uses the lap time equivalence factor  $q_t$  as an actuator in power-limited regions to stabilize the deviation in weighted energy consumption  $\delta E_c = E_c - \bar{E}_c^*$ , whereas the weights  $q_f$  and  $q_{\text{K2ES}}$  are used by two PID controllers in grip-limited regions to stabilize the fuel and K2ES deviations  $\delta E_f = E_f - \bar{E}_f^*$  and  $\delta E_{\text{K2ES}} = E_{\text{K2ES}} - \bar{E}_{\text{K2ES}}^*$ , respectively.

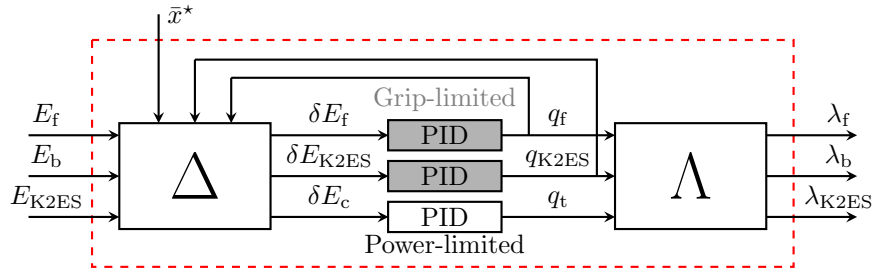


Figure 6.3: Controller of the ELTMS shown in Fig. 6.2 for the adaptation of the costate variables. The  $\Delta$  block computes the value of  $E_c$  as in (6.6) and the deviations of this variable, the fuel and the K2ES energy from their nominal trajectories. The PIDs of fuel and K2ES (grey) operate only in grip-limited regions, whereas the PID of the energy consumption (white) operates only in power-limited regions. The  $\Lambda$  block computes the variables  $(\lambda_f, \lambda_b, \lambda_{K2ES})$  from the values of  $q_t$ ,  $q_f$ , and  $q_{K2ES}$ , as in Eq. (6.2).

### 6.3 Numerical Results

This section presents the results obtained by implementing the ELTMS on the benchmark simulator from Section 2.3 in the presence of a realistic race disturbance. As in Section 5.4, we simulate the car mounting fresh tires, which allow the driver to corner faster than expected. This effect is simulated by increasing the maximum kinetic energy profile by 10%, as shown in Fig. 5.5. We compare the proposed feedback control scheme with the two-level MPC scheme presented in Chapter 5 on both simulators introduced in Section 2.3 over multiple laps. All simulations were carried out using the circuit of Barcelona, with a nominal fuel load of  $r_f = 100\%$ , and in charge-sustained battery operation  $\Delta E_{b,0} = 0$  MJ.

#### Benchmark Simulator

In this section, we implement the ELTMS controller and the two-level MPC scheme presented in Chapter 5 on the benchmark simulator and compare their performance to the globally optimal solution computed numerically for each disturbance, using the framework presented in Chapter 3. Figures 6.4 and 6.5 show the state and input trajectories in the first lap. The tracking performance of the ELTMS algorithm is comparable to that of the MPC, and both show a close-to-optimal behaviour in terms of lap time deviation from the optimal solution. The ELTMS has a faster lap time than the MPC, while drifting more in terms of battery consumption. Figure 6.6, however, demonstrates that with both algorithms the solution converges close to the desired energy budgets while avoiding any dangerous drifts. Moreover, the ELTMS appears to perform better than the MPC in terms of lap time, losing less than 20 milliseconds per lap with respect to the global optimum.

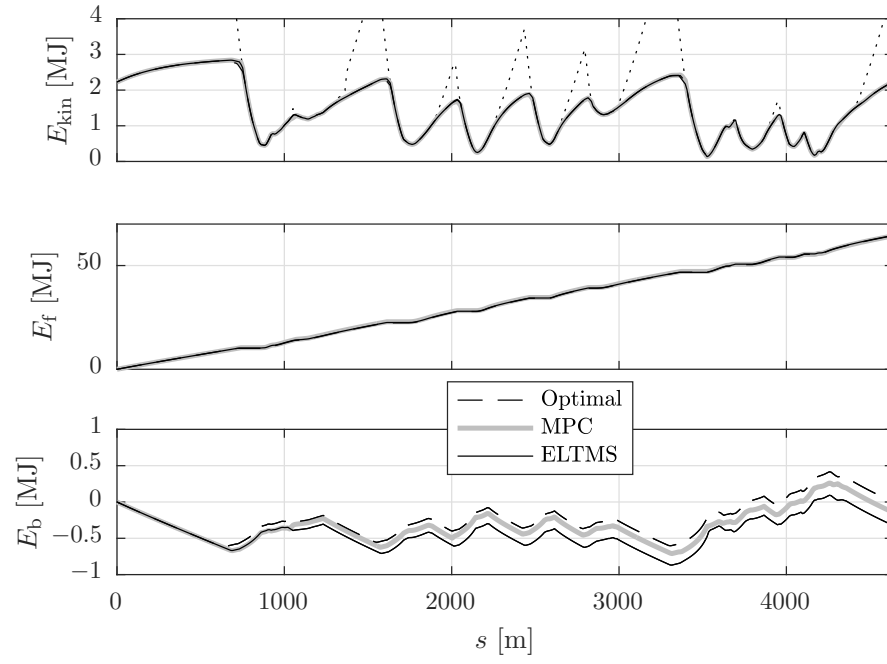


Figure 6.4: State trajectories over one lap for the fresh tires scenario.

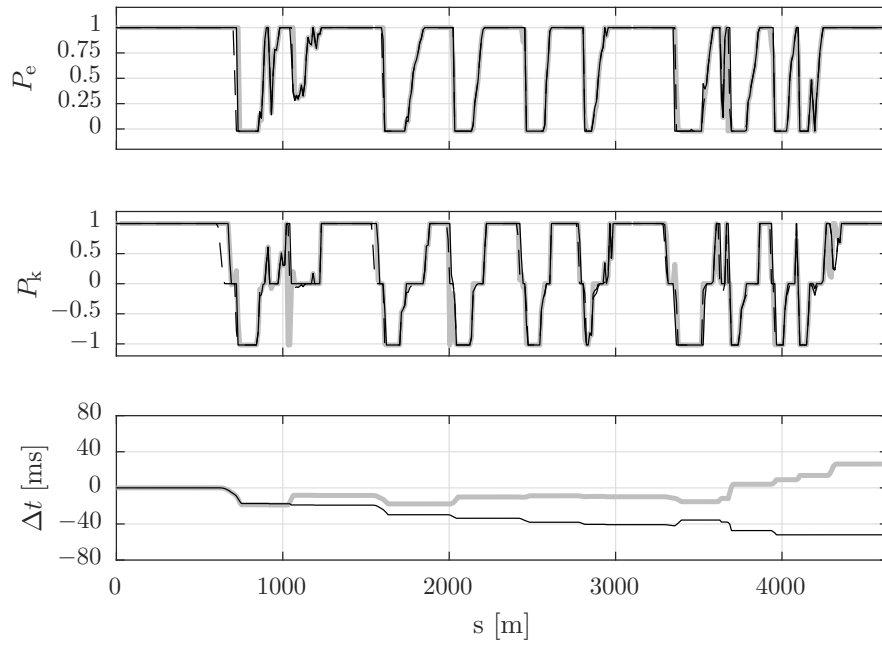


Figure 6.5: Normalized input trajectories and lap time difference over one lap for the fresh tires scenario.



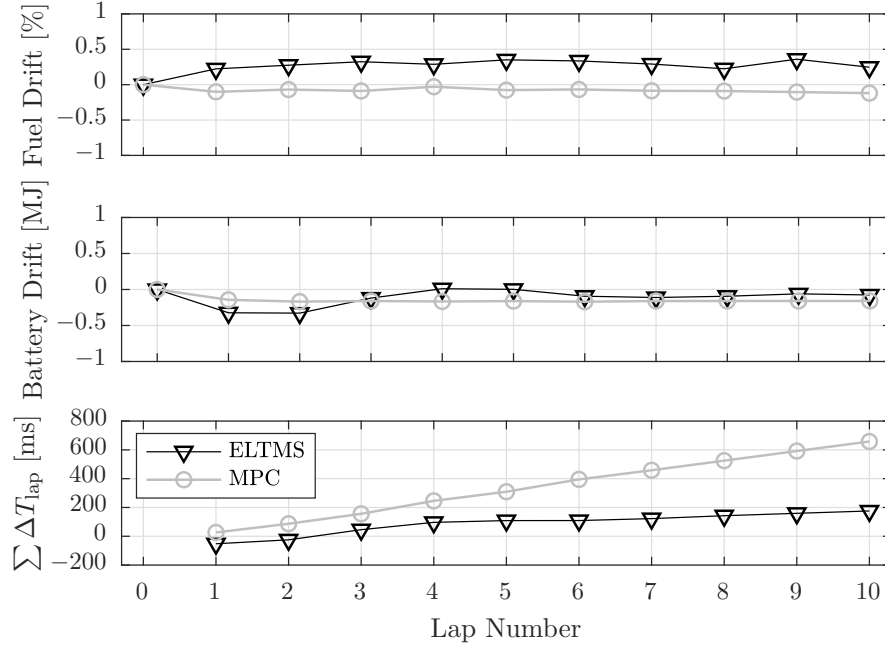


Figure 6.6: Fuel, battery, and cumulative lap time drift with respect to the globally optimal solution for the fresh tires scenario.

### High-fidelity Nonlinear Simulator

In order to test the ELTMS controller presented, we implement it on the high-fidelity nonlinear simulator introduced in Section 2.3 and compare its performance to the one achieved by the two-level MPC scheme designed in Chapter 5. Figure 6.7 shows the trajectory of the kinetic energy, the fuel and the battery energy achieved by the ELTMS controller and the MPC scheme, together with the global optimum computed for the benchmark simulator as a reference, but it does not represent the optimal solution for the nonlinear simulator. Figure 6.8 shows the results achieved over ten laps. Overall, the ELTMS controller performs better than the MPC scheme, exhibiting similar drifts in terms of fuel and battery consumption, but achieving slightly faster lap times.

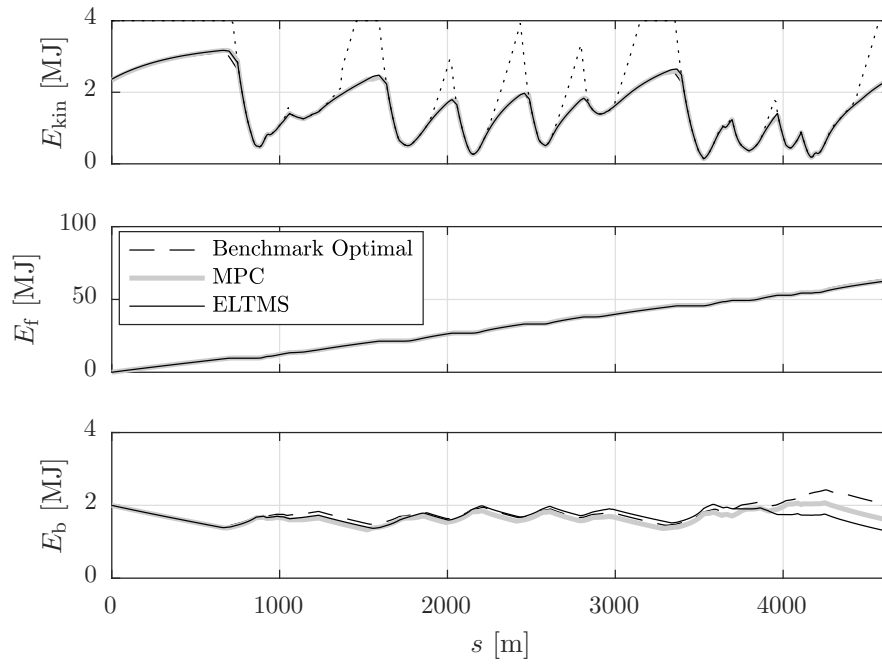


Figure 6.7: Kinetic, fuel and battery energy on the high-fidelity nonlinear simulator for the fresh tires scenario.

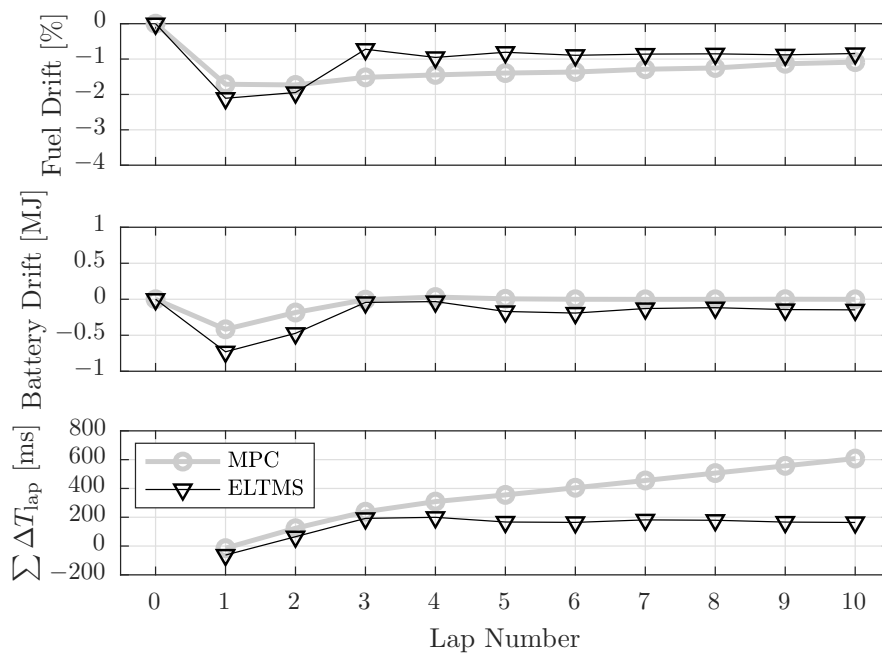


Figure 6.8: Fuel, battery and cumulative lap time drift with respect to the benchmark solution on the high-fidelity nonlinear simulator for the fresh tires scenario.

## Conclusion and Future Directions

In this thesis we presented models and control algorithms for the time-optimal energy management of the Formula 1 (F1) hybrid electric power unit. First, we developed an efficient methodology to numerically compute the time-optimal control strategies. The system dynamics were derived, validated and expressed in a convex form. This structure facilitates the rapid computation of the optimal strategies, and therefore also allows for parameter studies, which play a significant role in the choice of the best vehicle configuration and energy management approach for each track and for both race and qualifying scenarios. Second, we analytically derived the time-optimal control policy by combining Pontryagin's Minimum Principle (PMP) with non-smooth convex analysis, in order to implement the optimal solution on the car in real-time and in accordance with the sporting regulations. This policy was shown to be a piecewise affine function of one particular costate variable that corresponds to the kinetic energy of the vehicle. Therefore, nine characteristic values are sufficient to fully describe the optimal control policy for a given racing scenario and allow the optimal inputs to be determined in power- and grip-limited regions. Moreover, every strategy related to a specific energy budget can be stored within one position-dependent and four constant costate variables. Third, we turned our attention to the synthesis of feedback control algorithms, that can be implemented in real-time. We presented a two-level MPC scheme which consists of a high-level MPC that periodically updates the optimal strategies in the course of the lap and a low-level zone MPC algorithm that tracks them in a minimum-lap-time fashion. Fourth, we presented equivalent lap time minimization strategies (ELTMS) with the scope of achieving the same performance as the two-level MPC, whilst avoiding its computational burden. To take the non-smooth nature of the problem into account, we leveraged PMP to adapt the optimal control policy online with simple PID controllers. We tested both control algorithms in the presence of disturbances typical for a F1 race. The optimality of the feedback controllers presented was verified on a benchmark simulator, whereby a close-to-optimal behaviour was observed. The implementation on a high-fidelity nonlinear simulator of the vehicle provided satisfying results, and a robust behaviour was observed over subsequent laps.

This work opens the field for several possible extensions. First, the feedback controllers presented should be combined with parameter estimation algorithms in order to adapt the model parameters to the current state of the racetrack and of the car, as well as to

the driver's mood, feeling and style. A preliminary study is to be found in [6]. Second, we would like to study the energy management strategies for the entire race, explicitly considering pit-stops and possible safety-car scenarios. It would be worth extending the optimal control problem presented to account for stochastic effects. Third, it would be challenging to extend the traffic-free model employed to account for the presence of opponents. To this end, we would like to consider game-theoretical aspects to understand how to best interact with the drivers of other teams, depending on the stage of the race and on the state of the car. Fourth, the algorithms presented should be extended to qualifying scenarios, where fuel consumption is not restricted and the boundary conditions are different, since in such a scenario it is of paramount importance to quickly react to exogenous disturbances and maximize the efforts on the single flying lap. A preliminary study can be found in [7]. Fifth, we recognize the importance of extending the quasi-static model of the internal combustion engine (ICE) to take transient phenomena into account and exploit the vast potential offered by the prime mover of the F1 car. We would like to tackle the low-level optimal control of the ICE numerically. A preliminary study has been carried out in [8]. Thereafter, we would like to study the optimal solutions and devise control policies to operate the engine in a lap-time-optimal way, whereby nonlinear MPC techniques might be applied in real-time. Finally, it could be advantageous to study the interaction of such a framework with the one presented in this thesis in order to couple and implement them in the most favourable way. Last, but not least, we hope to see Scuderia Ferrari and her drivers shine in the F1 championship in the years to come.

*Forza Ferrari!*

# A

## Appendix

### A.1 Second-order Conic Constraints

A convex optimization problem can be written as

$$\begin{aligned} & \min_x f(x) \\ & \text{subject to } g(x) = 0 \\ & \quad h(x) \leq 0 \end{aligned} \tag{A.1}$$

where the objective function  $f(x)$  is convex in  $x \in \mathbb{R}^n$ . The function  $g(x)$  is affine in  $x$ , whereas  $h(x)$  is convex in  $x$ . Robust and efficient algorithms are available to solve (A.1) with global optimality guarantees [95].

A special case of convex inequality constraints is the second-order conic constraint

$$\|Ax + b\|_2 \leq c^\top x + d \ , \tag{A.2}$$

with  $A \in \mathbb{R}^{m \times n}$ ,  $b \in \mathbb{R}^m$ ,  $c \in \mathbb{R}^n$ , and  $d \in \mathbb{R}$ . A geometric mean inequality constraint

$$\sqrt{x_1 \cdot x_2} \geq x_3 \ , \tag{A.3}$$

where  $x_i \in \mathbb{R}_+$ , can be formulated as a second-order conic constraint as follows:

$$\left\| \begin{array}{c} 2 \cdot x_3 \\ x_1 - x_2 \end{array} \right\|_2 \leq x_1 + x_2 \ . \tag{A.4}$$

This result is frequently used in Chapter 3. Note that specialized methods are required to solve convex optimization problems with second-order conic constraints, such as [85]. However, these conic programs can be solved in roughly the same time as quadratically constrained linear programs of the same size. Further material is to be found in [96]–[98].

## A.2 Non-smooth Pontryagin's Minimum Principle

Consider the optimization problem

$$\begin{aligned} J^*(0, x_0) &= \min_u \int_0^T g(x(t), u(t)) dt + h(x(T)) \\ \text{s.t. } \dot{x}(t) &= f(x(t), u(t)) \quad \forall t \in [0, T] \\ x(0) &= x_0 \quad , \end{aligned} \tag{A.5}$$

where  $x(t) \in \mathbb{R}^n$  are the state variables,  $u(t) \in \mathbb{R}^m$  are the input trajectories,  $g(\cdot)$  is the stage cost function,  $h(\cdot)$  the terminal cost function, and  $f(\cdot)$  the function describing the system's dynamics. This problem can be solved using PMP by defining the Hamiltonian as

$$H(x, u, \lambda) = g(x, u) + \lambda^\top f(x, u) \quad , \tag{A.6}$$

where the trajectories of the optimal state variables and co-state variables  $\lambda(t) \in \mathbb{R}^n$  are subject to

$$\begin{cases} \dot{x}^*(t) = \left( \frac{\partial}{\partial \lambda} H(x^*(t), u^*(t), \lambda(t)) \right)^\top \\ x^*(0) = x_0 \\ \dot{\lambda}(t) = - \left( \frac{\partial}{\partial x} H(x^*(t), u^*(t), \lambda(t)) \right)^\top \\ \lambda(T) = \left( \frac{\partial}{\partial x} h(x^*(T)) \right)^\top . \end{cases} \tag{A.7}$$

Assuming uniqueness of the optimal solution, at every point in time  $t \in [0, T]$  the optimal input  $u^*(t)$  can be found using the necessary condition of optimality

$$u^*(t) = \underset{u}{\operatorname{argmin}} H(x^*(t), u, \lambda(t)) \quad . \tag{A.8}$$

Moreover, if the Hamiltonian is strictly convex in  $u$ , the unique minimizer is found as

$$\frac{\partial}{\partial u} H(x^*(t), u, \lambda(t)) \Big|_{u=u^*(t)} = 0 \quad . \tag{A.9}$$

In order to deal with inequality constraints, a Lagrangian function can be constructed, defining complementary multipliers, and minimized, imposing several complementarity conditions, as shown in [99]. An equivalent solution consists of including the hard con-

straints in the cost functions using the indicator function

$$\Psi_{\mathcal{X}}(x) = \begin{cases} 0 & \text{if } x \in \mathcal{X} \\ \infty & \text{if } x \notin \mathcal{X} \end{cases} . \quad (\text{A.10})$$

As this function is non-smooth, the following theoretical concepts derived from [98], [100] will be used to define a more general gradient for this class of functions.

**Definition 1** (Subdifferential)

For a lower semi-continuous convex function  $f : \mathbb{R}^n \rightarrow (-\infty, \infty]$ , with the property  $\exists x \in \mathbb{R}^n : f(x) < \infty$  (proper), we define the **subdifferential** of  $f$  at  $x \in \mathbb{R}^n$

$$\partial f(x) = \{y \in \mathbb{R}^n | f(\bar{x}) \geq f(x) + y^\top(\bar{x} - x) \quad \forall \bar{x}\} . \quad (\text{A.11})$$

The subdifferential  $\partial f(x)$  is a set-valued function. If  $f$  is differentiable at  $x$ , then  $\partial f(x) = \nabla f(x)$ .  $\square$

**Definition 2** (Normal Cone)

Let  $\mathcal{X} \subseteq \mathbb{R}^n$  be a closed convex set. The normal cone to  $\mathcal{X}$  at  $x \in \mathcal{X}$  is

$$N_{\mathcal{X}}(x) = \{y \in \mathbb{R}^n | y^\top(\bar{x} - x) \leq 0, \quad x \in \mathcal{X}, \quad \forall \bar{x} \in \mathcal{X}\} \quad (\text{A.12})$$

and  $N_{\mathcal{X}}(x) = \emptyset$  if  $x \notin \mathcal{X}$ .  $\square$

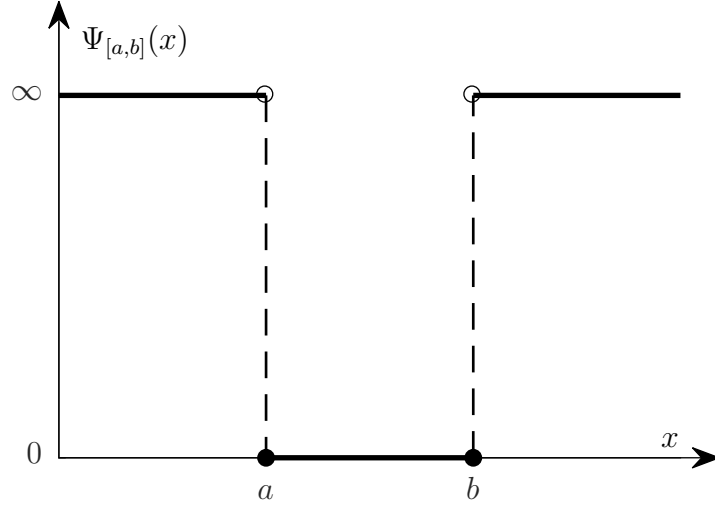
If  $\mathcal{X}$  is closed and convex,  $\Psi_{\mathcal{X}}(x)$  is lower semi-continuous and convex and its subdifferential for  $x \in \mathcal{X}$  is

$$\begin{aligned} \partial_x \Psi_{\mathcal{X}}(x) &= \{y \in \mathbb{R}^n | \Psi_{\mathcal{X}}(\bar{x}) \geq \underbrace{\Psi_{\mathcal{X}}(x)}_{=0} + y^\top(\bar{x} - x), \quad \forall \bar{x}\} \\ &= \{y \in \mathbb{R}^n | 0 \geq y^\top(\bar{x} - x), \quad \forall \bar{x} \in \mathcal{X}\} = N_{\mathcal{X}}(x) , \end{aligned} \quad (\text{A.13})$$

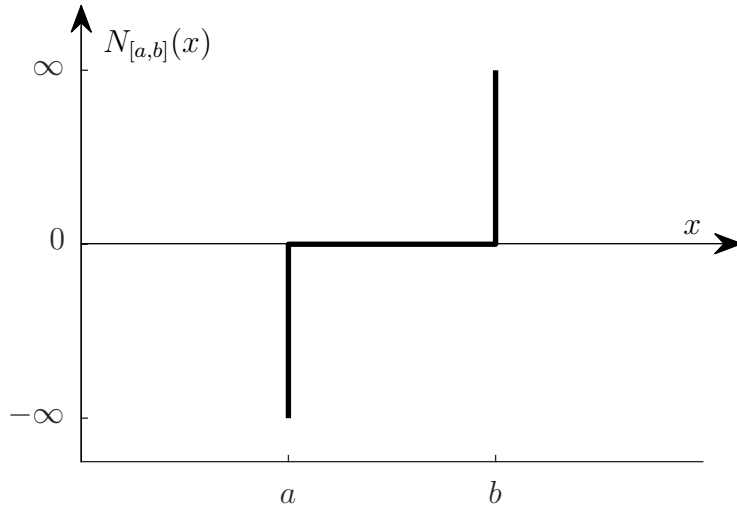
i.e. the subdifferential of the indicator function to a closed convex set is the normal cone to that set. Considering the closed convex set  $[a, b] \subseteq \mathbb{R}$  with  $a < b$ , the indicator function to this set and the normal cone are shown in Figure A.1.

This generalized gradient for convex functions can be used when the Hamiltonian is composed of a differentiable and locally bounded component  $H_d(\cdot)$ , a convex part with a polyhedral epigraph  $H_p(\cdot)$  and an indicator function on a closed, non-empty convex set  $\mathcal{C}$   $\Psi_{\mathcal{C}}(\cdot)$ , i.e.,

$$H(q) = H_d(q) + H_p(q) + \Psi_{\mathcal{C}}(q) , \quad (\text{A.14})$$



(a) Indicator function to the set  $[a, b]$ .



(b) Normal cone to the set  $[a, b]$ .

Figure A.1: Indicator function and normal cone to the set  $[a, b]$ . The full dots represent inclusion, the empty ones exclusion.

where  $q := (x^\top, u^\top, \lambda^\top)^\top$  is a general vector containing the arguments of  $H(\cdot)$ . Then, for the subdifferential of the Hamiltonian function we obtain

$$\partial_q H(q) = \nabla_q H_d(q) + \partial_q H_p(q) + N_c(q) . \quad (\text{A.15})$$

The input and state constraints

$$u(t) \in \mathcal{U} \quad (\text{A.16})$$

$$x(t) \in \mathcal{X} \quad (\text{A.17})$$

$$x(T) \in \mathcal{X}_f , \quad (\text{A.18})$$



where  $\mathcal{U} \subseteq \mathbb{R}^m$ ,  $\mathcal{X} \subseteq \mathbb{R}^n$ , and  $\mathcal{X}_f \subseteq \mathbb{R}^n$  are assumed to be non-empty closed convex sets, can be expressed as additional costs as

$$\bar{g}(x, u) = g(x, u) + \Psi_{\mathcal{X}}(x) + \Psi_{\mathcal{U}}(u) \quad (\text{A.19})$$

$$\bar{h}(x(T)) = h(x(T)) + \Psi_{\mathcal{X}_f}(x(T)) \quad . \quad (\text{A.20})$$

The Hamiltonian is then redefined as

$$H(x, u, \lambda) = \bar{g}(x, u) + \lambda^\top f(t, x, u) \quad . \quad (\text{A.21})$$

The optimal state and co-state trajectories are given by

$$\begin{cases} \dot{x}^*(t) = \left( \frac{\partial}{\partial \lambda} H(x^*(t), u^*(t), \lambda(t)) \right)^\top \\ x^*(0) = x_0 \\ \dot{\lambda}(t) \in - \left( \partial_x H(x^*(t), u^*(t), \lambda(t)) \right)^\top \\ \lambda(T) \in \left( \partial_x \bar{h}(x^*(T)) \right)^\top \end{cases} \quad (\text{A.22})$$

It can be shown that (A.22) is equivalent to the result obtained employing Lagrangian multipliers, as in [99]. Assuming a convex Hamiltonian, the optimal inputs can be obtained from

$$0 \in \partial_u H(x^*(t), u, \lambda(t)) \Big|_{u=u^*(t)} \quad . \quad (\text{A.23})$$

### A.3 Derivation of the Optimal Control Policy

From the first inclusion of (4.13) we obtain

$$P_f^* = \begin{cases} P_{f,\max} & \text{if } \lambda_{\text{kin}} \leq \lambda_{f,\max} \\ 0 & \text{if } \lambda_{\text{kin}} \geq \lambda_{f,0} \end{cases}, \quad (\text{A.24})$$

where

$$\begin{aligned} \lambda_{f,\max} &:= \left( -\lambda_f + \left( \lambda_b \cdot (2 \cdot \alpha_b \cdot P_b \cdot (P_{k,\text{fmax}}, -\eta_h \cdot P_{f,\max}) + 1) \right. \right. \\ &\quad \left. \left. - \lambda_{\text{ES2K}} \cdot \bar{\sigma}(P_{k,\text{dc}}(P_{k,\text{fmax}}) + P_{h,\text{dc}}(-\eta_h \cdot P_{f,\max})) \cdot (2\alpha_h \cdot \eta_h^2 \cdot P_{f,\max} - \eta_h) \right) \right) \\ &\quad \cdot \frac{1}{\eta_e \cdot (2 \cdot c_{s,1} \cdot (\eta_e \cdot P_{f,\max} - P_{e,0} + P_{k,\text{fmax}}) + c_{s,2})} \\ \lambda_{f,0} &:= \frac{\left( \lambda_b \cdot (2 \cdot \alpha_b \cdot P_b(P_{k,\text{f0}}, 0) + 1) - \lambda_{\text{ES2K}} \cdot \underline{\sigma}(P_{k,\text{f0}}) \right) (-\eta_h) - \lambda_f}{\eta_e \cdot (2 \cdot c_{s,1} \cdot (-P_{e,0} + P_{k,\text{f0}}) + c_{s,2})}. \end{aligned} \quad (\text{A.25})$$

The functions  $\bar{\sigma}(\cdot) := \mathbf{1}_{[0,\infty)}(\cdot)$  and  $\underline{\sigma}(\cdot) := \mathbf{1}_{(0,\infty)}(\cdot)$  are single-valued Heaviside functions for which  $\bar{\sigma}(0) = 1$  and  $\underline{\sigma}(0) = 0$ . The value of  $P_f^*(\lambda_{\text{kin}})$  could be computed analytically for  $\lambda_{\text{kin}} \in [\lambda_{f,\max}, \lambda_{f,0}]$ . To this end, a third-order polynomial equation should be solved. However, it can be shown that the second- and third-order terms are combined with squared and cubic efficiency parameters  $\alpha_j$ , which strongly reduce the importance of these terms, such that an affine behaviour can be assumed. The  $\lambda_{\text{kin}}$  values for a given optimal fuel power  $P_f^*$  inside the constraint set  $[0, P_{f,\max}]$  are obtained from the first inclusion of (4.13), where the normal cone  $N_{[0, P_{f,\max}]}(P_f^*)$  is zero, as

$$\begin{aligned} \lambda_{\text{fuel}} &= \left( -\lambda_f + \left( \lambda_b \cdot (2 \cdot \alpha_b \cdot P_b(P_k^*, -\eta_h \cdot P_f^*) + 1) \right. \right. \\ &\quad \left. \left. - \lambda_{\text{ES2K}} \cdot \sigma(P_{k,\text{dc}}(P_k^*) + P_{h,\text{dc}}(-\eta_h \cdot P_f^*)) \cdot (2 \cdot \alpha_h \cdot \eta_h^2 \cdot P_f^* - \eta_h) \right) \right) \\ &\quad \cdot \frac{1}{\eta_e \cdot (2 \cdot c_{s,1} \cdot (\eta_e \cdot P_f^* - P_{e,0} + P_k^*) + c_{s,2})}. \end{aligned} \quad (\text{A.26})$$

The value of  $P_k^*(\lambda_{\text{fuel}}, P_f^*)$  for these points can be computed substituting  $\lambda_{\text{kin}} = \lambda_{\text{fuel}}$  into the second inclusion of (4.13) and solving numerically the arising inclusion

$$0 \in \left( \lambda_b \cdot (2 \cdot \alpha_b \cdot P_b(P_k^*, -\eta_h \cdot P_f^*) + 1) - \lambda_{\text{ES2K}} \cdot \sigma(P_{k,\text{dc}}(P_k^*) + P_{h,\text{dc}}(-\eta_h \cdot P_f^*)) \right) \cdot \left( \frac{2 \cdot \alpha_h \cdot \eta_h^2 \cdot P_f^* - \eta_h}{\eta_e} - (2 \cdot \alpha_k \cdot P_k^* + 1) \right) + \lambda_{\text{K2ES}} \cdot \sigma(-P_k^*)(2 \cdot \alpha_k \cdot P_k^* + 1) - \frac{\lambda_f}{\eta_e} + N_{[P_{k,\min}, P_{k,\max}]}(P_k^*) , \quad (\text{A.27})$$

for the specific value of  $P_f^*$ .

From the second inclusion of (4.13) we derive

$$P_k^* = \begin{cases} P_{k,\max} & \text{if } \lambda_{\text{kin}} \leq \lambda_{k,\max} \\ P_{k,h}(-\eta_h P_{f,kh}) & \text{if } \lambda_{\text{kin}} \in \Lambda_{k,h} \\ 0 & \text{if } \lambda_{\text{kin}} \in \Lambda_{k,0} \\ P_{k,\min} & \text{if } \lambda_{\text{kin}} \geq \lambda_{k,\min} \end{cases} , \quad (\text{A.28})$$

whereby  $P_{kh}(P_h) = P_{k,\text{dc}}^{-1}(-P_{h,\text{dc}}(P_h))$  represents the operational mode where the MGU-K is operated exclusively with the power extracted from the MGU-H, and the values of  $\lambda_{\text{kin}}$  are computed as

$$\begin{aligned} \lambda_{k,\max} := & \left( \lambda_b \cdot (2 \cdot \alpha_b \cdot P_b(P_{k,\max}, -\eta_h \cdot P_{f,k\max}) + 1) \right. \\ & \left. - \lambda_{\text{ES2K}} \cdot \underbrace{\bar{\sigma}(P_{k,\text{dc}}(P_{k,\max}) + P_{h,\text{dc}}(-\eta_h \cdot P_{f,k\max}))}_{=1} \right) \\ & - \lambda_{\text{K2ES}} \cdot \underbrace{\sigma(-P_{k,\max})}_{=0} \cdot \frac{2 \cdot \alpha_k \cdot P_{k,\max} + 1}{2 \cdot c_{s,1} \cdot (\eta_e \cdot P_{f,k\max} - P_{e,0} + P_{k,\max}) + c_{s,2}} , \end{aligned} \quad (\text{A.29})$$

$$\begin{aligned} \Lambda_{k,h} := & \left[ \left( \lambda_b \cdot (2 \cdot \alpha_b \cdot P_{\text{aux}}, -\eta_h \cdot P_{f,kh}) + 1 \right) - \lambda_{\text{ES2K}} \cdot \underbrace{\bar{\sigma}(0)}_{=1} - \lambda_{\text{K2ES}} \cdot \underbrace{\sigma(P_{k,h}(-\eta_h \cdot P_{f,kh}))}_{=0}^{\leq 0} \right) \\ & \cdot \frac{2 \cdot \alpha_k \cdot P_{k,h}(-\eta_h \cdot P_{f,kh}) + 1}{2 \cdot c_{s,1} \cdot (\eta_e \cdot P_{f,kh} - P_{e,0} + P_{k,h}(-\eta_h \cdot P_{f,kh})) + c_{s,2}} , \\ & \left( \lambda_b \cdot (2 \cdot \alpha_b \cdot P_{\text{aux}} + 1) - \lambda_{\text{ES2K}} \cdot \underbrace{\sigma(0)}_{=0} - \lambda_{\text{K2ES}} \cdot \underbrace{\sigma(P_{k,h}(-\eta_h \cdot P_{f,kh}))}_{=0}^{\leq 0} \right) \\ & \cdot \frac{2 \cdot \alpha_k \cdot P_{k,h}(-\eta_h \cdot P_{f,kh}) + 1}{2 \cdot c_{s,1} \cdot (\eta_e \cdot P_{f,kh} - P_{e,0} + P_{k,h}(-\eta_h \cdot P_{f,kh})) + c_{s,2}} \Big] , \end{aligned} \quad (\text{A.30})$$

$$\Lambda_{k,0} := \left[ \begin{aligned} & \left( \lambda_b \cdot (2 \cdot \alpha_b \cdot P_b(0, -\eta_h \cdot P_{f,k0+}) + 1) - \lambda_{\text{ES2K}} \cdot \underbrace{\bar{\sigma}(-\eta_h \cdot P_{f,k0+})}_{\in \{0,1\}} \right. \\ & \quad \left. - \lambda_{\text{K2ES}} \cdot \underbrace{\underline{\sigma}(0)}_{=0} \right) \frac{1}{2 \cdot c_{s,1} \cdot (\eta_e \cdot P_{f,k0+} - P_{e,0}) + c_{s,2}} , \\ & \left( \lambda_b \cdot (2 \cdot \alpha_b \cdot P_b(0, -\eta_h \cdot P_{f,k0-}) + 1) \right. \\ & \quad \left. - \lambda_{\text{ES2K}} \cdot \underbrace{\underline{\sigma}(-\eta_h \cdot P_{f,k0-})}_{=0} - \lambda_{\text{K2ES}} \cdot \underbrace{\bar{\sigma}(0)}_{=1} \right) \frac{1}{2 \cdot c_{s,1} \cdot (\eta_e \cdot P_{f,k0-} - P_{e,0}) + c_{s,2}} \end{aligned} \right] \quad (\text{A.31})$$

and

$$\lambda_{k,\min} := \left( \lambda_b \cdot (2 \cdot \alpha_b \cdot P_b(P_{k,\min}, -\eta_h \cdot P_{f,\min}) + 1) + \right. \\ \left. - \lambda_{\text{ES2K}} \cdot \underbrace{\underline{\sigma}(P_{k,\text{dc}}(P_{k,\min}) + P_{h,\text{dc}}(-\eta_h \cdot P_{f,\min}))}_{=0} \right) + \\ \left. - \lambda_{\text{K2ES}} \cdot \underbrace{\bar{\sigma}(-P_{k,\min})}_{=1} \right) \frac{2 \cdot \alpha_k \cdot P_{k,\min} + 1}{2 \cdot c_{s,1} \cdot (\eta_e \cdot P_{f,\min} - P_{e,0} + P_{k,\min}) + c_{s,2}} . \quad (\text{A.32})$$

The intervals  $\Lambda_{k,h}$  and  $\Lambda_{k,0}$  are related to the values of  $\lambda_{\text{ES2K}}$  and  $\lambda_{\text{K2ES}}$ , respectively. They exist only if the ES2K and K2ES constraints are active, and they arise from the set-valued form of  $\sigma(\cdot)$ . The  $\lambda_{\text{kin}}$  value for a given optimal MGU-K power  $P_k^*$  inside the constraint set  $[P_{k,\min}, P_{k,\max}]$  is obtained from the second inclusion of (4.13), where the normal cone  $N_{[P_{k,\min}, P_{k,\max}]}(P_k^*)$  is zero, as

$$\lambda_k = \left( \lambda_b \cdot (2 \cdot \alpha_b \cdot P_b(P_k^*, -\eta_h \cdot P_f^*) + 1) - \lambda_{\text{ES2K}} \cdot \sigma(P_k^* - P_{kh}(-\eta_h \cdot P_f^*)) \right. \\ \left. - \lambda_{\text{K2ES}} \cdot \sigma(-P_k^*) \right) \frac{2 \cdot \alpha_k \cdot P_k^* + 1}{2 \cdot c_{s,1} \cdot (\eta_e \cdot P_f^* - P_{e,0} + P_k^*) + c_{s,2}} . \quad (\text{A.33})$$

For these values, the value of  $P_f^*(\lambda_k, P_k^*)$  can be obtained by substituting  $\lambda_{\text{kin}} = \lambda_k$  into the first inclusion of (4.13) and solving numerically the arising inclusion

$$0 \in \left( \lambda_b \cdot (2 \cdot \alpha_b \cdot P_b(P_k^*, -\eta_h \cdot P_f^*) + 1) - \lambda_{\text{ES2K}} \cdot \sigma(P_k^* - P_{kh}(-\eta_h \cdot P_f^*)) \right) \\ \cdot \left( \eta_e \cdot (2 \cdot \alpha_k \cdot P_k^* + 1) - (2 \cdot \alpha_h \cdot \eta_h^2 \cdot P_f^* - \eta_h) \right) + \lambda_f \\ - \lambda_{\text{K2ES}} \cdot \sigma(-P_k^*) \eta_e \cdot (2 \cdot \alpha_k \cdot P_k^* + 1) + N_{[0, P_{f,\max}]}(P_f^*) . \quad (\text{A.34})$$

To summarize, the switch-points in  $\lambda_{\text{kin}}$  for the ICE and the MGU-K optimal modes are

$$\begin{aligned}
 \lambda_{f,\max} &= \left( (2 \cdot \alpha_h \cdot \eta_h^2 \cdot P_{f,\max} - \eta_h) \cdot \left( \lambda_b \cdot (2 \cdot \alpha_b \cdot P_b(P_{k,\max}, -\eta_h \cdot P_{f,\max}) + 1) \right. \right. \\
 &\quad \left. \left. - \lambda_{\text{ES2K}} \cdot \bar{\sigma}(P_{k,\text{dc}}(P_{k,\max}) + P_{h,\text{dc}}(-\eta_h \cdot P_{f,\max})) \right) - \lambda_f \right) \\
 &\quad \cdot \frac{1}{\eta_e \cdot (2 \cdot c_{s,1} \cdot (\eta_e \cdot P_{f,\max} - P_{e,0} + P_{k,\max}) + c_{s,2})} \\
 \lambda_{f,0} &= \frac{\left( \lambda_b \cdot (2 \cdot \alpha_b \cdot P_b(P_{k,f0}, 0) + 1) - \lambda_{\text{ES2K}} \cdot \bar{\sigma}(P_k^*) \right) \cdot (-\eta_h) - \lambda_f}{\eta_e \cdot (2 \cdot c_{s,1} \cdot (-P_{e,0} + P_{k,f0}) + c_{s,2})} \\
 \lambda_{k,\max} &= \left( \lambda_b \cdot (2 \cdot \alpha_b \cdot P_b(P_{k,\max}, -\eta_h \cdot P_{f,k\max}) + 1) - \lambda_{\text{ES2K}} \right) \\
 &\quad \cdot \frac{(2 \cdot \alpha_k \cdot P_{k,\max} + 1)}{2 \cdot c_{s,1} \cdot (\eta_e \cdot P_{f,k\max} - P_{e,0} + P_{k,\max}) + c_{s,2}} \\
 \Lambda_{k,h} &= \left[ \frac{\left( \lambda_b \cdot (2 \cdot \alpha_b \cdot P_{\text{aux}} + 1) - \lambda_{\text{ES2K}} \right) \cdot (2 \cdot \alpha_k \cdot P_{k,h}(-\eta_h \cdot P_{f,kh+}) + 1)}{2 \cdot c_{s,1} \cdot (\eta_e \cdot P_{f,kh+} - P_{e,0} + P_{k,h}(-\eta_h \cdot P_{f,kh+})) + c_{s,2}}, \right. \\
 &\quad \left. \frac{\lambda_b \cdot (2 \cdot \alpha_b \cdot P_{\text{aux}} + 1) \cdot (2 \cdot \alpha_k \cdot P_{k,h}(-\eta_h \cdot P_{f,kh-}) + 1)}{2 \cdot c_{s,1} \cdot (\eta_e \cdot P_{f,kh-} - P_{e,0} + P_{k,h}(-\eta_h \cdot P_{f,kh-})) + c_{s,2}} \right] \\
 \Lambda_{k,0} &= \left[ \frac{\lambda_b \cdot (2 \cdot \alpha_b \cdot P_b(0, -\eta_h \cdot P_{f,k0+}) + 1) - \lambda_{\text{ES2K}} \cdot \bar{\sigma}(-P_{f,k0+})}{2 \cdot c_{s,1} \cdot (\eta_e \cdot P_{f,k0+} - P_{e,0}) + c_{s,2}}, \right. \\
 &\quad \left. \frac{\lambda_b \cdot (2 \cdot \alpha_b \cdot P_b(0, -\eta_h \cdot P_{f,k0-}) + 1) - \lambda_{\text{K2ES}}}{2 \cdot c_{s,1} \cdot (\eta_e \cdot P_{f,k0-} - P_{e,0}) + c_{s,2}} \right] \\
 \lambda_{k,\min} &= \left( \lambda_b \cdot (2 \cdot \alpha_b \cdot P_b(P_{k,\min}, -\eta_h \cdot P_{f,k\min}) + 1) - \lambda_{\text{K2ES}} \right) \\
 &\quad \cdot \frac{(2 \cdot \alpha_k \cdot P_{k,\min} + 1)}{2 \cdot c_{s,1} \cdot (\eta_e \cdot P_{f,k\min} - P_{e,0} + P_{k,\min}) + c_{s,2}}.
 \end{aligned} \tag{A.35}$$

The values of  $P_{k,i}$  with  $i=f_{\max}$ ,  $f_0$  and  $P_{f,j}$  with  $j=k_{\max}$ ,  $kh+$ ,  $kh-$ ,  $k0+$ ,  $k0-$ ,  $k_{\min}$  can be computed by numerically solving the inclusions (A.27) and (A.34), respectively. The optimal control policy for the ICE power can be inferred by using the relation  $P_e^* = \eta_e \cdot P_f^* - P_{e,0}$  and the fact that  $\lambda_{e,\max} = \lambda_{f,\max}$  and  $\lambda_{e,0} = \lambda_{f,0}$ .

## A.4 Linearized System

The state space matrices of system (5.12) are

$$A = \begin{pmatrix} 1 - a_d & 0 & 0 \\ 0 & 1 & 0 \\ a_b & 0 & 1 \end{pmatrix}, \quad B = \begin{pmatrix} b_p & b_p \\ b_f & 0 \\ b_h & -b_k \end{pmatrix}, \quad (\text{A.36})$$

where

$$\begin{aligned} a_d &= \left( \overbrace{-c_{s,1} \left\langle \frac{\bar{F}_u^o}{\bar{v}^o} \right\rangle}^{\approx 0} + (c_{d,0} + c_{d,1} \cdot \langle \gamma \rangle) \right) \cdot \frac{2}{m} \cdot \Delta s \\ a_b &= \left\langle \left( \alpha_b \bar{F}_b^{o2} + (2 \cdot \alpha_b \cdot \bar{v}^o \cdot \bar{F}_b^o + 1) \right. \right. \\ &\quad \left. \left. \cdot \left( \alpha_k \cdot \bar{F}_k^{o2} + \alpha_h \cdot \bar{F}_h^{o2} - \frac{P_{\text{aux}}}{\bar{v}^o} \right) \right) \frac{2}{m \cdot \bar{v}^o} \right\rangle \cdot \Delta s \approx 0, \\ b_p &= (2 \cdot c_{s,1} \cdot \langle (\bar{F}_e^o + \bar{F}_k^o) \cdot \bar{v}^o \rangle + c_{s,2}) \cdot \Delta s \\ b_f &= 1/\eta_e \cdot \Delta s \\ b_h &= \langle (2 \cdot \alpha_b \cdot \bar{F}_b^o \cdot \bar{v}^o + 1) \cdot (2 \cdot \alpha_h \cdot \bar{F}_h^o \cdot \bar{v}^o + 1) \cdot \eta_h/\eta_e \rangle \cdot \Delta s \\ b_k &= \langle (2 \cdot \alpha_b \cdot \bar{F}_b^o \cdot \bar{v}^o + 1) \cdot (2 \cdot \alpha_k \cdot \bar{F}_k^o \cdot \bar{v}^o + 1) \rangle \cdot \Delta s \end{aligned} \quad (\text{A.37})$$

and  $\langle \cdot \rangle$  is the mean-value operator applied over one lap.

# References

- [1] S. Ebbesen, M. Salazar, P. Elbert, C. Bussi, and C. H. Onder, “Time-optimal control strategies for a hybrid electric race car”, *IEEE Transactions on Control Systems Technology*, vol. 26, no. 1, pp. 233–247, 2018.
- [2] M. Salazar, P. Elbert, S. Ebbesen, C. Bussi, and C. H. Onder, “Time-optimal control policy for a hybrid electric race car”, *IEEE Transactions on Control Systems Technology*, vol. 25, no. 6, pp. 1921–1934, 2017.
- [3] M. Salazar, C. Balerna, P. Elbert, F. P. Grando, and C. H. Onder, “Real-time control algorithms for a hybrid electric race car using a two-level model predictive control scheme”, *IEEE Transactions on Vehicular Technology*, vol. 66, no. 12, pp. 10 911–10 922, 2017.
- [4] M. Salazar, C. Balerna, E. Chisari, C. Bussi, and C. H. Onder, “Equivalent lap time minimization strategies for a hybrid electric race car”, in *57th IEEE Conference on Decision and Control (CDC)*, IEEE, 2018.
- [5] M. Salazar, C. Bussi, F. P. Grando, and C. H. Onder, “Optimal control policy tuning and implementation for a hybrid electric race car”, in *IFAC Symposium on Advances in Automotive Control (AAC)*, vol. 49, 2016, pp. 147–152.
- [6] C. Balerna, M. Salazar, N. Lanzetti, C. Bussi, and C. H. Onder, “Adaptation algorithms for the hybrid electric powertrain of a race car”, in *Proceedings of the FISITA World Automotive Congress*, 2018.
- [7] M. Salazar, P. Duhr, C. Balerna, L. Arzilli, and C. H. Onder, “Minimum lap time control of hybrid electric race cars in qualifying scenarios”, *submitted to IEEE Transactions on Vehicular Technology*, 2018.
- [8] C. Balerna, N. Lanzetti, M. Salazar, A. Cerofolini, and C. H. Onder, “Optimal low-level control strategies for a high performance hybrid electric power unit”, *submitted to IEEE Transactions on Control Systems Technology*, 2019.
- [9] S. Van Dooren, C. Balerna, M. Salazar, and C. H. Onder, “Convex modeling of pareto frontiers for optimal engine calibration”, *in preparation*, 2018.
- [10] R. Hedinger, N. Zsiga, M. Salazar, and C. H. Onder, “Model-based iterative learning control strategies for precise reference tracking in gasoline engines”, *submitted to IFAC Control Engineering Practice*, 2018.

## REFERENCES

- [11] N. Robuschi, M. Salazar, P. Duhr, F. Braghin, and C. H. Onder, “Minimum-fuel engine on/off control for the energy management of hybrid electric vehicles via iterative linear programming”, in *IFAC Symposium on Advances in Automotive Control (AAC)*, submitted, 2019.
- [12] M. Salazar, F. Rossi, M. Schiffer, C. H. Onder, and M. Pavone, “On the interaction between autonomous mobility-on-demand and the public transportation systems”, in *Proceedings of the IEEE Intelligent Transportation Systems Conference (ITSC)*, Extended Version Available at <https://arxiv.org/abs/1804.11278>, 2018.
- [13] M. Tsao, D. Milojevic, C. Ruch, M. Salazar, E. Frazzoli, and M. Pavone, “Model predictive control of ride-sharing autonomous mobility on demand systems”, in *IEEE International Conference on Robotics and Automation (ICRA)*, submitted, 2019.
- [14] M. Salazar, M. Tsao, I. Aguiar, M. Schiffer, and M. Pavone, “A congestion-aware routing scheme for autonomous mobility-on-demand systems”, in *European Control Conference (ECC)*, submitted, 2019.
- [15] FIA, “2009 formula one technical regulations”, FIA, Geneva, Switzerland, Tech. Rep., 2009.
- [16] FIA, “2014 formula one technical regulations”, FIA, Geneva, Switzerland, Tech. Rep., 2011.
- [17] FIA, “2017 formula one technical regulations”, FIA, Geneva, Switzerland, Tech. Rep., 2017.
- [18] A. Picarelli and M. Dempsey, “Simulating the complete 2014 hybrid electric formula 1 cars”, *Hybrid and Electric Vehicles Conference (HEVC)*, Nov. 2014.
- [19] L. Guzzella and A. Sciarretta, *Vehicle propulsion systems*, 3rd ed. Berlin: Springer, 2013.
- [20] D. P. Bertsekas, *Dynamic programming and optimal control*. Athena Scientific, Belmont, MA, 1995, vol. 1.
- [21] A. E. Bryson and Y.-C. Ho, *Applied optimal control: optimization, estimation and control*. Washington, D.C.: Hemisphere Publishing Corporation, 1975.
- [22] A. Sciarretta and L. Guzzella, “Control of hybrid electric vehicles”, *Control systems, IEEE*, vol. 27, no. 2, pp. 60–70, 2007.
- [23] A. Sciarretta, M. Back, and L. Guzzella, “Optimal control of parallel hybrid electric vehicles”, *IEEE Transactions on Control Systems Technology*, vol. 12, no. 3, pp. 352–363, 2004.
- [24] S. G. Wirasingha and A. Emadi, “Classification and review of control strategies for plug-in hybrid electric vehicles”, *IEEE Transactions on Vehicular Technology*, vol. 60, no. 1, pp. 111–122, 2011.



- [25] C. H. Kim and B. K. Kim, “Energy-saving 3-step velocity control algorithm for battery-powered wheeled mobile robots”, in *Robotics and Automation, 2005. ICRA 2005. Proceedings of the 2005 IEEE International Conference on*, IEEE, 2005, pp. 2375–2380.
- [26] S. Ebbesen, C. Dönitz, and L. Guzzella, “Particle swarm optimization for hybrid electric drive-train sizing”, *International Journal of Vehicle Design*, vol. 58, no. 2/3/4, pp. 181–199, 2012.
- [27] S. Ebbesen, P. Elbert, and L. Guzzella, “Engine downsizing and electric hybridization under consideration of cost and drivability”, in *Proceedings of the International Conference on Hybrid and Electric Vehicles, RHEVE*, IFP, Dec. 2011.
- [28] D. Petitjean, L. Bernardini, C. Middlemass, and S. Shahed, “Advanced gasoline engine turbocharging technology for fuel economy improvements”, SAE Technical Paper, Warrendale, PA, USA, Tech. Rep. 2004-01-0988, 2004.
- [29] M. Algrain, “Controlling an electric turbo compound system for exhaust gas energy recovery in a diesel engine”, in *2005 IEEE International Conference on Electro Information Technology*, IEEE, 2005.
- [30] K. Kishishita, K. Miyajima, and K. Hirai, “A study of an electrical turbo-compound system”, *JSAE review*, vol. 16, no. 1, pp. 66–68, 1995.
- [31] T. Katrašnik, S. Rodman, F. Trenc, A. Hribernik, and V. Medica, “Improvement of the dynamic characteristic of an automotive engine by a turbocharger assisted by an electric motor”, *Journal of engineering for gas turbines and power*, vol. 125, no. 2, pp. 590–595, 2003.
- [32] W. Wei, W. Zhuge, Y. Zhang, and Y. He, “Comparative study on electric turbo-compounding systems for gasoline engine exhaust energy recovery”, in *ASME Turbo Expo 2010: Power for Land, Sea, and Air*, American Society of Mechanical Engineers, 2010, pp. 531–539.
- [33] A. M. Mamat, A. Romagnoli, and R. F. Martinez-Botas, “Design and development of a low-pressure turbine for turbocompounding applications”, *International Journal of Gas Turbine, Propulsion and Power Systems*, vol. 4, no. 3, pp. 1–8, 2012.
- [34] L. V. Pérez and E. A. Pilotta, “Optimal power split in a hybrid electric vehicle using direct transcription of an optimal control problem”, *Mathematics and Computers in Simulation*, vol. 79, no. 6, pp. 1959–1970, 2009.
- [35] P. Elbert, S. Ebbesen, and L. Guzzella, “Implementation of dynamic programming for  $n$ -dimensional optimal control problems with final state constraints”, *IEEE Transactions on Control Systems Technology*, vol. 21, no. 3, pp. 924–931, 2013.
- [36] N. Murgovski, L. Johannesson, J. Sjöberg, and B. Egardt, “Component sizing of a plug-in hybrid electric powertrain via convex optimization”, *Mechatronics*, vol. 22, no. 1, pp. 106–120, 2012.

## REFERENCES

- [37] P. Elbert, T. Nüesch, A. Ritter, N. Murgovski, and L. Guzzella, “Engine on/off control for the energy management of a serial hybrid electric bus via convex optimization”, *IEEE Transactions on Vehicular Technology*, vol. 63, no. 8, pp. 3549–3559, 2014.
- [38] T. Nüesch, P. Elbert, M. Flankl, C. Onder, and L. Guzzella, “Convex optimization for the energy management of hybrid electric vehicles considering engine start and gearshift costs”, *Energies*, vol. 7, no. 2, pp. 834–856, 2014.
- [39] L. S. Pontryagin, *Mathematical theory of optimal processes*. CRC Press, 1987.
- [40] V. Ngo, T. Hofman, M. Steinbuch, and A. Serrarens, “Optimal control of the gearshift command for hybrid electric vehicles”, *IEEE Transactions on Vehicular Technology*, vol. 61, no. 8, pp. 3531–3543, Oct. 2012.
- [41] G. Paganelli, S. Delprat, T.-M. Guerra, J. Rimaux, and J.-J. Santin, “Equivalent consumption minimization strategy for parallel hybrid powertrains”, in *Vehicular Technology Conference, 2002. VTC Spring 2002. IEEE 55th*, IEEE, vol. 4, 2002, pp. 2076–2081.
- [42] L. Serrao, S. Onori, and G. Rizzoni, “A comparative analysis of energy management strategies for hybrid electric vehicles”, *Journal of Dynamic Systems, Measurement, and Control*, vol. 133, no. 3, p. 031012, 2011.
- [43] H. Pham, P. Van Den Bosch, J. Kessels, and R. Huisman, “Integrated energy and thermal management for hybrid electric heavy duty trucks”, in *Vehicle Power and Propulsion Conference (VPPC), 2012 IEEE*, IEEE, 2012, pp. 932–937.
- [44] S. Ebbesen, P. Elbert, and L. Guzzella, “Battery state-of-health perceptive energy management for hybrid electric vehicles”, *IEEE Transactions on Vehicular technology*, vol. 61, no. 7, pp. 2893–2900, 2012.
- [45] T. Nüesch, A. Cerofolini, G. Mancini, N. Cavina, C. Onder, and L. Guzzella, “Equivalent consumption minimization strategy for the control of real driving nox emissions of a diesel hybrid electric vehicle”, *Energies*, vol. 7, no. 5, pp. 3148–3178, 2014.
- [46] H. A. Borhan, A. Vahidi, A. M. Phillips, M. L. Kuang, and I. V. Kolmanovsky, “Predictive energy management of a power-split hybrid electric vehicle”, in *American Control Conference, 2009. ACC’09.*, IEEE, 2009, pp. 3970–3976.
- [47] H. Borhan, A. Vahidi, A. M. Phillips, M. L. Kuang, I. V. Kolmanovsky, and S. Di Cairano, “Mpc-based energy management of a power-split hybrid electric vehicle”, *IEEE Transactions on Control Systems Technology*, vol. 20, no. 3, pp. 593–603, 2012.
- [48] T. Hofman, M. Steinbuch, R. Van Druten, and A. Serrarens, “Rule-based energy management strategies for hybrid vehicles”, *International Journal of Electric and Hybrid Vehicles*, vol. 1, no. 1, pp. 71–94, 2007.
- [49] J. Hooker, “Optimal driving for single-vehicle fuel economy”, *Transportation Research Part A: General*, vol. 22, no. 3, pp. 183–201, 1988.

- [50] G. Heppeler, M. Sonntag, and O. Sawodny, “Fuel efficiency analysis for simultaneous optimization of the velocity trajectory and the energy management in hybrid electric vehicles”, *IFAC Proceedings Volumes*, vol. 47, no. 3, pp. 6612–6617, 2014.
- [51] Y. Saboohi and H. Farzaneh, “Model for developing an eco-driving strategy of a passenger vehicle based on the least fuel consumption”, *Applied Energy*, vol. 86, no. 10, pp. 1925–1932, 2009.
- [52] T. van Keulen, B. de Jager, D. Foster, and M. Steinbuch, “Velocity trajectory optimization in hybrid electric trucks”, in *American Control Conference (ACC), 2010*, IEEE, 2010, pp. 5074–5079.
- [53] E. Hellström, J. Åslund, and L. Nielsen, “Management of kinetic and electric energy in heavy trucks”, in *SAE 2010 World Congress & Exhibition, April 2010, Detroit, MI, USA, Session: Transmission and Driveline: Hybrid*, SAE International, 2010, pp. 1152–1163.
- [54] A. Sciarretta, G. De Nunzio, and L. L. Ojeda, “Optimal ecodriving control: Energy-efficient driving of road vehicles as an optimal control problem”, *Control Systems, IEEE*, vol. 35, no. 5, pp. 71–90, 2015.
- [55] B. Asadi and A. Vahidi, “Predictive cruise control: Utilizing upcoming traffic signal information for improving fuel economy and reducing trip time”, *IEEE transactions on control systems technology*, vol. 19, no. 3, pp. 707–714, 2011.
- [56] L. Johannesson, N. Murgovski, E. Jonasson, J. Hellgren, and B. Egardt, “Predictive energy management of hybrid long-haul trucks”, *Control Engineering Practice*, vol. 41, pp. 83–97, 2015.
- [57] D. Casanova, “On minimum time vehicle manoeuvring: The theoretical optimal lap”, PhD thesis, Cranfield University, School of Mechanical Engineering, Nov. 2000.
- [58] D. P. Kelly, “Lap time simulation with transient vehicle and tyre dynamics”, PhD thesis, Cranfield University, School of Mechanical Engineering, May 2008.
- [59] M. Thommyppillai, S. Evangelou, and R. Sharp, “Car driving at the limit by adaptive linear optimal preview control”, *Vehicle system dynamics*, vol. 47, no. 12, pp. 1535–1550, 2009.
- [60] J. P. Timings and D. J. Cole, “Minimum maneuver time calculation using convex optimization”, *Journal of Dynamic Systems, Measurement, and Control*, vol. 135, no. 3, p. 031 015, 2013.
- [61] A. Rucco, G. Notarstefano, and J. Hauser, “An efficient minimum-time trajectory generation strategy for two-track car vehicles”, *IEEE Transactions on Control Systems Technology*, vol. 23, no. 4, pp. 1505–1519, 2015.
- [62] J. Hauser and A. Saccon, “Motorcycle modeling for high-performance maneuvering”, *Control Systems, IEEE*, vol. 26, no. 5, pp. 89–105, 2006.

## REFERENCES

- [63] R. Lot and S. Evangelou, “Lap time optimization of a sports series hybrid electric vehicle”, in *2013 World Congress on Engineering*, 2013, pp. 1–6.
- [64] G. Perantoni and D. Limebeer, “Optimal control for a formula one car with variable parameters”, *Vehicle System Dynamics*, vol. 52, no. 5, pp. 653–678, 2014.
- [65] D. Limebeer, G. Perantoni, and A. Rao, “Optimal control of formula one car energy recovery systems”, *International Journal of Control*, vol. 87, no. 10, pp. 2065–2080, 2014.
- [66] M. I. Masouleh and D. J. Limebeer, “Optimizing the aero-suspension interactions in a formula one car”, *IEEE Transactions on Control Systems Technology*, vol. 24, no. 3, pp. 912–927, 2016.
- [67] G. Perantoni and D. Limebeer, “Optimal control of a formula one car on a three-dimensional track – part 1: Track modeling and identification”, *Journal of Dynamic Systems, Measurement, and Control*, vol. 137, no. 5, 2015.
- [68] D. Limebeer and G. Perantoni, “Optimal control of a formula one car on a three-dimensional track – part 2: Optimal control”, *Journal of Dynamic Systems, Measurement, and Control*, vol. 137, no. 5, 2015.
- [69] D. J. Limebeer and A. V. Rao, “Faster, higher and greener: Vehicular optimal control”, *IEEE Control Systems Magazine*, pp. 36–56, Apr. 2015.
- [70] P. Falcone, F. Borrelli, J. Asgari, H. E. Tseng, and D. Hrovat, “Predictive active steering control for autonomous vehicle systems”, *IEEE Transactions on Control Systems Technology*, vol. 15, no. 3, pp. 566–580, 2007.
- [71] T. Faulwasser, B. Kern, and R. Findeisen, “Model predictive path-following for constrained nonlinear systems”, in *Decision and Control, 2009 held jointly with the 2009 28th Chinese Control Conference. CDC/CCC 2009. Proceedings of the 48th IEEE Conference on*, IEEE, 2009, pp. 8642–8647.
- [72] C. E. Beal and J. C. Gerdes, “Model predictive control for vehicle stabilization at the limits of handling”, *IEEE Transactions on Control Systems Technology*, vol. 21, no. 4, pp. 1258–1269, 2013.
- [73] R. Verschueren, S. De Bruyne, M. Zanon, J. V. Frasch, and M. Diehl, “Towards time-optimal race car driving using nonlinear mpc in real-time”, in *Decision and Control (CDC), 2014 IEEE 53rd Annual Conference on*, IEEE, 2014, pp. 2505–2510.
- [74] A. Liniger, A. Domahidi, and M. Morari, “Optimization-based autonomous racing of 1:43 scale rc cars”, *Optimal Control Applications and Methods*, vol. 36, no. 5, pp. 628–647, 2015.
- [75] V. A. Laurence, J. Y. Goh, and J. C. Gerdes, “Path-tracking for autonomous vehicles at the limit of friction”, in *American Control Conference (ACC), 2017*, IEEE, 2017, pp. 5586–5591.

- [76] J. Funke, M. Brown, S. M. Erlien, and J. C. Gerdes, “Collision avoidance and stabilization for autonomous vehicles in emergency scenarios”, *IEEE Transactions on Control Systems Technology*, vol. 25, no. 4, pp. 1204–1216, 2017.
- [77] M. Brown, J. Funke, S. Erlien, and J. C. Gerdes, “Safe driving envelopes for path tracking in autonomous vehicles”, *Control Engineering Practice*, vol. 61, pp. 307–316, 2017.
- [78] F. Zhang, J. Gonzales, S. E. Li, F. Borrelli, and K. Li, “Drift control for cornering maneuver of autonomous vehicles”, *Mechatronics*, 2018.
- [79] L. Guzzella and C. H. Onder, *Introduction to modeling and control of internal combustion engine systems*, 2nd ed. Berlin: Springer, 2010.
- [80] D. Verscheure, B. Demeulenaere, J. Swevers, J. De Schutter, and M. Diehl, “Time-optimal path tracking for robots: A convex optimization approach”, *IEEE Transactions on Automatic Control*, vol. 54, no. 10, pp. 2318–2327, 2009.
- [81] T. Lipp and S. Boyd, “Minimum-time speed optimisation over a fixed path”, *International Journal of Control*, vol. 87, no. 6, pp. 1297–1311, 2014.
- [82] R. de Castro, M. Tanelli, R. E. Araújo, and S. M. Savaresi, “Minimum-time path-following for highly redundant electric vehicles”, *IEEE Transactions on Control Systems Technology*, vol. 24, no. 2, pp. 487–501, 2016.
- [83] N. Murgovski, L. Johannesson, X. Hu, B. Egardt, and J. Sjöberg, “Convex relaxations in the optimal control of electrified vehicles”, in *American Control Conference (ACC), 2015*, IEEE, 2015, pp. 2292–2298.
- [84] J. Löfberg, “Yalmip : A toolbox for modeling and optimization in MATLAB”, in *Proceedings of the CACSD Conference*, Taipei, Taiwan, 2004. [Online]. Available: <http://users.isy.liu.se/johanl/yalmip>.
- [85] A. Domahidi, E. Chu, and S. Boyd, “ECOS: An SOCP solver for embedded systems”, in *European Control Conference (ECC)*, 2013, pp. 3071–3076.
- [86] X. Zuhua and Z. Jun, “Zone model predictive control algorithm using soft constraint method”, in *Intelligent Control and Automation, 2004. WCICA 2004. Fifth World Congress on*, IEEE, vol. 1, 2004, pp. 650–653.
- [87] A. H. González and D. Odloak, “A stable mpc with zone control”, *Journal of Process Control*, vol. 19, no. 1, pp. 110–122, 2009.
- [88] A. Ferramosca, D. Limon, A. González, D. Odloak, and E. Camacho, “Mpc for tracking zone regions”, *Journal of Process Control*, vol. 20, no. 4, pp. 506–516, 2010.
- [89] B. Grosman, E. Dassau, H. C. Zisser, L. Jovanović, and F. J. Doyle, “Zone model predictive control: A strategy to minimize hyper- and hypoglycemic events”, *Journal of diabetes science and technology*, vol. 4, no. 4, pp. 961–975, 2010.

## REFERENCES

- [90] R. Gondhalekar, E. Dassau, and F. J. Doyle, “Periodic zone-mpc with asymmetric costs for outpatient-ready safety of an artificial pancreas to treat type 1 diabetes”, *Automatica*, vol. 71, pp. 237–246, 2016.
- [91] P. S. Rivadeneira, A. Ferramosca, and A. H. González, “Impulsive zone model predictive control with application to type 1 diabetic patients”, in *Control Applications (CCA), 2016 IEEE Conference on*, IEEE, 2016, pp. 544–549.
- [92] R. Gondhalekar, F. Oldewurtel, and C. N. Jones, “Least-restrictive robust periodic model predictive control applied to room temperature regulation”, *Automatica*, vol. 49, no. 9, pp. 2760–2766, 2013.
- [93] R. F. Stengel, *Optimal control and estimation*. New York: Dover Publications, 1994.
- [94] A. Domahidi and J. Jerez, *FORCES Professional*, embotech GmbH (<http://embotech.com/FORCES-Pro>), Feb. 2017.
- [95] D. P. Bertsekas, *Convex optimization algorithms*. Athena Scientific, 2015.
- [96] S. Boyd and L. Vandenberghe, *Convex optimization*. Cambridge University Press, 2004.
- [97] D. P. Bertsekas, *Convex optimization theory*. Athena Scientific Belmont, 2009.
- [98] R. T. Rockafellar, *Convex Analysis*. Princeton University Press, 1997.
- [99] R. F. Hartl, S. P. Sethi, and R. G. Vickson, “A survey of the maximum principles for optimal control problems with state constraints”, *SIAM review*, vol. 37, no. 2, pp. 181–218, 1995.
- [100] R. T. Rockafellar and R. J.-B. Wets, *Variational Analysis*. New York: Springer Science & Business Media, 2009, vol. 317.

# Curriculum Vitae

**Mauro Rubén Ulisse Salazar Villalon**

Swiss and Spanish citizen

samauro@ethz.ch

## EDUCATION

---

<b>Ph.D., ETH Zürich, Switzerland</b>	2015-present
Institute for Dynamic Systems and Control, Dept. of Mechanical and Process Engineering	
Advisor: Prof. C. H. Onder	
<b>M.Sc., ETH Zürich, Switzerland</b>	2012-2015
Mechanical and Process Engineering, GPA: 5.95/6.0	
<b>B.Sc., ETH Zürich, Switzerland</b>	2009-2011
Mechanical and Process Engineering, GPA: 5.68/6.0	

## AWARDS

---

<b>Best Student Paper Award – IEEE ITSC</b>	2018
For the contribution “On the Interaction between Autonomous Mobility-on-Demand and Public Transportation Systems”	
<b>ETH Medal</b>	2016
For the outstanding Master thesis in Mechanical and Process Engineering	
<b>Outstanding D-MAVT Bachelor Award – ETH Zürich</b>	2012
For being ranked 1st out of more than 229 students	
<b>Excellence Scholarship and Opportunity Award – ETH Zürich</b>	2012
For the Master studies in Mechanical and Process Engineering	
<b>European Patent Office Originality Prize</b>	2010
European Union Contest for Young Scientists, design of a heterogeneous catalyst using the horse’s spongy bone’s micro- and nanoporous structure, Matura project	
<b>Schweizer Jugend Forscht Award</b>	2010
National competition for young researchers, design of a heterogeneous catalyst using the horse’s spongy bone’s micro- and nanoporous structure, Matura project	

- SGCI Simply Science Prize** 2010  
National competition for young researchers, design of a heterogeneous catalyst using the horse's spongy bone's micro- and nanoporous structure, Matura project
- Prix des matériaux EPFL** 2009  
For the design of a heterogeneous catalyst using the horse's spongy bone's micro- and nanoporous structure, Matura project
- Fernando Zappa Prize** 2009  
Best Latin student at the highschool Lugano 2

INVITED TALKS

---

- INFORMS, Annual Meeting, USA** 2018  
Invited talk, "Intermodal Autonomous Mobility-on-Demand"
- TU/Eindhoven, Netherlands** 2018  
Invited talk at the Control Systems Technology Group (Prof. T. Hofman), "From Urban Mobility to Formula 1 Racing"
- EPFL, Switzerland** 2018  
Invited talk at the Chair of Risk Analytics and Optimization (Prof. D. Kuhn), "Autonomous Mobility-on-Demand"
- ETH Zürich, Switzerland** 2018  
Invited talk at the Institute for Transport Planning and Systems (Prof. K.W. Axhausen), "Autonomous Mobility-on-Demand"
- ETH Zürich, Switzerland** 2018  
Invited talk at the Automatic Control Laboratory (Prof. R. Smith, Prof. J. Lygeros, Prof. F. Dörfler, Prof. M. Morari), "Autonomous Mobility-on-Demand"
- EPFL, Switzerland** 2018  
Invited talk at the Automatic Control Laboratory (Prof. C. Jones, Prof. G. Ferrari), "The Interaction between Autonomous Mobility-on-Demand and Public Transit"
- Georgia Tech, USA** 2018  
Invited talk at the DCL Seminar Series (Prof. B. German, Prof. E. Feron, Prof. M. Costello), "From Urban Mobility to Formula 1 Racing"
- International Conference on Innovations in Travel Modeling, USA** 2018  
Invited talk, "Multimodal Autonomous Mobility-on-Demand"
- UC Berkeley, USA** 2018  
Invited talk at the MPC Lab (Prof. F. Borrelli), "Time-optimal Control of the Formula 1 Hybrid Electric Power Unit"
- Stanford University, USA** 2018  
Invited talk at the Autonomous Systems Lab and the Center of Automotive Research (Prof. M. Pavone and Prof. C. Gerdes), "Time-optimal Control of the Formula 1 Hybrid



Electric Power Unit”

**EPFL, Switzerland**

2017

Invited talk at the Automatic Control Laboratory (Prof. C. Jones, Prof. T. G. Ferrari),  
“Time-optimal Control of the Formula 1 Hybrid Electric Power Unit”

**ETH Zürich, Switzerland**

2017

Invited talk at the Automatic Control Laboratory (Prof. R. Smith, Prof. J. Lygeros, Prof.  
F. Dörfler), “Time-optimal Control of the Formula 1 Hybrid Electric Power Unit”

## TEACHING EXPERIENCE

---

**System Modeling, ETH Zürich, Switzerland** 2018

Lecturer for undergraduate course, approximately 300 students. Responsibilities included giving lecture courses, organizing exercise classes, offering office hours, developing and grading final exams, maintaining the class web page, and overall class administration.

**Control Systems I/II, ETH Zürich, Switzerland** 2015-2016

Teaching assistant and lecturer for undergraduate course, approximately 400 students. Responsibilities included active participation in the lectures, organizing exercises classes, offering office hours, developing and grading final exams, maintaining the class web page, and overall class administration.

**Engine Systems, ETH Zürich, Switzerland** 2014

Teaching weekly exercise classes, answering questions during weekly office hours. Co-examiner in the oral exams.

**Quantum Mechanics for Engineers, ETH Zürich, Switzerland** 2013-2014

Teaching weekly exercise classes, answering questions during weekly office hours, grading written midterm and final exams and holding some of the lectures.

**Fluid Dynamics II, ETH Zürich, Switzerland** 2012

Teaching weekly exercise classes, answering questions during weekly office hours and grading midterm exams.

**Mechanics I/II, ETH Zürich, Switzerland** 2011-2012

Teaching weekly exercise classes, answering questions during weekly office hours and grading midterm exams. Topics included kinematics and structural mechanics.

**Analysis II, ETH Zürich, Switzerland** 2011-2012

Teaching weekly exercise classes, answering questions during weekly office hours.

## PUBLIC COMMUNICATION

---

**RSI, Rete Uno, Millevoci** 2018

Lavorare e vivere in California nel mondo delle tecnologie di punta

**ETH Zürich D-MAVT Master Ceremony Speech** 2016

On the importance of humanities in engineering studies

**Schweizer Jugend Forscht Presentation, Switzerland** 2011

Presentation on the EUCYS experience to the President of the Swiss Confederation Johann Schneider-Ammann, to the ETH board and to the audience present at the awards ceremony of Schweizer Jugend Forscht at ETH Zürich

**Swiss Confederation Presidency, Switzerland** 2010

Presentation of the highschool qualification project to the President of the Swiss Confederation Doris Leuthard

## PUBLICATIONS

---

### Journal Publications

- [1] S. Ebbesen, M. Salazar, P. Elbert, C. Bussi and C. H. Onder, “*Time-optimal Control Strategies for a Hybrid Electric Race Car*”, IEEE Transactions on Control Systems Technology, 2017
- [2] M. Salazar, P. Elbert, S. Ebbesen, C. Bussi and C. H. Onder, “*Time-optimal Control Policy for a Hybrid Electric Race Car*”, IEEE Transactions on Control Systems Technology, 2017
- [3] M. Salazar, C. Balerna, P. Elbert, F. P. Grando and C. H. Onder, “*Real-time Control Algorithms for a Hybrid Electric Race Car Using a Two-level Model Predictive Control Scheme*”, IEEE Transactions on Vehicular Technology 2017
- [4] M. Salazar, P. Duhr, C. Balerna, L. Arzilli and C. H. Onder, “*Minimum Lap Time Control of Hybrid Electric Race Cars in Qualifying Scenarios*”, Submitted to IEEE Transactions on Vehicular Technology, 2018
- [5] C. Balerna, N. Lanzetti, M. Salazar, A. Cerofolini and C. H. Onder, “*Optimal Low-level Control Strategies for a High Performance Hybrid Electric Power Unit*”, submitted to IEEE Transactions on Control Systems Technology, 2019
- [6] S. Van Dooren, C. Balerna, M. Salazar and C. H. Onder, “*Convex Modeling of Pareto Frontiers for Optimal Engine Calibration*”, in preparation.
- [7] R. Hedinger, N. Zsiga, M. Salazar and C. H. Onder, “*Model-based Iterative Learning Control Strategies for Precise Reference Tracking in Gasoline Engines*”, IFAC Control Engineering Practice, under review, 2018

**Conference Proceedings** (full-paper-refereed)

- [1] M. Salazar, M. Tsao, I. Aguiar, M. Schiffer and M. Pavone, “*A Congestion-aware Routing Scheme for Autonomous Mobility-on-Demand Systems*”, Submitted to the European Control Conference (ECC), 2019
- [2] N. Robuschi, M. Salazar, P. Duhr, F. Braghin and C. H. Onder, “*Minimum-fuel Engine On/Off Control for the Energy Management of Hybrid Electric Vehicles using Iterative Linear Programming*”, Submitted to the IFAC Symposium on Advances in Automotive Control (AAC), 2019
- [3] M. Tsao, D. Milojevic, C. Ruch, M. Salazar, E. Frazzoli and M. Pavone, “*Model Predictive Control of Ride-sharing Autonomous Mobility-on-Demand Systems*”, Submitted to the International Conference on Robotics and Automation (ICRA), 2019
- [4] M. Salazar, C. Balerna, E. Chisari, C. Bussi and C. H. Onder, “*Equivalent Lap Time Minimization Strategies for a Hybrid Electric Race Car*”, Proceedings of the IEEE International Conference on Decision and Control (CDC), 2018
- [5] M. Salazar, F. Rossi, M. Schiffer, C. H. Onder and M. Pavone, “*On the Interaction between Autonomous Mobility-on-Demand and Public Transportation Systems*”, Proceedings of the IEEE International Conference on Intelligent Transportation Systems (ITSC), 2018 (Best Student Paper Award)
- [6] C. Balerna, M. Salazar, N. Lanzetti, C. Bussi and C. H. Onder, “*Adaptation Algorithms for the Hybrid Electric Powertrain of a Race Car*”, Proceedings of the FISITA World Congress, 2018
- [7] M. Salazar, F. P. Grando, C. Bussi and C. H. Onder, “*Optimal Control Policy Tuning and Implementation for a Hybrid Electric Race Car*”, Proceedings of the IFAC Symposium on Advances in Automotive Control (AAC), 2016
- [8] M. Salazar, A. Alessandretti, A. P. Aguiar and C. Jones, “*An Energy Efficient Trajectory Tracking Controller for Car-like Vehicles Using Model Predictive Control*”, Proceedings of the IEEE International Conference on Decision and Control (CDC), 2015

**Master Level****M.Sc. Thesis** (6 months, full-time research project)

- [1] Dejan Milojevic, Mechanical Engineering, ETH Zürich and Stanford University, “Ride-sharing Autonomous Mobility-on-Demand”, 2018
- [2] Pol Duhr, Mechanical Engineering, ETH Zürich, “Minimum Lap Time Control for Hybrid Electric Race Cars”, 2018
- [3] Camillo Balerna, Mechanical Engineering, ETH Zürich, “Real-time Control of the Power Unit of Hybrid Electric Race Cars Using Model Predictive Control”, 2016

**Master Semester Project** (semester-long research project)

- [1] Friedrich Prinz, Mechanical Engineering, ETH Zürich, “Optimization of a Battery-supercapacitor-based HESS for an Electric Race Car”, 2018
- [2] José Mastrangelo, Mechanical Engineering, ETH Zürich, “Time-optimal Race Strategies for Hybrid Electric Race Cars”, 2018
- [3] Nicolas Lanzetti, Mechanical Engineering, ETH Zürich, “NN-based Modeling and Optimization of an E-Turbocharged Internal Combustion Engine”, 2017
- [4] Davide Frey, Mechanical Engineering, ETH Zürich, “Time-optimal Control Strategies for Hybrid Electric Race Cars Using Homotopic NLP”, 2017
- [5] Danylo Malyuta, Mechanical Engineering, ETH Zürich, “An Optimal Endurance Power Limiter for an Electric Race Car”, 2016
- [6] Wolfgang Gentzcke, Mechanical Engineering, ETH Zürich, “Time-optimal Control Strategies for Hybrid Electric Race Cars Using Nonlinear Programming”, 2016

## **Bachelor Level**

### **B.Sc. Thesis** (semester-long research project)

- [1] Moritz Patriarca, Mechanical Engineering, ETH Zürich, “Trajectory Tracking MPC Algorithms for an Autonomous Car”, 2017
- [2] Eugenio Chisari, Mechanical Engineering, ETH Zürich, “Equivalent Lap Time Minimization Strategies for a Hybrid Electric Race Car”, 2017
- [3] Nicolas Lanzetti, Mechanical Engineering, ETH Zürich, “Real-time Adaptation Algorithms for Hybrid Electric Race Cars”, 2016
- [4] Laura Gasser, Mechanical Engineering, ETH Zürich, “Real-time Control of the Power Unit of Hybrid Electric Race Cars Using ECMS-inspired Algorithms”, 2016

### **Studies on Mechatronics** (semester-long literature research project)

- [1] Eugenio Chisari, Mechanical Engineering, ETH Zürich, “Multivariable ECMS Control Algorithms”, 2017
- [2] Nicolas Lanzetti, Mechanical Engineering, ETH Zürich, “Adaptive Control”, 2016
- [3] Laura Maria Gasser, Mechanical Engineering, ETH Zürich, “Equivalent Consumption Minimization Strategies with State Constraints”, 2016